

N 82-25600

Casefile Copy

A PRELIMINARY STUDY OF THE APPLICATION OF HCMM SATELLITE DATA
TO DEFINE INITIAL AND BOUNDARY CONDITIONS FOR NUMERICAL MODELS:
A CASE STUDY IN ST. LOUIS, MISSOURI

Fred M. Vukovich
Research Triangle Institute
P. O. Box 12194
Research Triangle Park, North Carolina 27709

May 1982
Final Report

Prepared for

GODDARD SPACE FLIGHT CENTER
Greenbelt, Maryland

BIBLIOGRAPHIC DATA SHEET

1. Report No.	2. Government Accession No.	3. Recipient's Catalog No.	
4. Title and Subtitle A PRELIMINARY STUDY OF THE APPLICATION OF HCMM SATELLITE DATA TO DEFINE INITIAL AND BOUNDARY CONDITIONS FOR NUMERICAL MODELS: A CASE STUDY IN ST. LOUIS, MISSOURI		5. Report Date May 1982	6. Performing Organization Code
		8. Performing Organization Report No. 4182-2155-F	
7. Author(s) Fred M. Vukovich		10. Work Unit No.	
9. Performing Organization Name and Address Research Triangle Institute P. O. Box 12194 Research Triangle Park, NC 27709		11. Contract or Grant No. NAS5-26442	
		13. Type of Report and Period Covered	
12. Sponsoring Agency Name and Address Mr. Harold Oseroff, Technical Monitor NASA/Goddard Space Flight Center Greenbelt, Maryland		14. Sponsoring Agency Code	
		15. Supplementary Notes	
16. Abstract <p>HCMM infrared and visible data were used to examine the potential application of these data to define initial and boundary conditions for mesoscale numerical models. Various boundary layer models were used to calculate the distribution of the surface heat flux, specific humidity depression (the difference between the specific humidity in the air at approximately the 10-m level and the specific humidity at the ground), and the eddy viscosity in a 72-km by 72-km area centered about St. Louis, Missouri. Various aspects of the implications of the results on the meteorology of St. Louis were discussed. Overall, the results indicated that a reasonable estimate of the surface heat flux, urban albedo, ground temperature, and specific humidity depression can be obtained using HCMM satellite data. Values of the ground-specific humidity can be obtained if the distribution of the air-specific humidity was available. However, more research is required in estimating the absolute magnitude of the specific humidity depression because calculations may be sensitive to model parameters.</p>			
17. Key Words (Selected by Author(s)) Urban meteorology, initial conditions, ground temperatures, urban albedo		18. Distribution Statement	
19. Security Classif. (of this report)	20. Security Classif. (of this page)	21. No. of Pages 108	22. Price*

FOREWORD

This report by the Geosciences Department of the Research Triangle Institute, Research Triangle Park, North Carolina, presents the results of a study on the application of HCMM satellite data to define initial and boundary conditions for numerical models. The study was performed for the Goddard Space Flight Center, National Aeronautics and Space Administration, under Contract No. NAS5-26442. The author wishes to acknowledge the assistance of Mr. J. W. Dunn in the development of computer algorithms of the various models; the assistance of Mr. Ashwin Gajar of the St. Louis County Air Pollution Control Department, Mr. William Hagger of the St. Louis City Air Pollution Control Department, and Mr. Terry Switzer of the East St. Louis Air Pollution Control Department for providing in situ observations in and around the City of St. Louis; and the assistance of the Army Corps of Engineers for providing Mississippi River temperatures. The author also wishes to acknowledge the interest and assistance of Mr. Locke Stuart and Mr. Harold Oseroff of NASA/GSFC, and Mr. Alan Royal of General Electric Company for helping to obtain the HCMM satellite data and for their useful discussions on the HCMM data.

PREFACE

The primary purpose of this study is to examine the potential application of HCMM satellite data to define initial and boundary conditions for mesoscale numerical models. In order to meet this objective, various boundary layer models were used to calculate the distribution of the surface heat flux, the specific humidity depression (the difference between the specific humidity in the air at approximately the 10-m level and the specific humidity at the ground), and the eddy viscosity in a 72-km x 72-km area centered about St. Louis, Missouri. Data for the models were derived from the HCMM satellite and from observations obtained through 15 stations across the urban region. Six case studies were performed.

It was shown that if the HCMM infrared data are properly calibrated, reasonable estimates of the ground temperature and temperature pattern can be obtained. The ground temperature values obtained from the HCMM satellite had approximately the same magnitude as that obtained from aircraft radiometer measurements. The analyses of the HCMM ground temperature pattern demonstrated marked seasonal and day-night differences. In the warm season and during the day, the ground temperature distribution was markedly influenced by small-scale land use features. Temperature contrasts across the urban and rural regions reached values ranging from 2.0° to 6.0°C. In the cold season and during the day, the pattern was similar to that found in the warm season but the temperature contrasts were not as large. At night, the ground temperature pattern did not show a dependence on small-scale land use features as it did during the day. Furthermore, the temperature contrasts were not as large.

The reflectivity measurements made by the HCMM satellite had a slightly larger magnitude than the albedo measurements previously made in St. Louis. However, the contrast between the urban and rural regions were similar to previous measurements and consistent with modeling results. The reflectivity pattern across the region generally showed low values of reflectivity in the central portions of St. Louis relative to the surrounding suburban and rural region.

The magnitude and pattern of the surface heat flux, which was computed using the HCMM and in situ data, were consistent with the results of previous investigators. The distribution of the specific humidity depression suggested a pattern for the ground-specific humidity which called for relatively smaller values of the ground-specific humidity in the central urban region relative to the surrounding suburban and rural region. This interpretation was consistent with previous results. During the day and in the warm season, low values of evaporation characterized the central urban region. This result was also consistent with previous observations.

The calculated distribution of eddy viscosity was governed by the distribution of wind speeds and stability. The stability was determined by the air-ground temperature difference. There was no available observational evidence with which to compare the calculated distributions of eddy viscosity. A limited comparison was performed with turbulent intensity measurements made in St. Louis. This comparison suggested that the relative distributions of the eddy viscosity were reasonable.

Overall, the results indicated that a reasonable estimate of the surface heat flux, the urban albedo, the ground temperature, and specific humidity depression can be obtained using HCMM satellite data. Values of the ground-specific humidity can be obtained if the distribution of the air-specific humidity are available. However, more research is required in estimating the absolute magnitude of the specific humidity depression because the calculations may be sensitive to model parameters.

The three parameters (the ground temperature distribution, the albedo distribution, and the ground-specific humidity distribution) are needed by mesoscale modelers for proper specification of initial and boundary conditions. The eddy viscosity is not a parameter necessary for input into most hydrodynamic models. However, there is a potential utilization for the eddy viscosity distribution in diffusion models. As in the case of the specific humidity depression, more research is required with fundamental comparisons between calculated and observed values. Furthermore, recommendation of the application of satellite data in mesoscale modeling must be qualified until studies are performed in which satellite data are actually used in a numerical model, even though this preliminary effort indicated that the potentials for application are good.

TABLE OF CONTENTS

	<u>Page</u>
1.0 Introduction	1
2.0 Methodology	5
2.1 HCMM Data and Data Processing	5
2.2 Geographical Location of HCMM Data	13
2.3 The Surface Observations	15
2.4 Boundary Layer Parameters	17
3.0 St. Louis Urban Boundary Layer Characteristics	25
3.1 Model Parameters and General Meteorology	25
3.2 The HCMM Ground Temperature Analysis	28
3.3 Urban Reflectivity Measurements	34
3.4 The Surface Heat Flux Distribution	40
3.5 The Distribution of the Specific Humidity Depression	45
3.6 Eddy Viscosity Distribution	51
4.0 Discussion of Results	56
5.0 Recommended Research	62
6.0 References	63
APPENDIX A: HCMM Daytime Ground Temperature Analyses for St. Louis, MO	68
APPENDIX B: HCMM Nighttime Ground Temperature Analyses for St. Louis, MO	73
APPENDIX C: HCMM Reflectivity Analyses for St. Louis, MO	76
APPENDIX D: Daytime Surface Heat Flux Analyses	81
APPENDIX E: Nighttime Surface Heat Flux Analyses	86
APPENDIX F: The Daytime Specific Humidity Depression Distribution	89
APPENDIX G: The Nighttime Specific Humidity Depression Distribution	94
APPENDIX H: The Distribution of the Eddy Viscosity for the Daytime Cases	97
APPENDIX I: The Distribution of the Eddy Viscosity for the Nighttime Cases	102
APPENDIX J: Estimation of the Surface Roughness Distribution Using HCMM Satellite Data	105

LIST OF ILLUSTRATIONS

<u>Figure</u>		<u>Page</u>
1	Location of areas of interest and of stations used to determine surface wind and temperature analyses	11
2	HCMM daytime ground temperature ($^{\circ}\text{C}$) distribution for 26 June 1978 in the region about St. Louis, MO	29
3	HCMM nighttime ground temperature ($^{\circ}\text{C}$) distribution for 14 June 1978 in the region about St. Louis, MO	31
4	HCMM daytime ground temperature ($^{\circ}\text{C}$) distribution for 26 February 1979 in the region about St. Louis, MO	35
5	HCMM reflectivity distribution for 26 June 1978 for the St. Louis area	36
6	HCMM reflectivity distribution for 26 February 1979 for the St. Louis area	39
7	Surface heat flux ($\text{kJ m}^{-2} \text{s}^{-1}$) distribution for 26 June 1978	41
8	Surface heat flux ($\text{kJ m}^{-2} \text{s}^{-1}$) distribution for 26 February 1979	42
9	Surface heat flux ($\text{kJ m}^{-2} \text{s}^{-1}$) distribution for 14 June 1978	46
10	The distribution of the specific humidity depression (10^{-1}g kg^{-1}) for 26 June 1978	47
11	The distribution of the specific humidity depression (10^{-1}g kg^{-1}) for 26 February 1979	49
12	The distribution of the specific humidity depression (10^{-1}g kg^{-1}) for 14 June 1978	50
13	The distribution of the eddy viscosity, K_m , ($\text{m}^2 \text{s}^{-1}$) for 26 June 1978	52
14	The distribution of the eddy viscosity, K_m , ($\text{m}^2 \text{s}^{-1}$) for 26 February 1979	53
15	The distribution of the eddy viscosity, K_m , ($\text{m}^2 \text{s}^{-1}$) for 14 June 1978	55

LIST OF ILLUSTRATIONS (continued)

<u>Figure</u>		<u>Page</u>
1A	HCMM daytime ground temperature ($^{\circ}\text{C}$) analysis for 10 June 1978	69
2A	HCMM daytime ground temperature ($^{\circ}\text{C}$) analysis for 26 June 1978	70
3A	HCMM daytime ground temperature ($^{\circ}\text{C}$) analysis for 26 February 1979	71
4A	HCMM daytime ground temperature ($^{\circ}\text{C}$) analysis for 27 September 1979	72
1B	HCMM nighttime ground temperature ($^{\circ}\text{C}$) analysis for 9 June 1978	74
2B	HCMM nighttime ground temperature ($^{\circ}\text{C}$) analysis for 14 June 1978	75
1C	Reflectivity distribution for 10 June 1978	77
2C	Reflectivity distribution for 26 June 1978	78
3C	Reflectivity distribution for 26 February 1979	79
4C	Reflectivity distribution for 27 September 1979	80
1D	Surface heat flux ($\text{kJ m}^{-2} \text{s}^{-1}$) distribution for 10 June 1978	82
2D	Surface heat flux ($\text{kJ m}^{-2} \text{s}^{-1}$) distribution for 26 June 1978	83
3D	Surface heat flux ($\text{kJ m}^{-2} \text{s}^{-1}$) distribution for 26 February 1979	84
4D	Surface heat flux ($\text{kJ m}^{-2} \text{s}^{-1}$) distribution for 27 September 1979	85
1E	Surface heat flux ($\text{kJ m}^{-2} \text{s}^{-1}$) distribution for 9 June 1978	87
2E	Surface heat flux ($\text{kJ m}^{-2} \text{s}^{-1}$) distribution for 14 June 1978	88
1F	The distribution of the specific humidity (10^{-1}g kg^{-1}) depression for 10 June 1978	90

LIST OF ILLUSTRATIONS (continued)

<u>Figure</u>		<u>Page</u>
2F	The distribution of the specific humidity (10^{-1} g kg $^{-1}$) depression for 26 June 1978	91
3F	The distribution of the specific humidity (10^{-1} g kg $^{-1}$) depression for 26 February 1979	92
4F	The distribution of the specific humidity (10^{-1} g kg $^{-1}$) depression for 27 September 1979	93
1G	The distribution of the specific humidity (10^{-1} g kg $^{-1}$) depression for 9 June 1978	95
2G	The distribution of the specific humidity (10^{-1} g kg $^{-1}$) depression for 14 June 1978	96
1H	The distribution of the eddy viscosity ($m^2 s^{-1}$) for 10 June 1978	98
2H	The distribution of the eddy viscosity ($m^2 s^{-1}$) for 26 June 1978	99
3H	The distribution of the eddy viscosity ($m^2 s^{-1}$) for 26 February 1979	100
4H	The distribution of the eddy viscosity ($m^2 s^{-1}$) for 27 September 1979	101
1I	The distribution of the eddy viscosity ($m^2 s^{-1}$) for 9 June 1978	103
2I	The distribution of the eddy viscosity ($m^2 s^{-1}$) for 14 June 1978	104
1J	Distribution of the surface roughness (m) for 9 June 1978	108

LIST OF TABLES

<u>Table</u>		<u>Page</u>
1	HCMM case studies of St. Louis heat island	6
2	Mississippi River temperatures	10
3	Mean transmissivity and values for the calibrated intercept term, b'	12
4	Identification of stations that provided data for the wind and temperature analyses	16
5	Values of parameters for the model for the friction velocity	19
6	Model parameters	26
7	The general meteorological conditions at the time of each case study derived from the observations from the National Weather Station at Lambert Field, St. Louis, MO., and an estimate of the characteristic Richardson Number in the first 10 meters	27
8	Horizontal gradient of air and ground temperature between the urban region represented by Stations #1 and #11, and the outlying suburban and rural region, represented by Stations #6, #8, #10, and #12	33
9	Characteristic values of $\Delta T (= T_a - T_g)$ in the urban and rural regions for the four daytime case studies	44

1.0 Introduction

Considerable resources have been used in an effort to develop an understanding of the urban climate because of the effect of air pollution on plants and animals, of Federal requirements on air quality, and of the environmental effects of energy consumption (Landsberg, 1970; Chandler, 1970; Kellogg, 1977; Vukovich, 1981; and Landsberg, 1981). Furthermore, a 5-year research project held in St. Louis in the early 1970's (METROMEX) has shown that a city can act as a catalyst for an increase in summer thunderstorms and precipitation. Precipitation maxima were found downwind of the city. The results are apparently extrapolatable to other urban regions (Huff and Schlessman, 1973; Huff and Changnon, 1973; Schickendanz, 1974; and Semonin and Changnon, 1974). The increased precipitation can benefit the region by increasing farm yields and can also be a detriment by increasing the frequency of violent storms.

The urban climate is principally characterized by the so-called "urban heat island" (Mitchell, 1961; Hage, 1972; and Oke and East, 1971). In the late afternoon, the temperature difference begins to increase and the urban region becomes warmer. The temperature difference reaches a maximum at around 3 to 5 hours after sunset in all seasons. Daytime differences also are found, but are generally smaller. Factors that influence the urban heat island are urban air pollution, surface roughness, soil moisture, soil thermal diffusivity, and anthropogenic heating.

Mateer (1961) noted an increase in the amount of solar radiation received in an urban area at the surface on Sunday compared to that for the remainder of the week, suggesting the influence of anthropogenic activity (air pollution). Craig and Lowry (1972) developed a model that indicated that the urban albedo should be 20 percent less than the rural albedo due to the buildings in the area. Measurements by Bray et al. (1966) in St. Paul, Minnesota, indicated that the albedo is 50 percent greater than that for the rural regions. They attributed the larger urban albedo to the use of light-colored construction material, the removal of vegetation, and the increased amounts of suspended particles over the urban region. Data presented by McCormack and Ludwig (1967) indicated that the presence of aerosols would increase the surface albedos. Welch et al. (1978) have shown that the presence of air pollution should lead to a 2° to 7°C surface

temperature decrease during the day due to the reflection of solar radiation.

Calculations (Nappo, 1972) have suggested that soil moisture is one of the most important parameters in the production of the urban heat island. Moisture in the soil in cities is considerably less than that in the rural regions because cities are generally made up of rock-like, impervious substances. Precipitation in the form of rain is quickly removed from the surface by drain pipes, gutters, and sewers. Snow is cleared from the surface by plow shovels, and significant amounts are carried away. However, in the country, most of the precipitation remains in the soil, and the water is available for evaporation. Therefore, in the urban area, solar radiation is used more to heat the surface; whereas in the rural region, some of the solar radiation is used for evaporation, reducing the amount available to heat the ground.

Mitchell (1961) has suggested that home heating plants sustained the heat island during the daylight hours of the wintertime. Welch et al. (1978) calculated that artificial heat sources can increase the air temperature by approximately 4°C. It has been suggested that the relative absence of this factor during the summer would lead to an apparent equality between the urban and rural temperatures.

There have been a number of efforts to model the urban heat island (Myrup, 1969; McElroy, 1973; Pandolpho et al., 1971; and Nappo, 1972), and its associated circulation system (Bornstein, 1975; Vukovich, 1971; Vukovich, 1973; Vukovich et al., 1976; Vukovich and Dunn, 1978; and Vukovich et al., 1979). The urban heat island is a mesoscale phenomenon, and like all mesoscale phenomena, the initial and boundary conditions required for proper execution of the models are not available. In order to define proper initial and boundary conditions, observations are required commensurate with the space resolution of the model which is, in many cases, on the order of 1 km or less. Observational networks of this caliber are generally only used in special studies. Therefore, "best estimates" are used to define the initial and boundary conditions for the models.

Efforts have been made to utilize satellite data to study the urban climate, and these efforts have recently increased. One of the initial efforts was performed by Rao (1972) who used thermal infrared data from the

radiometer on board the Improved TIROS Operational Satellite to demonstrate that the New York City-Philadelphia-Baltimore-Washington, DC urban corridor can be delineated. Carlson et al. (1977) used NOAA-3 infrared data to study the ground temperature pattern in Los Angeles and vicinity. They found the highest morning temperatures in the industrial zones and the highest evening temperatures in the central business district and the densely populated residential areas. Matson et al. (1978) used NOAA-5 satellite infrared data to detect more than 50 urban heat islands in the midwestern and northeastern portions of the United States. Their analysis of digital infrared data for selected cities yielded maximum urban-rural ground temperature differences ranging from 2.6° to 6.5°C. They also demonstrated that the distribution of ground temperatures associated with various heat islands can be depicted using the NOAA data.

Price (1979) used infrared data from the Heat Capacity Mapping Mission (HCMM) to quantify the urban-rural ground temperature differences for urban areas in the New England area. Temperature differences ranged from 10° to 15°C. Carlson et al. (1981) used thermal infrared data from the HCMM satellite to estimate the surface energy balance, the moisture availability, and the thermal inertia in Los Angeles and St. Louis. They found a marked reduction in evaporation and moisture availability and a corresponding increase in the sensible heat flux over the urbanized areas. They also found little variation in the thermal inertia between the urban and rural areas. Unfortunately, the HCMM thermal infrared data that they used had an inherent 5.5°C calibration error (Heat Capacity Mapping Mission User's Guide, 1980) which may not have been properly accounted for, and which may have significantly influenced the magnitude of the terms they estimated. However, the work of Carlson et al. has suggested that the satellite data may be used to study various properties of the urban boundary layer and may be used to estimate some of the parameters needed to numerically model the urban heat island as well as other mesoscale phenomena.

The present study has a twofold purpose: 1) to use satellite data to study the urban climate, and 2) to determine the applicability of satellite data to find various boundary layer parameters that may be used in modeling the urban climate. Results pertaining to the applicability of satellite data to determine various boundary layer parameters which may be used for

modeling purposes, are extrapolatable to other mesoscale phenomena. The study focuses on the City of St. Louis because past research programs (the Regional Air Pollution Study (RAPS) and the METROMEX program) have yielded information which well characterizes the St. Louis urban climate. That information was used for comparative purposes with the results of this study.

2.0 Methodology

2.1 HCMM Data and Data Processing

The HCMM satellite was the first of a planned series of applications explorer missions that involved the placement of small, dedicated spacecrafts in special orbits to satisfy mission-unique data acquisition requirements. The satellite was specifically designed to support exploratory scientific investigation on the feasibility of utilizing thermal infrared remote sensing measurements of the earth's surface to estimate the thermal inertia. It was launched on April 26, 1978, and subsequently completed over 6500 orbits before the experiment was terminated in October 1980.

The HCMM satellite had a two-channel scanning radiometer; one spectral channel was in the visible band from 0.5 to 1.1 μm , and the other channel viewed the thermal infrared band from 10.5 to 12.5 μm . The measurement accuracy of the two channels was limited by the analog telemetry system to 0.2 mW cm^{-2} in the 0.5 to 1.1 μm channel and to 0.4°K at 280°K in the 10.5 to 12.5 μm channel. The orbital altitude of the satellite was 620 km, and the angular resolution was 0.83 milliradians which yielded a resolution at the surface of the earth at nadir of $600 \times 600 \text{ m}$ in the infrared channel and $500 \times 500 \text{ m}$ in the visible channel.

The HCMM spacecraft orbit was sun-synchronous with a nominal ascending equatorial crossing time of 1400 Local Standard Time (LST), in order to provide north mid-latitude crossing times of 1330 LST and 0230 LST. The mission was designed to acquire repetitive thermal data at the time when the ground temperature was at a maximum or a minimum. The repeat cycle of the spacecraft was 16 days, but mid-latitude sites received repeated coverage approximately every 5 days.

Six case studies were chosen of the heat island of St. Louis. Three of these were in the late spring of 1978, one in the early summer of 1978, one in the winter of 1979, and one in the early fall of 1979. Four of the case studies treated a daytime heat island and two, a nighttime heat island. Specific information on the case studies is given in Table 1.

The HCMM data were processed to remove the extraneous influence of the atmosphere and to calibrate the infrared measurements. The signal from the ground reaching the radiometer was influenced by absorption and reradiation

Table 1. HCMM Case Studies of St. Louis Heat Island

DATE	SEASON	TIME (LST)
9 June 1978	Spring	0230
10 June 1978	Spring	1330
14 June 1978	Spring	0230
26 June 1978	Summer	1330
26 February 1979	Winter	1330
27 September 1979	Fall	1330

in the atmosphere by water vapor and carbon dioxide. In order to obtain the precise value of the ground temperature, the influence of the atmosphere must be accounted for. The procedure used to account for atmosphere attenuation and to calibrate the data is described below.

The radiation received by the satellite, N_s , can be determined through the radiative transfer equation:

$$N_s = \int_{\lambda} \phi_{\lambda} \tau_{\lambda} R_{\lambda} d\lambda + \int_{\lambda} \phi_{\lambda} \int_{\tau_{\lambda}} R'_{\lambda} d\tau_{\lambda} d\lambda \quad , \quad (1)$$

where λ is the wavelength, ϕ_{λ} is the spectral response, τ_{λ} is the transmissivity, R_{λ} is the blackbody radiation from the surface, R'_{λ} is the blackbody radiation from the atmosphere. Letting

$$\bar{\tau} = \int_{\lambda} \tau_{\lambda} d\lambda / \int_{\lambda} d\lambda \quad , \quad (2)$$

and defining

$$N_o \equiv \int_{\lambda} \phi_{\lambda} R_{\lambda} d\lambda \quad (3)$$

and

$$\delta N \equiv \int_{\lambda} \phi_{\lambda} \int_{\tau_{\lambda}} R'_{\lambda} d\tau_{\lambda} d\lambda \quad , \quad (4)$$

where N_o is the blackbody radiation emitted at the surface in the spectral interval, and δN is the increment of radiation emitted by the atmosphere and received by the satellite in the spectral interval, then the following approximation is made

$$\bar{N}_s \sim \bar{\tau} N_o + \delta N \quad . \quad (5)$$

Assuming that δN is invariant in a small area (i.e., the air mass characteristics do not change markedly over a small area), then differentiating

Equation (5) gives

$$\frac{dN_s}{dN_o} = \bar{\tau} \quad . \quad (6)$$

Equation (6) states that the gradient of (temperature or) radiation emitted from the ground would be reduced due to atmospheric absorption.

For the satellite infrared data, the digital counts, C, are related to radiation received by the satellite by a simple linear relationship; i.e.,

$$N_s = a C + b \quad , \quad (7)$$

where a and b are parameters derived from the satellite calibration data. For the HCMM satellite, a = 1.0 and b = 118.214 (HCMM User's Guide, 1980). In order to correct for the atmospheric absorption, the following inversion procedure was used. Equation (6) was differentiated:

$$\frac{dN_s}{dC} = a \quad . \quad (8)$$

This differential equation was written in the following form:

$$\frac{dN_o}{dC} \frac{dN_s}{dN_o} = a \quad . \quad (9)$$

Substitution of Equation (8) into Equation (9) and integration gave:

$$N_o = a' C + b' \quad , \quad (10)$$

where $a' = a/\bar{\tau}$. The new intercept term, b', may be expressed as a function of the old intercept term, b, by combining Equations (5), (7), and (10):

$$b' = (b - \delta N) \bar{\tau}^{-1} \quad . \quad (11)$$

Equation (10) gives the radiation emitted at the surface which is directly related to the ground temperature. The ground temperature was derived through the inversion of the Planck function:

$$T_g = \lambda_o [\ln(\lambda_1/N_o - 1.0)]^{-1} , \quad (12)$$

where T_g is the ground temperature, $\lambda_o = 1251.159$, and $\lambda_1 = 14421.587$.

The mean transmissivity was determined by calculating the optical path for water vapor using the upper-air data collected at the Upper Air Weather Station at Salem, Illinois, for those days and time periods which most closely correspond to the time that the HCMM data were collected, and by computing the optical path for carbon dioxide, assuming that carbon dioxide is thoroughly mixed in the atmosphere with a mixing ratio of 0.5 grams/kilogram (Haltiner and Martin, 1957). The optical paths for carbon dioxide and water vapor were used to develop the mean transmissivity in the thermal wavelength band of HCMM from the data presented by Wyatt *et al.* (1964a, 1964b). The corrected intercept term, b' , may be computed using Equation (11). However, because there was a controversial 5.5°C error in the HCMM-derived temperatures (see the HCMM User's Guide, 1980)--which implied that the intercept term, b , could be in error--it was decided to use an alternative approach to determine the intercept term b' . Mississippi River temperatures were acquired from the Army Corps of Engineers for the dates in question (see Table 2). The observations of the Mississippi River temperature were made near the Chain of Rocks Bridge which is located near Mosenthein Island in the Mississippi River (see Figure 1) immediately north of the central portions of St. Louis. The river temperatures were used to derive a value for the surface radiation through the Planck function. The derived value of the surface radiation was matched with the digital count located in that region. These two values were combined in Equation (10) to determine the intercept term b' . By referencing the digital counts to the Mississippi River temperature, the procedure accounted for the calibration and a portion of the atmospheric effect. The computed values of the mean transmissivity in the infrared wavelength band and of the intercept term b' are given in Table 3.

Table 2. Mississippi River Temperatures*

DATE	RIVER TEMPERATURES (°C)
9 June 1978	23.3
10 June 1978	23.3
14 June 1978	23.3
26 June 1978	26.7
26 February 1979	2.2
27 September 1979	22.2

*Source: Army Corps of Engineers

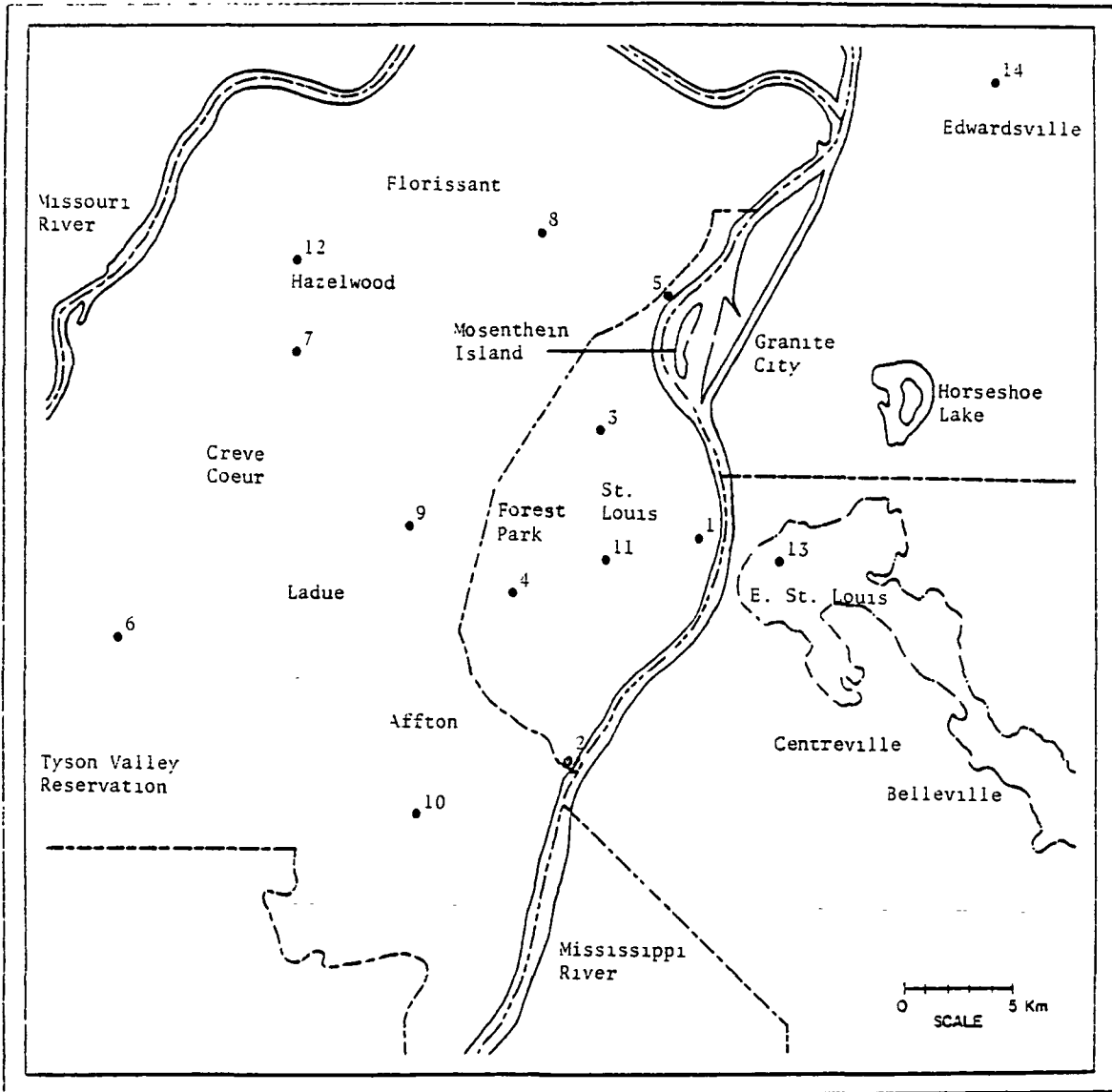


Figure 1. Location of areas of interest and of stations used to determine surface wind and temperature analyses. Station #15 is not shown because it is off the map in Alton, Illinois. See Table 4 for identification of stations. Various regions pertinent to the analyses are also identified.

Table 3. Mean Transmissivity and Values for the Calibrated Intercept Term, b'

DATE	$\bar{\tau}$	b' (Watt cm ⁻² μm ⁻¹ steradian ⁻¹)
9 June 1978	0.80	134.25
10 June 1978	0.72	102.07
14 June 1978	0.70	143.14
26 June 1978	0.62	89.78
26 February 1979	0.85	134.59
27 September 1979	0.74	108.47

The calibration data for the HCMM satellite yielded a simple linear expression to derive the reflectivity in the visible band; i.e.,

$$r = m C \quad , \quad (13)$$

where r is the reflectivity, m is the slope and is equal to $1/255$, and C is the digital count which, in this case, is in the visible band.

2.2 Geographical Location of HCMM Data

A conformal mapping procedure was used to locate the HCMM data in space. A Mercator projection of the region of interest was developed which will hereafter be referred to as the base map. A contour analysis of the HCMM digital counts for either the IR or the visible data was developed. The area of HCMM analysis was always selected to be larger than the area covered by the base map. The analysis of the digital counts will hereafter be referred to as the analysis map.

The coordinates of identifiable points such as bends in the river, confluences of rivers, edges of lakes, etc., on the base and analysis maps were determined relative to a fixed origin. The origin in the analysis map was not the same for each case study. Coordinates were determined as distances from the origin. Matrices of the two sets of corresponding coordinates were created, and the equation relating the two coordinate systems was established; i.e.,

$$A \cdot Z = B \quad , \quad (14)$$

$$A = \begin{pmatrix} x_1, y_1, 1 \\ x_2, y_2, 1 \\ \vdots \\ \vdots \\ \vdots \\ x_n, y_n, 1 \end{pmatrix} \quad , \quad B = \begin{pmatrix} a_1, b_1, 1 \\ a_2, b_2, 1 \\ \vdots \\ \vdots \\ \vdots \\ a_n, b_n, 1 \end{pmatrix} \quad , \quad (15)$$

where (x_i, y_i) are the coordinates of the points $i = 1, 2, \dots, n$ in the analysis map, (a_i, b_i) are the coordinates of corresponding points $i = 1, 2,$

..., n in the base map, and Z is an unknown transform matrix which relates the two sets of coordinates. If the transform matrix is determined, then the HCMM data can be projected into the base map.

In order to determine the transform matrix, the transpose matrix of A, A^T , was computed, and both sides of Equation (14) were multiplied by the transpose of A:

$$(A^T \cdot A) \cdot Z = A^T \cdot B \quad (16)$$

The transform matrix Z was determined by first computing the inversion matrix of the product of the transpose of A times A and multiplying both sides of the Equation (16) by the inversion matrix:

$$Z = (A^T \cdot A)^{-1} \cdot (A^T \cdot B) \quad (17)$$

In the analysis map, each data value (digital count, for example), V_k , has a corresponding grid point (x_k, y_k) . Each coordinate in the analysis map was postmultiplied by the transform matrix to determine a coordinate (a_k, b_k) in the base map. If the computed coordinate fell outside of the domain defined by the base map, the coordinate and the associated HCMM data value were discarded. However, if the coordinates fell within the domain of the base map, the HCMM data value was stored in an array $F_{i,j}$. The array $F_{i,j}$ corresponded to the base map, and the i,j locations were determined by knowing the length scale and defining the i and/or j grid spacing of the base map. The array then becomes

$$F_{i,j} = F_{i,j} + V_k \quad (18)$$

where initially

$$F_{i,j} = 0 \quad (19)$$

The procedure stored all HCMM data values, having transformed coordinates which fell within a certain ρ -neighborhood of a grid point within the $F_{i,j}$ array, at the grid point. Therefore, some grid points had more

than one HCMM data value. An array, $C_{i,j}$, was determined which accounted for the number of HCMM data values stored in each i,j location. Upon completion of the mapping, the average HCMM data value was determined in the array:

$$\bar{F}_{i,j} = F_{i,j}/C_{i,j} \quad , \quad C_{i,j} \neq 0 \quad . \quad (20)$$

After the average values were computed, a gravitationally weighted interpolation model was used to compute a data value at each i,j location where $C_{i,j} = 0$ (i.e., at each i,j location in the array $F_{i,j}$ where HCMM data values were not mapped from the analysis map because coordinates near or corresponding to the specific i,j location did not exist).

Errors in location of the satellite data occurred because it was not possible to locate precisely geographical features in the analysis map. Generally, a number of estimates were attempted until one was found that yielded the best geographic positioning. Even so, positioning errors as large as 3 km are noted in some of the analyses.

2.3 The Surface Observations

For this study, surface observations were utilized from 15 stations in and around the City of St. Louis. The principal meteorological observations available were the wind speed and air temperature at the 10-m level. Figure 1 provides the geographical location of the stations relative to St. Louis, and Table 4 identifies the station type. The meteorological data were used to develop an analysis of wind and temperature across the city using a gravitationally weighted interpolation scheme. The analyses were used to develop wind and temperature values for a grid with a 1-km resolution. Based on the distribution of stations in Figure 1, the results of the interpolation have credibility in the urban St. Louis and the immediately surrounding area. Because of the absence of stations, the results have no credibility in the northwest, southwest, and southeast portions of the analysis area. These interpolated data, together with the ground temperature and reflectance values from the HCMM satellite, were used to determine the surface heat flux, moisture flux, and exchange coefficients across the urban region.

Table 4. Identification of Stations That Provided Data for the Wind and Temperature Analyses.

STATION NUMBER	STATION TYPE
1	St. Louis City Air Pollution
2	St. Louis City Air Pollution
3	St. Louis City Air Pollution
4	St. Louis City Air Pollution
5	St. Louis City Air Pollution
6	St. Louis County Air Pollution
7	St. Louis County Air Pollution
8	St. Louis County Air Pollution
9	St. Louis County Air Pollution
10	St. Louis County Air Pollution
11	St. Louis University
12	National Weather Service Station at Lambert Field
13	E. St. Louis Air Pollution
14	Edwardsville Air Pollution
15*	Alton-Woodriver Air Pollution

*Station #15 is not shown in Figure 1 because it is off the map area.

2.4 Boundary Layer Parameters

2.4.1 Surface Heat Flux

The surface heat flux, H , was determined using the following equation:

$$H/c_p \rho = -kU_*T_* \quad , \quad (21)$$

where c_p is the specific heat at constant pressure, ρ is the air density, U_* is the friction velocity, k is the Von Kármán constant, and T_* is the scale temperature. The expression for the scale temperature was derived using the following set of boundary layer profile equations:

$$U(z) = \frac{U_*}{k} \left[\ln \left(\frac{z + z_0}{z_0} \right) + \phi_m(z) \right] \quad , \quad (22)$$
$$T(z) = T_g + \frac{T_*}{k} \left[\ln \left(\frac{z + z_0}{z_0} \right) + \phi_H(z) \right] \quad ;$$

where $U(z)$ is the wind speed at any level z , z_0 is the surface roughness, $\phi_m(z)$ and $\phi_H(z)$ are the stability parameters for momentum and heat, respectively, $T(z)$ is the temperature at any level z , and T_g is the temperature at the ground. Letting $z = 10$ m and rearranging terms in Equation (22) yields the following expression for T_* :

$$T_* = \frac{(T_a - T_g)}{\frac{\phi_H - \phi_m}{k} + \frac{U_a}{U_*}} \quad ,$$

where U_a and T_a are the wind and temperature at the 10-m level. It has been generally accepted that $\phi_H = \phi_m^2$. Assuming that $\phi_m \approx \bar{Ri}$, where \bar{Ri} is the mean value of the Richardson number in layer, then if $|\bar{Ri}| < 1.0$ and $u_a > 1.0$, $|U_a/U_*| > |\phi_H - \phi_m/k|$ since U_* is generally less than one. In the case studies to be presented, $|\bar{Ri}| < 1.0$ and $u_a > 1.0$ (see Table 7 for estimates of the characteristic value for \bar{Ri}). Therefore, for the case studies, the following expression was used to approximate T_* :

$$\tau_x = \frac{(T_a - T_g)U_x}{U_a} \quad (23)$$

Techniques such as this have been used previously with reasonable success (e.g., Estoque and Bhumraikar, 1969). The RMS error as a result of using Equation (23) is ± 10 percent for the case studies.

The expression for U_x was determined from the results of research performed by the U.S. Environmental Protection Agency[†] (EPA). Based on EPA's analysis of the station data from the Regional Air Pollution Study, an expression for U_x for St. Louis was derived. The correlation coefficient was approximately 0.8 and the RMS was about ± 9 percent, regardless of the stability. That expression is

$$U_x = a + bU_a + cU_a^2, \quad (24)$$

where a, b, and c are parameters derived from observed results. Table 5 yields the numerical values for the model parameters for the summer and winter seasons. Values for the spring and fall seasons were not available. In the spring and fall, the parameters for the summer and winter were used depending on whether the time period was closer to the winter or the summer season.

The surface heat flux was determined using the ground temperatures from the HCMM satellite, and the surface wind and temperature data from the 15 stations across St. Louis together with Equations (21), (23), and (24), and the information in Table 5.

2.4.2 Soil Moisture

An estimate of the relative distribution of the soil moisture and of the latent heat flux was determined through a solution of the energy balance equation. The general energy balance equation relates the soil heat flux, H_g , to the long-wave radiation emitted from the ground, R_g , the sensible heat flux, H , the latent heat flux, E , the solar radiation

[†]The model and parameters were established through the efforts of Dr. John Clarke (EPA) using data collected during EPA's RAPS program held in St. Louis. These results have not yet been published.

Table 5. Values of Parameters[†] for the Model for the Friction Velocity

SEASON	a	b	c
Summer	-0.046	0.188	-0.010
Winter	-0.076	0.164	-0.005

[†]The parameters were derived by Dr. John Clarke (EPA) using RAPS data, and have not yet been published.

reaching the ground, S_o , and the long-wave radiation from the atmosphere, R_a ; i.e.,

$$H_g = R_g + H + E - S_o - R_a \quad . \quad (25)$$

Arakawa (1972) has shown that to a good approximation, the local rate of change of ground temperature is proportional to the soil heat flux; i.e.,

$$\frac{\partial T_g}{\partial t} = -\alpha_g H_g \quad , \quad (26)$$

$$\alpha_g = \pi^{1/2} \rho_g^{-1} c_g^{-1} d_1^{-1} \quad , \quad (27)$$

where c_g is the specific heat of the soil, ρ_g is the density of the soil, and d_1 is the depth of influence and is defined by the following expression,

$$d_1 = (k_g \tau_o)^{1/2} \quad , \quad (28)$$

where k_g is the diffusivity of the soil, and τ_o is the period of one day. The HCMM experiment was designed to collect data around the time of maximum and/or minimum ground temperature. Therefore, the HCMM satellite measured a ground temperature which is, to within a reasonable approximation, in a quasi-steady state ($\partial T_g / \partial t \approx 0$); i.e., according to Equation (26),

$$H_g \approx 0 \quad : \quad \text{at the time HCMM data were collected.} \quad (29)$$

Deardorff's (1978) calculations have shown that T_g is at a maximum between 1200 and 1500 local time. This is consistent with the observations discussed by Geiger (1965). At night, Deardorff's calculations indicate that $\partial T_g / \partial t \approx 0$ between local midnight and 0600 local time. This is also consistent with the observations discussed by Geiger. Therefore, the assumption [Equation (29)] is reasonable. Deardorff (1978) has also shown

that Equation (26) is a reasonable model for the ground temperature, though other models, such as the force-restore model, will yield better approximations.

Application of the assumption in Equation (29) to Equation (25) yields the following expression for the latent heat flux:

$$E = S_o + R_a - H - R_g \quad (30)$$

The equations used to determine the long-wave radiation from the ground, the sensible heat flux, and the long-wave radiation emitted from the atmosphere are given below:

$$R_g = e_g \sigma T_g^4 \quad (31)$$

$$H = -\rho c_p k U_* T_* \quad (32)$$

$$R_a = e_a \sigma T_m^4 \quad (33)$$

where e_g is the emissivity of the ground, σ is the Stephen-Boltzman constant, e_a is the emissivity of the atmosphere, and T_m is a characteristic radiation temperature of the atmosphere. Deardorff (1978) has suggested that to a good approximation, $T_m = T_a$, the 10-m temperature. The emissivity of the atmosphere was computed using the model given by Deardorff:

$$e_a = 0.67(1670 q_a)^{0.08} \quad (34)$$

where q_a is the specific humidity at the 10-m level.

The solar radiation absorbed at the ground, S_o , was computed using the model developed by Davies et al. (1975); i.e.,

$$S_o = R_o \cos Z (1 - A) \psi_{aw} \psi_{ad} (\psi_{sw} \psi_p \psi_{sd} + 1) / 2 \quad (35)$$

where R_0 is the solar constant, Z is the solar zenith angle, A is the albedo, ψ_{aw} is the transmission function associated with the absorption due to water vapor, ψ_{ad} is the transmission function due to aerosol absorption, ψ_{sw} is the transmission function due to scattering by water vapor, ψ_p is the transmission function for molecular scattering and absorption, and ψ_{sd} is the transmission function due to aerosol scattering. The various expressions in Equation (35) were computed using the following equations:

$$\cos Z = \sin \phi \sin \delta + \cos \phi \cos \delta \cos \psi \quad , \quad (36)$$

$$\begin{aligned} \psi_p = & 0.972 - 0.0826 \sec Z + 0.0093 \sec^2 Z \\ & - 0.00095 \sec^3 Z + 0.000044 \sec^4 Z \quad , \end{aligned} \quad (37)$$

$$\psi_{aw} = 1 - 0.077 \left[m \sec Z \right]^{0.3} \quad , \quad (\text{McDonald, 1960}) \quad (38)$$

$$\psi_{sw} = 1 - 0.0225 m \sec Z \quad , \quad (\text{Houghton, 1954}) \quad (39)$$

$$\psi_D = \psi_{ad} \psi_{sd} = k_a^{\sec Z} \quad , \quad \text{and} \quad (40)$$

(Houghton, 1954)

$$\psi_{ad} = \psi_{sd} \quad ,$$

where ϕ is the latitude, δ is the solar declination, ψ is the solar hour angle, and k_a is the aerosol transmission factor which varies from 0.88 to 0.98 (Houghton, 1954). The albedo was estimated using the reflectivity measurements from the HCMM satellite. The optical path for water vapor, m , was determined through Equation (41):

$$m = \frac{1}{g} \int_0^{p_0} q dp \quad ; \quad (41)$$

where g is the acceleration due to gravity, p_0 is the surface pressure, q is the specific humidity, and p is the pressure.

In order to determine the relative distribution of the soil moisture, the latent heat flux was written in a finite difference form; i.e.,

$$E \approx - \rho L K_m \frac{\Delta q}{z_a}, \quad (42)$$

where L is the latent heat of evaporation; K_m is the eddy diffusion coefficient; z_a is, in this case, the 10-m level; and Δq , the specific humidity depression, is the difference between the specific humidity of the air at the 10-m level, q_a , and the specific humidity at the ground, q_g ; i.e.,

$$\Delta q = q_a - q_g \quad (43)$$

If the latent heat flux is determined using Equations (30)-(41), then the soil moisture depression, Δq , can be determined using the following formula:

$$\Delta q = - \frac{E z_a}{\rho L K_m} \quad (44)$$

The method by which the eddy exchange coefficient is evaluated will be given in the next section.

2.4.3 Eddy Exchange Coefficient

The expression for the vertical distribution of wind in the boundary layer given in Equation (22) was derived from a first-order differential equation; i.e.,

$$\frac{dU}{dz} = \frac{U_*}{k} \left(\frac{1}{z + z_0} \right) + \frac{d\phi}{dz} \quad (45)$$

Following the procedure of Monin and Obukhov (1954), the second term on the right-hand side of Equation (45) was given by the following expression:

$$\frac{d\phi}{dz} = \frac{\alpha}{L_*} , \quad (46)$$

where α is a constant and L is the so-called Monin stability length. The value of L was derived through the following expression:

$$L = \frac{1}{g} \left(\frac{U_*}{k} \right)^2 \frac{T_a}{T_*} , \quad (47)$$

where g is the acceleration due to gravity. Since the roughness length is generally small, Equation (45) was estimated with small error in the following manner:

$$\frac{dU}{dz} \approx \frac{U_*}{k} \left(\frac{1}{z} + \frac{\alpha}{L_*} \right) . \quad (48)$$

An expression for the eddy viscosity, K_m , is:

$$K_m = \frac{U_*^2}{\frac{dU}{dz}} . \quad (49)$$

Substitution of Equation (48) into Equation (49) yields the expression utilized to compute the eddy viscosity:

$$K_m \approx k U_* \left[\frac{1}{z} + \frac{\alpha}{L_*} \right]^{-1} . \quad (50)$$

The basic input parameters for the computation of the eddy viscosity are the same as previously mentioned: the surface air temperature and wind speed and the ground temperature.

3.0 St. Louis Urban Boundary Layer Characteristics

3.1 Model Parameters and General Meteorology

The results of the analysis of the ground temperatures and the reflectivity in the St. Louis area using the HCMM infrared and visible data are given in Appendixes A to C. The results of the computations of the heat fluxes, the specific humidity depression, and the eddy viscosity using the surface wind and temperature observation and the ground temperature and reflectivity distribution from the HCMM data, and the models given in Section 2.0 are given in Appendixes D to I. The basic parameters used in the models developed in Section 2.0 to compute the various boundary layer terms are given in Table 6. The atmospheric emissivities, e_a , do not account for the effect of pollution over the city. Upper-air pollution can produce a higher downward flux of radiation over the city (Ackerman, 1977 and Aida and Yaji, 1979). The data in Table 7, which gives the meteorological observations at the National Weather Service Station at Lambert Field for each case study, indicate that the visibility for each of the case studies is relatively high and the winds are strong which suggests that the influence of a pollution layer over the city may not have been great in these cases.

Clear skies and relatively large visibility (Table 7) characterize all the case studies. There was no precipitation between 9 and 14 June 1978; but between 14 and 26 June 1978, approximately 2 inches of rain fell with a little over an inch occurring between 22 and 24 June 1978, and there was no precipitation after 24 June. The precipitation between 22 and 24 June is associated with the passage of a warm front through the region; the temperatures rose 9°C over a period of two days.

Prior to 26 February 1979, the local climatological data indicated that there was precipitation in the form of rain on 22 and 23 February associated with a cold frontal passage. There was no precipitation the entire month of September 1979 in the St. Louis area. Conditions were rather dry as indicated by the relatively low dewpoint temperature on 27 September (Table 7).

In the following sections of this report, the results in Appendixes A through I will be discussed in detail. Only those analyses that make specific points are presented in the text. The reader is referred to the appendixes for detailed inspection of all analyses.

Table 6. Model Parameters

PARAMETER NAME	PARAMETER SYMBOL	PARAMETER VALUE
Von Kármán Constant	k	0.4
Gravity	g	9.8 m s ⁻¹
Surface pressure	p _o	100 cb
Boltzman Constant	σ	5.73 x 10 ⁻¹¹ kj m ⁻² A ⁻¹ s ⁻¹
Latent heat of evaporation	L	2.5 x 10 ⁶ kj t ⁻¹
System Constant	α	3.0
Solar Constant	R _o	1.36 kj m ⁻² s ⁻¹
Height of <u>in situ</u> measurement	z _a	10 m

Table 7. The General Meteorological Conditions at the Time of Each Case Study Derived From the Observations From the National Weather Service Station at Lambert Field, St. Louis, MO., and an Estimate of the Characteristic Richardson Number in the First 10 Meters.

	AIR TEMPERATURE (°C)	DEWPOINT TEMPERATURE (°C)	WIND SPEED AND DIRECTION (m s ⁻¹)	CLOUD COVER (tenths)	VISIBILITY (mi.)	ESTIMATE OF THE CHARACTERISTIC RICHARDSON NUMBER
9 June 1978	11.6	9.4	2.0/WSW	0	7	0.15
10 June 1978	28.3	15.6	4.5/SSW	0	10	-0.56
14 June 1978	13.3	7.8	4.0/ESE	0	10	0.08
26 June 1978	35.0	21.7	6.0/SW	0	10	-0.12
26 February 1979	2.2	-8.9	5.0/NW	0	10	-0.60
27 September 1979	27.8	8.3	3.5/S	0	7	-0.50

3.2 The HCMM Ground Temperature Analysis

Figure 2 shows the analysis of the HCMM ground temperature distribution for 26 June 1978. This analysis shows the general characteristics of the ground temperature distribution found in all daytime warm season analyses. The ground temperature distribution is markedly influenced by the land use pattern. The heat island of the cities of St. Louis, East St. Louis, Belleville, Centreville, and Granite City (Figure 1) characterizes the analysis with the highest temperatures. The lowest temperatures are associated with the Missouri and Mississippi Rivers and Horseshoe Lake. Low temperatures also characterize Forest Park. Similarly, in some of the other analyses, low temperatures were found to be associated with Bellefontaine Cemetery to the north of the center of the city and Tower Grove Park to the south (not shown in Figure 1). Both the HCMM infrared temperatures and reflectance data were smoothed in order to produce a more coherent analysis. The smoothing in some cases removed some of the small-scale features in the analysis. The smoothing technique is a low-pass filter.

There is also a region of low temperatures immediately west of Forest Park in the suburban regions of Ladue and Creve Coeur and to the southwest at the Tyson Valley Reservation. The cold temperatures around Tyson Valley Reservation may be the influence of the Meramec River, a very small river compared to the Missouri and Mississippi Rivers, which flows in that region. Creve Coeur and Ladue--like Forest Park, Tower Park, the Bellefontaine Cemetery, and the Tyson Valley Reservation--are characterized by grasslands and trees. It is suggested that the relatively low temperatures in those regions are due to the utilization of solar energy for evaporation and evapotranspiration rather than heating the ground.

There is a zone of relatively warm temperatures to the northwest characterized by three centers having temperatures around 37°C and one to the southwest having temperatures around 36°C. The zones to the northwest are in the suburban regions around Florissant and Hazelwood and to the southwest in the suburban regions around Affton. These regions are heavily populated, being characterized by a large number of housing projects and large shopping centers. Another relatively warm zone is noted

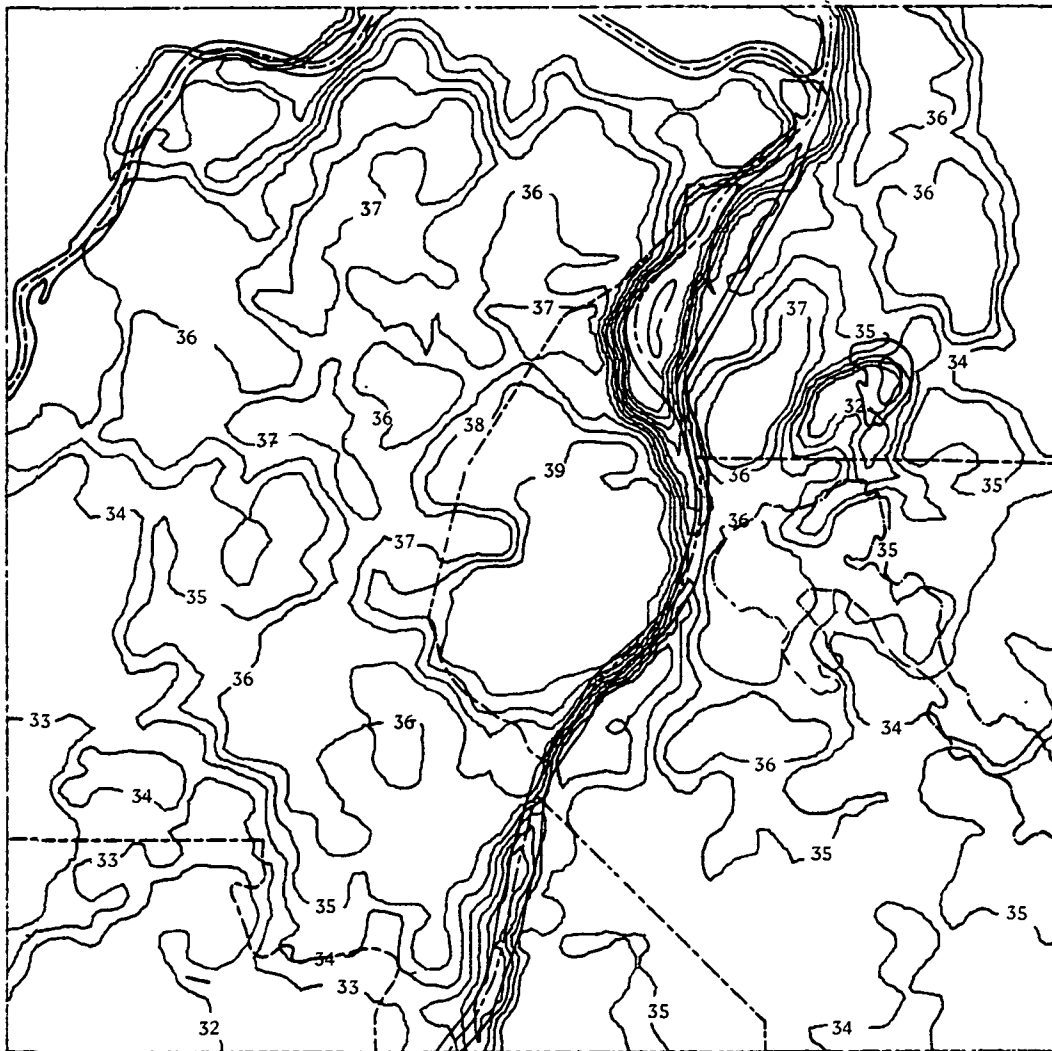


Figure 2. HCCM daytime ground temperature ($^{\circ}\text{C}$) distribution for 26 June 1978 in the region about St. Louis, MO.

northeast of the warm zone that characterizes Granite City. The approximate position of this warm zone is between Granite City and Edwardsville. This warm zone persisted in each of the warm season daytime cases. For the 10 June 1978 case, it was more intense than the warm zone associated with Granite City.

The maximum HCMM ground temperature in St. Louis on 26 June was between 39° and 40°C. White et al. (1978) measured values of the ground temperature of around 45°C in August 1976 as a part of a net radiation balance study in St. Louis. Many factors may account for the differences between these observations and those of White et al., including the fact that there was precipitation on 23 and 24 June prior to the observations on 26 June and the fact that the observations of White et al. were made in mid-August in the heart of the summer.

In contrast to the large variations in ground temperature that characterize the daytime temperature pattern around St. Louis and that are obviously influenced by the land use pattern, the nighttime ground temperature distribution shows considerably less variation and does not demonstrate the strong relationship with the small-scale land use pattern as did the daytime distribution. This is exemplified by the nighttime ground temperature analysis from HCMM for 14 June 1978 (Figure 3). The heat island associated with St. Louis, East St. Louis, and Belleville are indicated; but those associated with Centreville and Granite City are not as well represented. The rivers and lakes remain well represented, but the influence of regions such as Forest Park, Ladue and Creve Coeur, Tower Grove Park, and the Tyson Valley Reservation do not appear. However, there does appear to be an influence due to the Bellefontaine Cemetery to the north of the center of the city. Furthermore, the heavily populated suburban area around Florissant and Hazelwood to the northwest and Affton to the southwest do not appear to affect the ground temperature pattern. There is only a weak indication of the warm zone immediately northeast of Granite City.

Probably the most interesting aspect of the difference between the night and day ground temperature patterns is the fact that the horizontal gradients of temperature are considerably larger during the day. This is especially true when comparing the ground temperatures in the city of St.

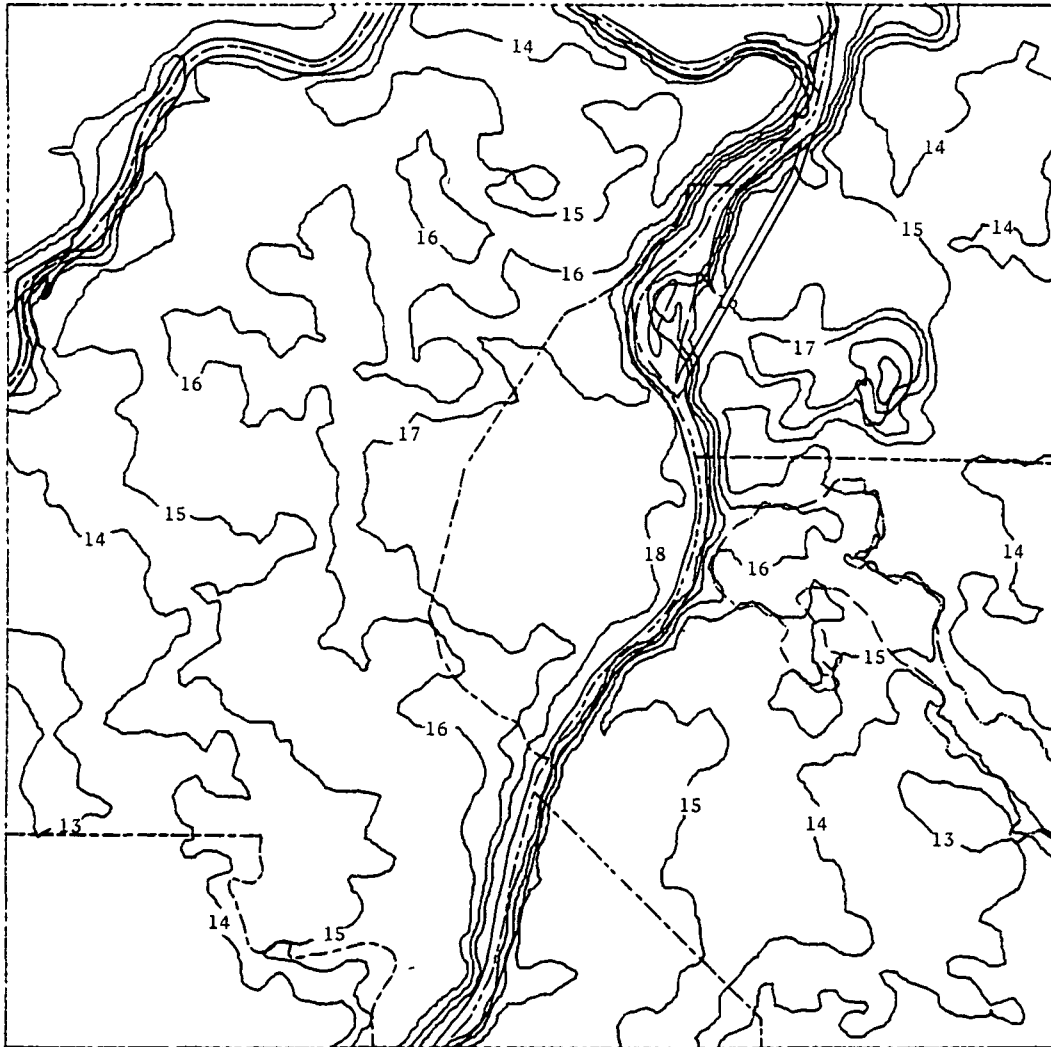


Figure 3. HCMM nighttime ground temperature ($^{\circ}\text{C}$) distribution for 14 June 1978 in the region about St. Louis, MO.

Louis with the surrounding rural regions to the northwest and southwest. This result is in contrast to the results of many other researchers pertaining to the contrast in air temperature in the daytime and nighttime heat island. The general result is that the air temperature difference between the urban and rural regions is greatest at night and smallest during the day (Steigerwald, 1981; Chandler, 1965; Hutcheon et al., 1967; Mitchell, 1961; Oke and East, 1971; Hage, 1972; and Vukovich, 1973). Table 8 yields the temperature differences between the urban regions (represented by the temperature at stations 1 and 11) and the rural region (represented by the temperature at Stations #6, #8, #10, and #12). The data presented are the average differences in air temperature between the urban and rural stations, and the average differences in ground temperatures which were determined at the locations of the various stations used in the computations. In all cases during the day, the mean difference in ground temperature between the urban and rural regions was greater than the mean difference in air temperature. That difference was as much as 3 to 5 times greater in some cases. A strong contrast in daytime ground temperatures would suggest a strong contrast in the heat flux pattern which should result in an air temperature contrast similar to that found in the ground temperature pattern. The fact that the air temperature contrasts are reduced relative to the ground temperature contrasts would indicate that some other process, most probably mixing, has markedly influenced the air temperature pattern.

At night, the air temperature contrasts are slightly greater than the ground temperature contrasts. This would indicate that the heat flux is not totally responsible for the air temperature contrasts. Other factors such as radiation processes must influence the air temperature pattern.

The data in Table 8 would suggest that the heat island intensity as defined by the urban-rural ground temperature difference, has a diurnal variation which appears to be 180 degrees out of phase with the heat island intensity as defined by the urban-rural air temperature difference. These are very preliminary results based on four discrete daytime observations and two discrete nighttime observations. Significantly more observations are necessary before the results are conclusive.

Table 8. Horizontal Gradient of Air and Ground Temperature Between the Urban Region, Represented by Stations #1 and #11, and the Outlying Suburban and Rural Region, Represented by Stations #6, #8, #10, and #12. Positive Values Indicate a Larger Urban Temperature.

DATE	AVERAGE AIR TEMPERATURE GRADIENT (°C)	AVERAGE GROUND TEMPERATURE GRADIENT (°C)
<u>Daytime Cases</u>		
10 June 1978	2.0	6.5
26 June 1978	3.0	3.8
26 February 1979	0.5	2.4
27 September 1979	4.2	4.4
<u>Nighttime Cases</u>		
9 June 1978	3.5	2.3
14 June 1978	3.1	2.7

The ground temperature pattern during the day and in the cold season, represented by the analysis of the HCMM data for 26 February 1979, shows many of the characteristics of the ground temperature patterns for the daytime during the warm season (compare Figure 2 with Figure 4). The heat island which characterizes the cities of St. Louis, East St. Louis, Belleville, Centreville, and Granite City, are easily distinguishable in the analysis for 26 February. The rivers and lakes are well represented. The cold temperatures to the southwest are a result of the Meramec River which flows almost parallel to the county line found in that region. The influence of Forest Park is noted on the 12° isotherm. The cold zone immediately west of Forest Park is the influence of the Creve Coeur and Ladue regions. It is interesting to note that the region immediately northeast of Granite City, which was an intense warm zone in the daytime warm season cases, is a cold zone in this daytime cold season case. The warming associated with the heavily populated suburbs to the northwest and southwest are also noted. However, the ground temperature contrast between warm and cold regions is reduced in the cold season analysis as compared to the warm season analysis. This is exemplified by comparing the ground temperature difference for the 26 February 1979 case with the other daytime case studies in Table 8. The air temperature difference for that case is also smaller than the other daytime cases. This factor was also noted by Lawrence (1971) and Mitchell (1961). A factor that may influence the reduced contrast in ground temperatures in the cold season is the lack of vegetation.

Though the influence of many of the land use features are indicated in the 26 February case study, the ground temperature pattern in many ways is similar to the nighttime distribution of the ground temperatures in the warm season. In particular, the ground temperature contrasts in the 26 February case study are small like the nighttime ground temperature contrasts in the 14 June case study. As indicated, this is most probably due to the absence of vegetation during the winter which smoothed out the radiation balance and the energy balance over the area.

3.3 Urban Reflectivity Measurements

Figure 5 shows the analysis of the 26 June reflectivity measurements. These data are typical of the warm season distribution of the reflectivity

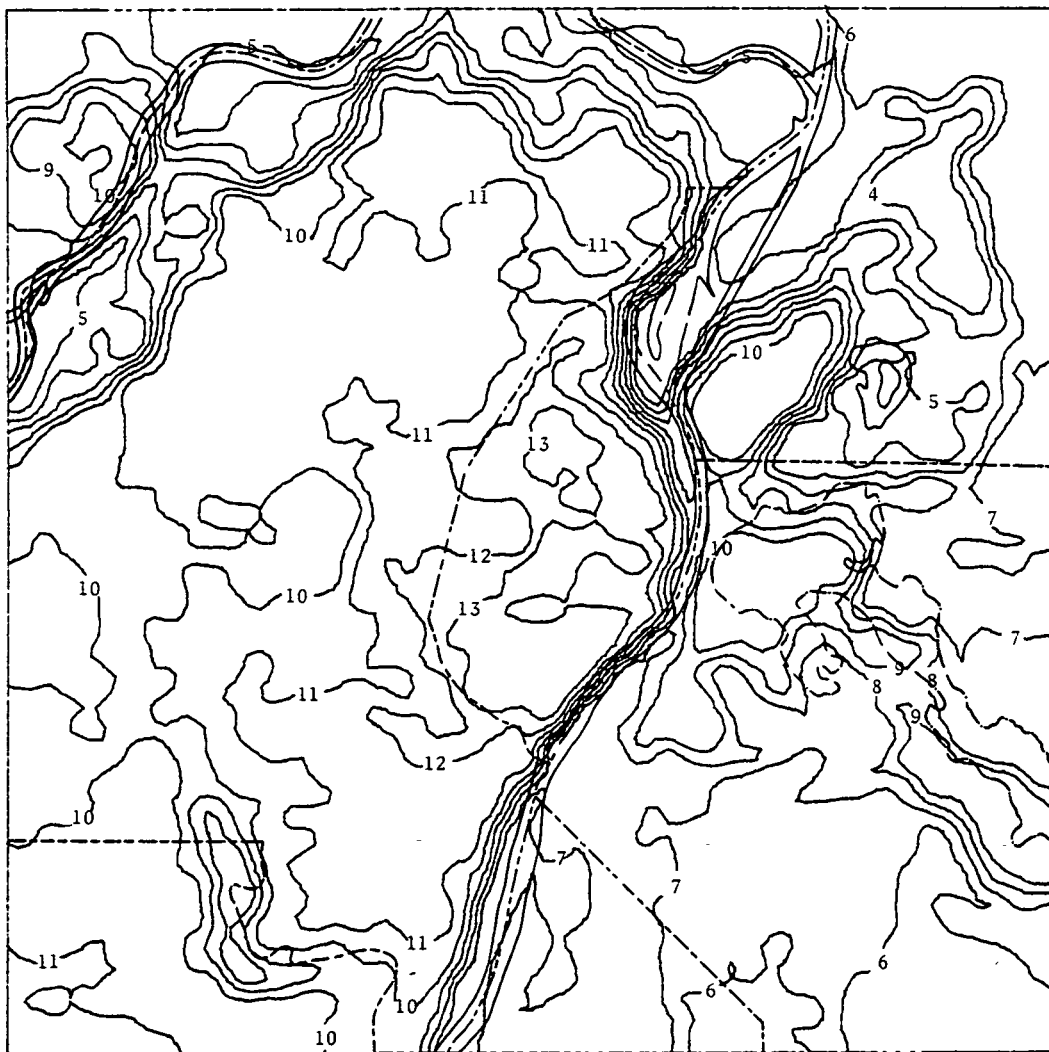


Figure 4. HCMM daytime ground temperature ($^{\circ}\text{C}$) distribution for 26 February 1979 in the region about St. Louis, MO.

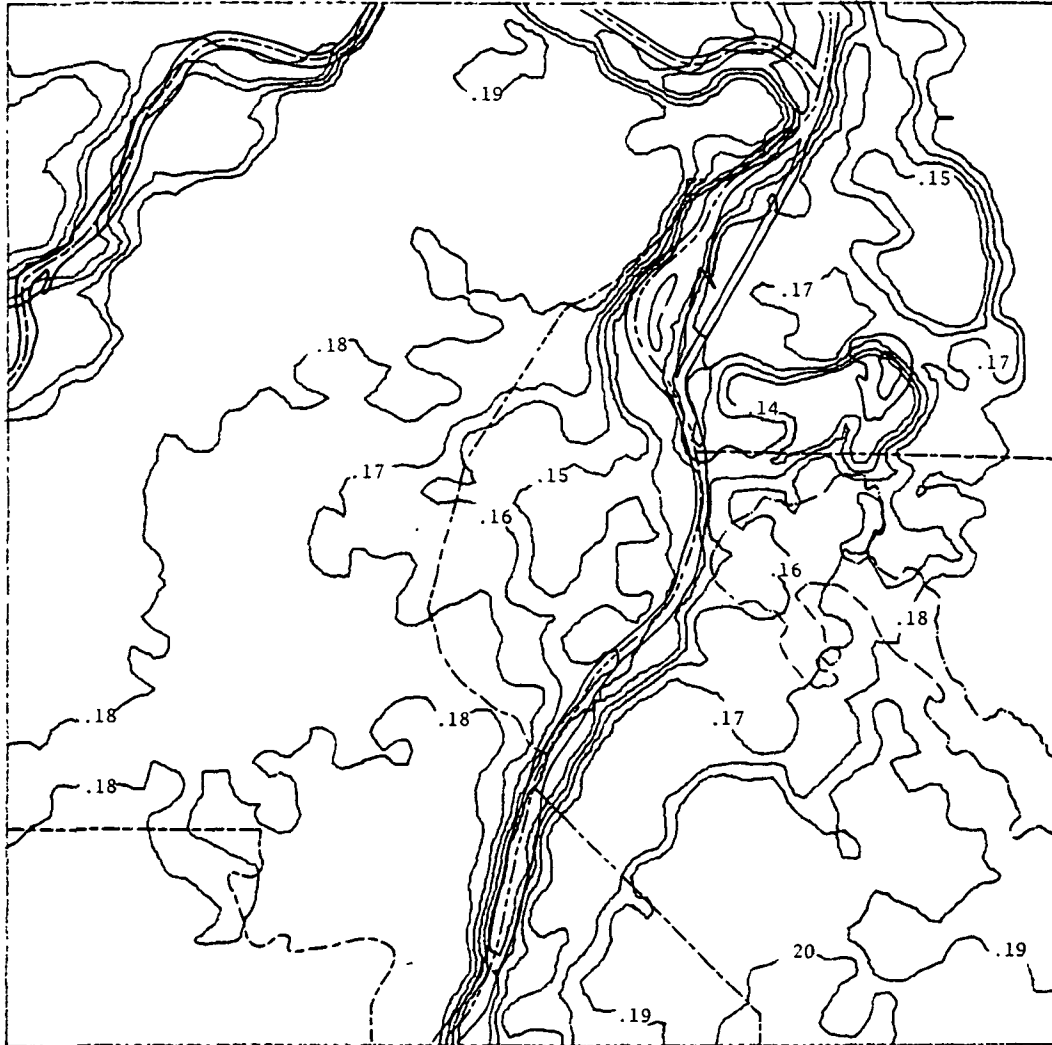


Figure 5. HCMM reflectivity distribution for 26 June 1978 for the St. Louis area.

across the city and surrounding regions. The rivers and lakes are well defined as regions of low reflectivity. The East St. Louis-Belleville complex is indicated in the analysis as a region of low reflectivity. The influence of Granite City is not apparent, but the region immediately northeast of Granite City where a warm zone was detected, is a region of low reflectivity.

The center of the City of St. Louis is a region of low reflectivity. In all the warm season case studies, the values in the center of the city ranged from 10 to 15 percent. The suburban and rural regions are characterized by relatively higher reflectivity with values ranging from 12 to 20 percent. The differences in reflectivity between the urban center and the surrounding suburban and rural regions ranged from 2 to 4 percentage points. The effect of small-scale features such as Bellefontaine Cemetery to the north and Tower Grove Park to the south of the center of the city was not evident. This may be a result of the smoothing performed for the analysis. However, the same smoothing was performed for the infrared temperatures, and in those cases, the effect of Forest Park was still evident in some cases. There was also no evidence of the influence of Forest Park in any of the reflectivity analyses.

White et al. (1978) made a number of measurements of the urban albedo in and around the city of St. Louis during the summer of 1976. Their solar noontime albedo values varied from 15 to 17 percent for rural land use and from 12 to 13 percent for most urban land uses. The differences between the urban and rural albedos range from 2 to 5 percentage points. Earlier, Dabberdt and Davis (1974) made measurements of the urban albedo in the summer of 1973. Their solar noon measurements of the albedo ranged from 12 percent in the urban region to 16.5 percent in the rural region, for a difference of 4.5 percentage points between the urban and rural regions. The measurements of the albedo made by White et al. and Dabberdt and Davis would be slightly higher at 1330 local time which is the time the HCMM satellite made its measurements of reflectivity. However, there would still be a difference between the HCMM measurements and those of White et al. and Dabberdt and Davis since HCMM measurements treat a narrow band reflectivity, and those of White et al. and Dabberdt and Davis treated the entire solar spectrum. Even so, the range of differences between the urban

and rural regions in the HCMM data appear to agree quite well with the measurements made by White et al. and Dabberdt and Davis.

The HCMM data suggest that the albedo may have a broader range in the urban and rural region than observed by White et al. However, low values of 10 percent in the urban region and 12 percent in the rural region were observed in the 27 September 1979 case. Though the seasonal period may be early fall, this case study could still be considered a warm season case study. The surface air temperature was comparable to the surface air temperature for the other two daytime warm season case studies, but the air mass was significantly drier as indicated by the lower value of the dewpoint temperature at the airport (Table 7). The visibility was slightly less for the September case study than the other two daytime warm season case studies which might indicate the presence of more aerosols over the region. However, McCormick and Ludwig (1967) have indicated that the presence of aerosols should increase the albedo. It is suggested that the decrease in water vapor content in the air mass was principally responsible for the lower albedo measurement in September. Differences in water vapor content, more than any other factor, may explain the differences in the albedo magnitudes between the HCMM measurements and the measurements made by White et al. and Dabberdt and Davis. White et al. and Dabberdt and Davis used a low-flying aircraft to make their measurements, and so their measurements were not influenced by as extensive a column of the atmosphere as were the measurements made by the HCMM satellite. Scattering by atmospheric constituents such as water vapor significantly influence the HCMM visible measurements.

The 26 February 1979 case study (Figure 6) is representative of the reflectivity distribution in the cold season. The rivers and lakes are indicated by low values of reflectivity, but are not as well represented as in the warm season case studies. The region immediately northeast of the Granite City urban complex is well-defined as a region of low reflectivity even though this region was a cold zone. There are indications of the East St. Louis-Bellefontaine complex; but, once again, Granite City is not apparent. The center of St. Louis is characterized by reflectivity values of around 9 percent, whereas the rural regions have values on the order of 11 percent. The difference between the urban and rural reflectivity

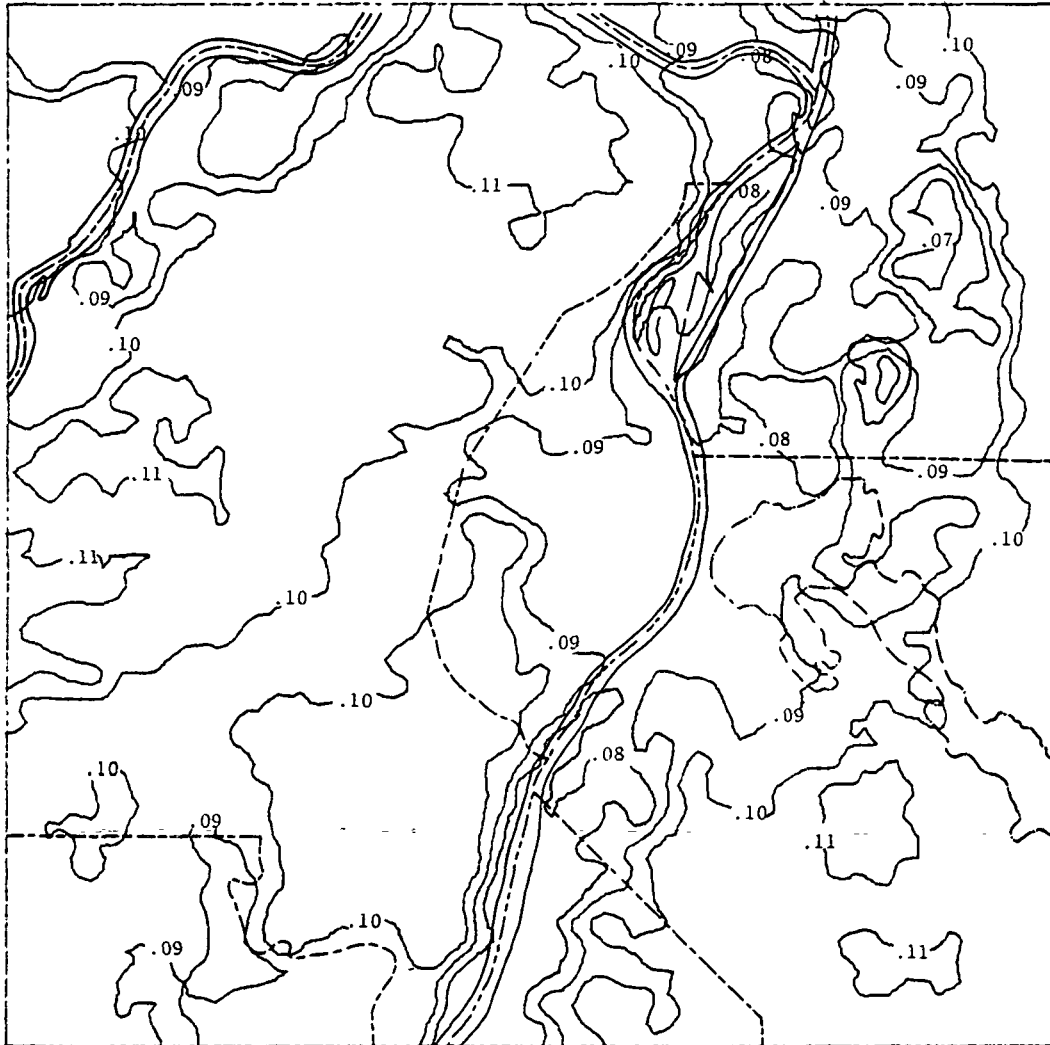


Figure 6. HCMM reflectivity distribution for 26 February 1979 for the St. Louis area.

regions is 2 percentage points. As in the warm season case studies, the effect of some of the small-scale features in and around St. Louis are not evident. The differences in the values are in part due to the reduced water vapor concentration in the atmosphere. However, part of the differences must be attributed to the lack of vegetation in the winter.

Peterson and Stoffel (1980) have estimated that the effect of atmospheric pollutants over the center of metropolitan St. Louis was to reduce the incident solar radiation by about 3 percentage points. The greatest reduction apparently took place in the winter period and the smallest in the summer. However, the HCMM measurements would suggest that there is about 2 to 4 percent greater absorption of solar radiation in the urban area than in the rural region. The combination of these two results would suggest that the amount of solar energy absorbed at the surface in the urban region was about equivalent to that in the rural region, indicating that other factors such as relative differences in soil moisture and in specific heats must be responsible for the production of the urban heat island (Nappo, 1972).

3.4 The Surface Heat Flux Distribution

The surface heat flux distribution on 26 June (Figure 7) represents the daytime heat flux in the warm season. The negative values characterize the rivers and lakes. The negative values in the southwest, southeast, and northwest have little credibility because they occur in regions where there is an absence of sampling stations. The negative values to the northeast may be a result of missing in situ data at Station #14. Only the negative values associated with the rivers and lakes have any credibility. Positive values of the heat flux characterize St. Louis and range from 0 to $0.1 \text{ kJ m}^{-2} \text{ s}^{-1}$. The largest positive values are centered about St. Louis. Large positive heat fluxes also characterize the Granite City-Edwardsville complex, but the magnitude is somewhat smaller than that characterizing St. Louis.

An example of the heat flux distribution in the daytime cold season is given in Figure 8, which is the analysis for 26 February. Positive heat fluxes characterize the entire region and range from approximately 0.05 to $0.25 \text{ kJ m}^{-2} \text{ s}^{-1}$. The largest values are found over the St. Louis urban complex. The smallest values are associated with the rivers and lakes.

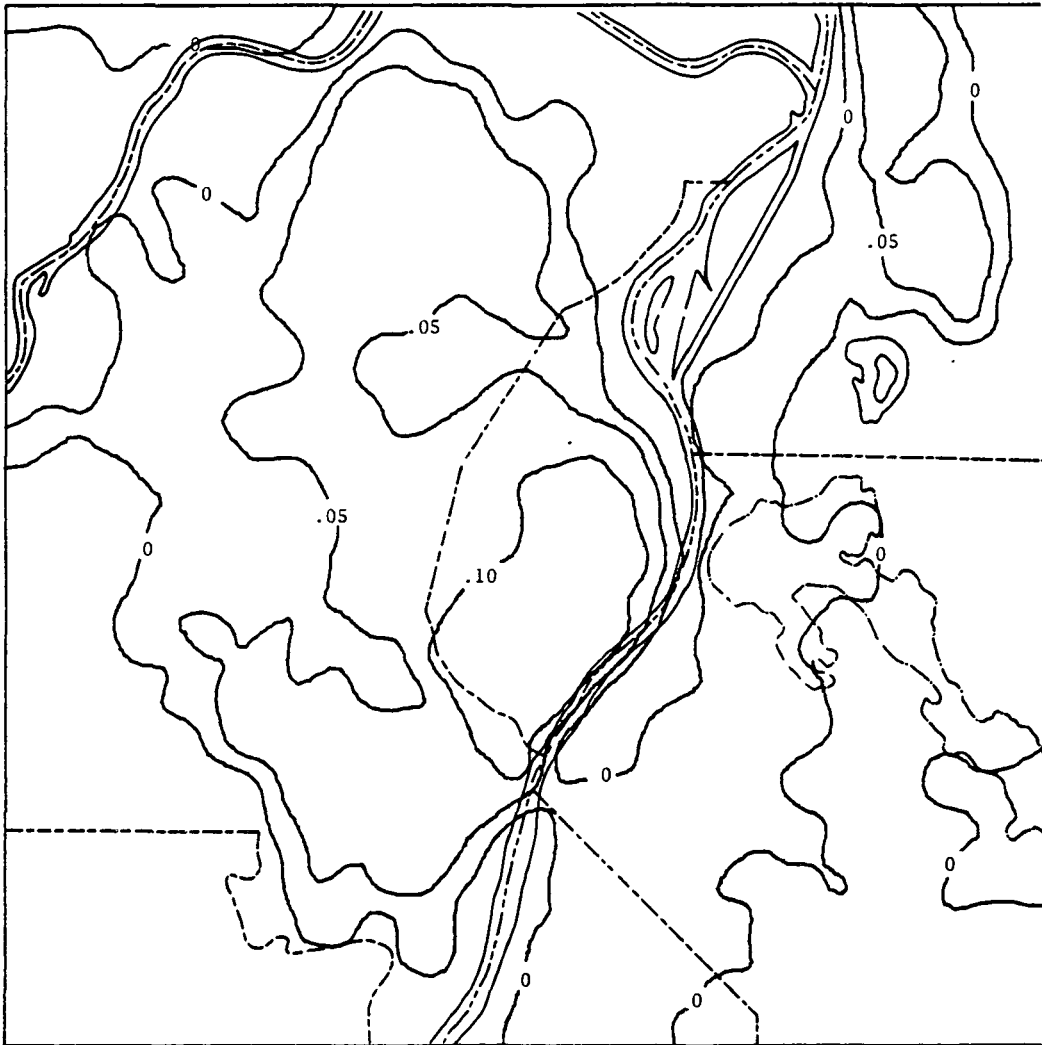


Figure 7. Surface heat flux ($\text{kJ m}^{-2} \text{s}^{-1}$) distribution for 26 June 1978.

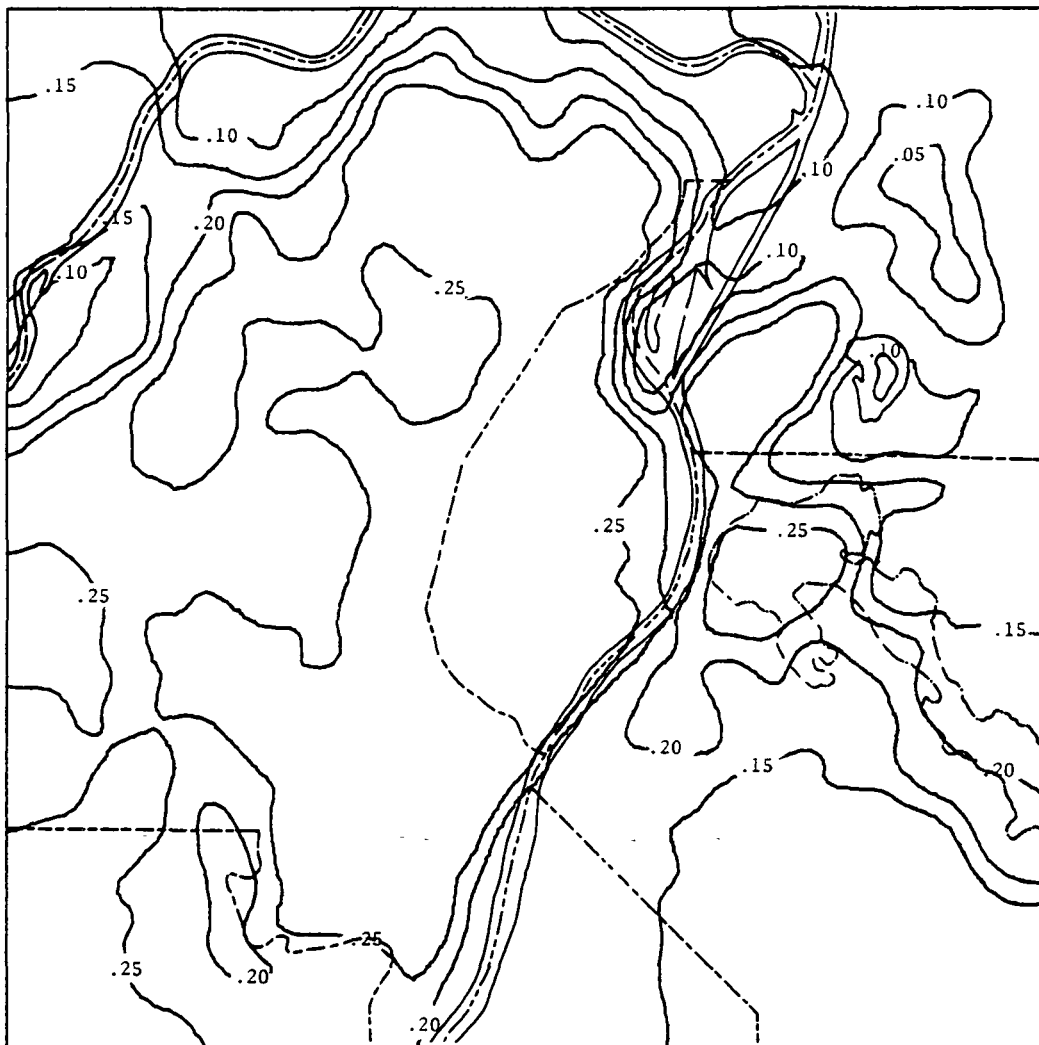


Figure 8. Surface heat flux ($\text{kJ m}^{-2} \text{s}^{-1}$) distribution for 26 February 1979.

Relatively large values of the heat flux are also associated with Granite City and the East St. Louis-Belleville complex. It is interesting to note that the heat flux in this case is 2 to 3 times larger than that for the 26 June case (Figure 7), a summertime case study. Since the wind speeds are roughly the same for the two case studies (Table 7), differences in the heat flux must be associated with differences in the air-ground temperature difference ($\Delta T = T_a - T_g$). Table 9 gives the characteristic ΔT for the urban and rural regions for the four daytime case studies.

In all cases, the ΔT 's are negative in both the urban and rural regions. In each case, the magnitude of the ΔT is greater in the urban region, and ranges, in the warm season, from -3.0°C (on 26 June) to -11.8°C (on 10 June). In the rural regions, the warm season values range from -2.0°C (on 26 June) to -7.1°C (on 10 June). The ΔT in either the urban or rural region for 26 February is roughly 3 times greater than that on 26 June, accounting for the increased heat flux on 26 February over the region.

The relatively small value for the ΔT 's on 26 June was, in part, due to the effect of warm air advection that was initiated on 24 June 1978 in the Central United States, producing temperatures in excess of 30°C in the St. Louis area. Chow *et al.* (1972) has shown that, on the synoptic scale, regions of warm air advection are characterized, on the average, by cooling at the surface (negative heat flux) and regions of cold air advection, by heating at the surface (positive heat flux). In certain time scales and at certain times of the day, however, positive heat fluxes can be found in regions of warm air advection and negative heat fluxes in regions of cold air advection. In the warm air advection, positive heat fluxes should be found at the time of maximum ground temperature, but the magnitude of the heat flux would not be as great as that for cold air advection at that time of day because the ΔT in the warm air advection case would be smaller, all other factors being generally the same. Since warm air advection characterized the 26 June case (winds from the southwest) and cold air advection characterized the 26 February case (winds from the northwest), it is not unexpected that larger positive heat fluxes are found in the winter case, particularly since the ground was free of snow cover as well as foliage in the winter case.

Table 9. Characteristic Values of $\Delta T (= T_a - T_g)$ in the Urban and Rural Regions for the Four Daytime Case Studies

DATE	URBAN ΔT ($^{\circ}\text{C}$)	SUBURBAN- RURAL ΔT ($^{\circ}\text{C}$)
10 June 1978	-11.8	-7.1
26 June 1978	-3.0	-2.0
26 February 1979	-10.4	-8.8
27 September 1979	-6.6	-4.9

The analysis for 14 June is given in Figure 9 and is representative of a nighttime warm season case. The region around the lakes and rivers are characterized by a positive heat flux. On the other hand, the urban region and surrounding suburban and rural regions are characterized by negative heat fluxes. The magnitude of the negative heat flux is smallest in the central portions of St. Louis and is on the order of $-0.02 \text{ kJ m}^{-2} \text{ s}^{-1}$. Larger magnitude negative heat fluxes are found in the surrounding suburban and rural regions. The small negative heat flux in St. Louis is indicative of a relatively small ΔT . This analysis dramatizes the relatively greater cooling expected in the suburban and rural regions than in the urban region.

Godowitch et al. (1981) and Ching et al. (1978) used RAPS data to determine the temporal variation of the heat flux at urban and rural sites in St. Louis for August 1976. They found that during the day, the urban sites had a greater sensible heat flux than the rural sites. The values in the urban site ranged from 0.1 to $0.3 \text{ kJ m}^{-2} \text{ s}^{-1}$. In the rural regions, the values ranged from 0.05 to $0.15 \text{ kJ m}^{-2} \text{ s}^{-1}$. In spite of the potential for errors which ranged from 10 to 20 percent discussed in the previous section, the heat flux calculations made using the HCMM satellite data appear to coincide quite well with those made by other investigators for the daytime cases. At night, Godowitch et al. and Ching et al. found that the values of the heat flux were generally small and negative. The values ranged from 0 to $-0.025 \text{ kJ m}^{-2} \text{ s}^{-1}$. They also found that the magnitude of the heat flux in the urban region was generally less than the heat flux in the rural region. These results coincide quite well with those obtained using the HCMM data for the nighttime cases.

3.5 The Distribution of the Specific Humidity Depression

The specific humidity depression (Δq) was defined in Section 2.0 as the difference between the specific humidity of the air and the specific humidity of the ground. The specific humidity depression was computed using the energy balance equation [Equation (30)], assuming that at the time of the HCMM ground temperature measurements, the ground temperature was in a quasi-steady state.

The analysis of the specific humidity depression for 26 June (Figure 10) is characteristic of the solutions of the daytime warm season case.

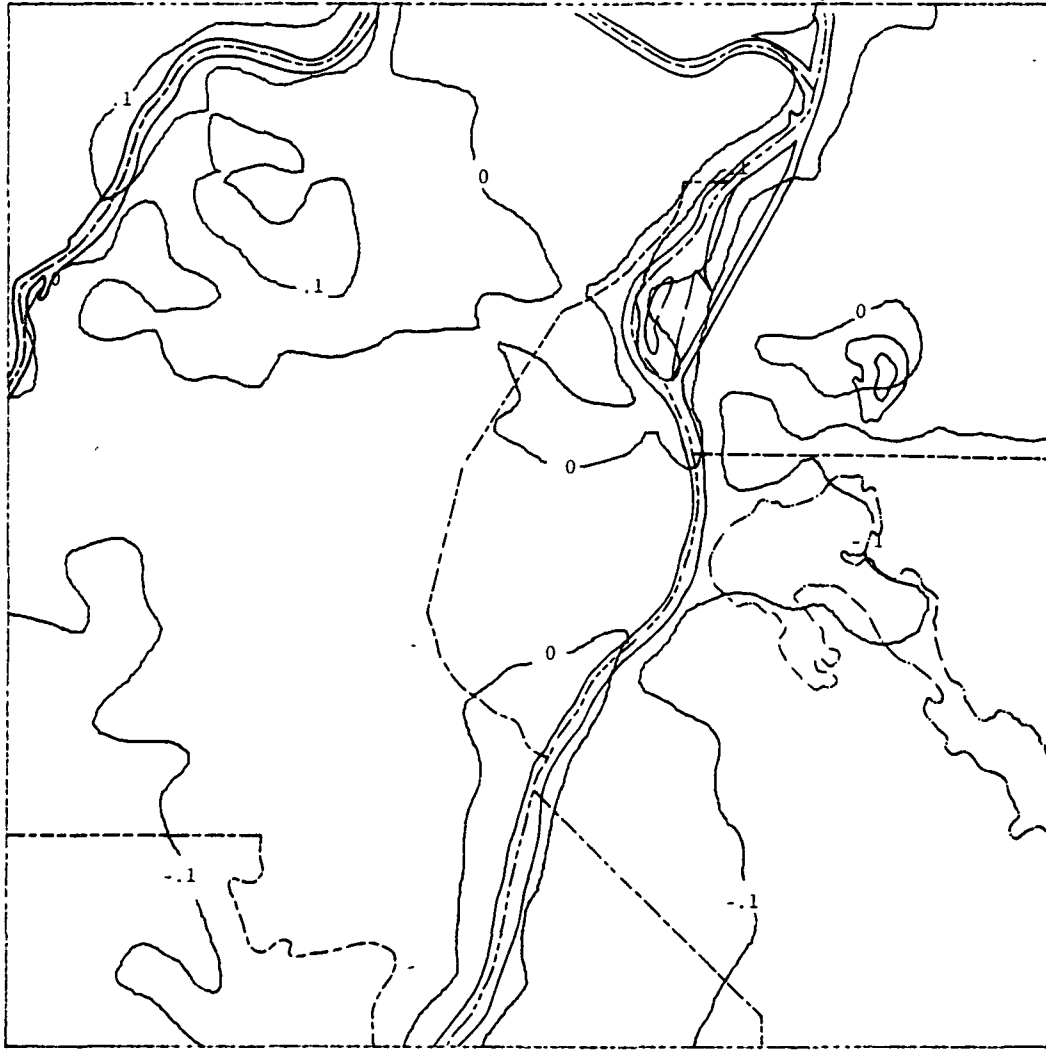


Figure 9. Surface heat flux ($\text{kJ m}^{-2} \text{s}^{-1}$) distribution for 14 June 1978.

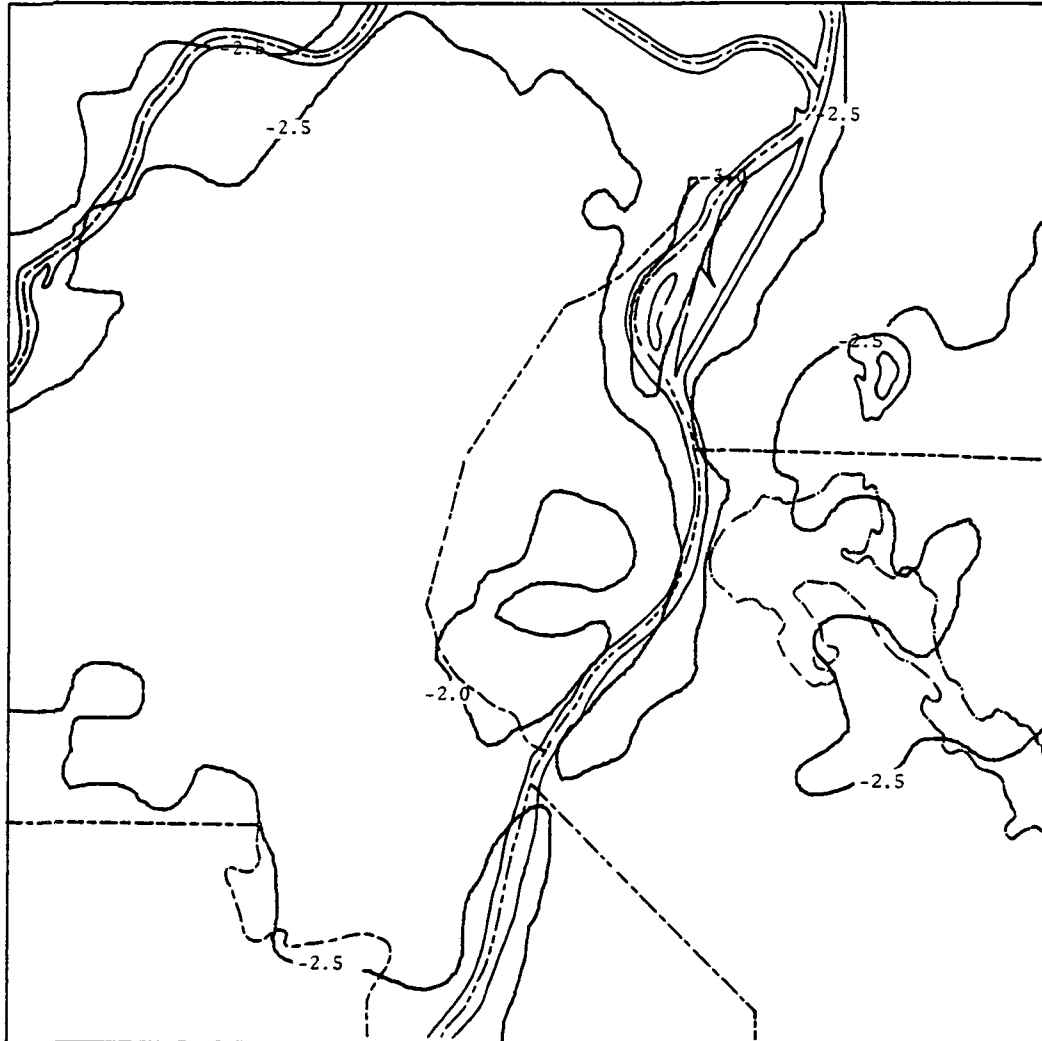


Figure 10. The distribution of the specific humidity depression ($10^{-1} \text{ g kg}^{-1}$) for 26 June 1978.

Negative values of the specific humidity depression indicate a flux of water vapor at the surface from the ground to the air (evaporation), and positive values, a flux of water vapor at the surface from the air to the ground. Because of problems with missing data and extrapolation, this analysis has most credibility around the central portions of St. Louis and around the lakes and the rivers. The entire region is characterized by negative values of the specific humidity depression (evaporation). Evaporation over the central portions of St. Louis is less than that in the suburban and rural regions. The greatest evaporation was found over the rivers and lakes. The specific humidity depression ranged from -0.2 to -0.3 g kg^{-1} for the entire area which yields a variation in evaporation from 0.6 to $0.9 \text{ kJ m}^{-2} \text{ s}^{-1}$.

The analysis of the specific humidity depression for 26 February 1979 is an example of the distribution of the specific humidity depression for the daytime cold season case studies (Figure 11). As in the warm season case studies, negative specific humidity depressions (evaporation) characterize the entire region. However, the specific humidity depression is roughly an order of magnitude smaller. As in the warm season case, the evaporation is greatest over the rivers and lakes and smallest over the St. Louis urban complex. The magnitude of specific humidity depression varies from -0.025 to -0.075 g kg^{-1} which will yield a range in evaporation from 0.08 to $0.23 \text{ kJ m}^{-2} \text{ s}^{-1}$.

The analysis of the specific humidity depression for 14 June 1978 is representative of a nighttime warm season case (Figure 12). There is a flux of water vapor from the air to the ground over the entire region except in southeastern sections where there were no observation stations for wind and temperature. The largest value of the specific humidity depression, and therefore the largest flux of water vapor from the air to the ground, is found over the rivers and lakes. In the energy balance equation [Equation (30)], the surface heat flux yields the major contribution to the solution for the evaporation at night since the net radiation (the difference between R_a and R_g) is generally small. Therefore, at night, regions of large positive heat flux are usually characterized by a relatively large flux of water vapor from the air to the ground in order to maintain the energy balance.

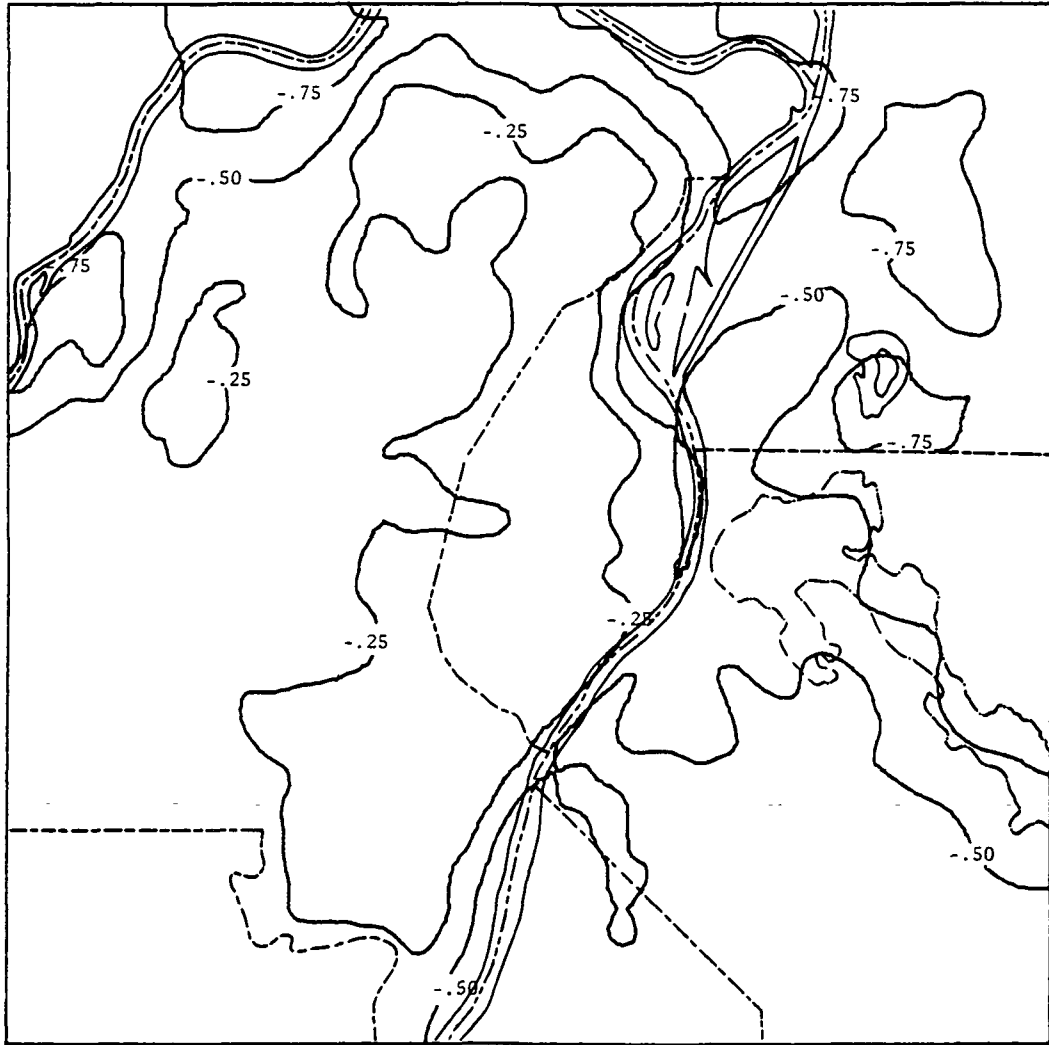


Figure 11. The distribution of the specific humidity depression ($10^{-1} \text{ g kg}^{-1}$) for 26 February 1979.

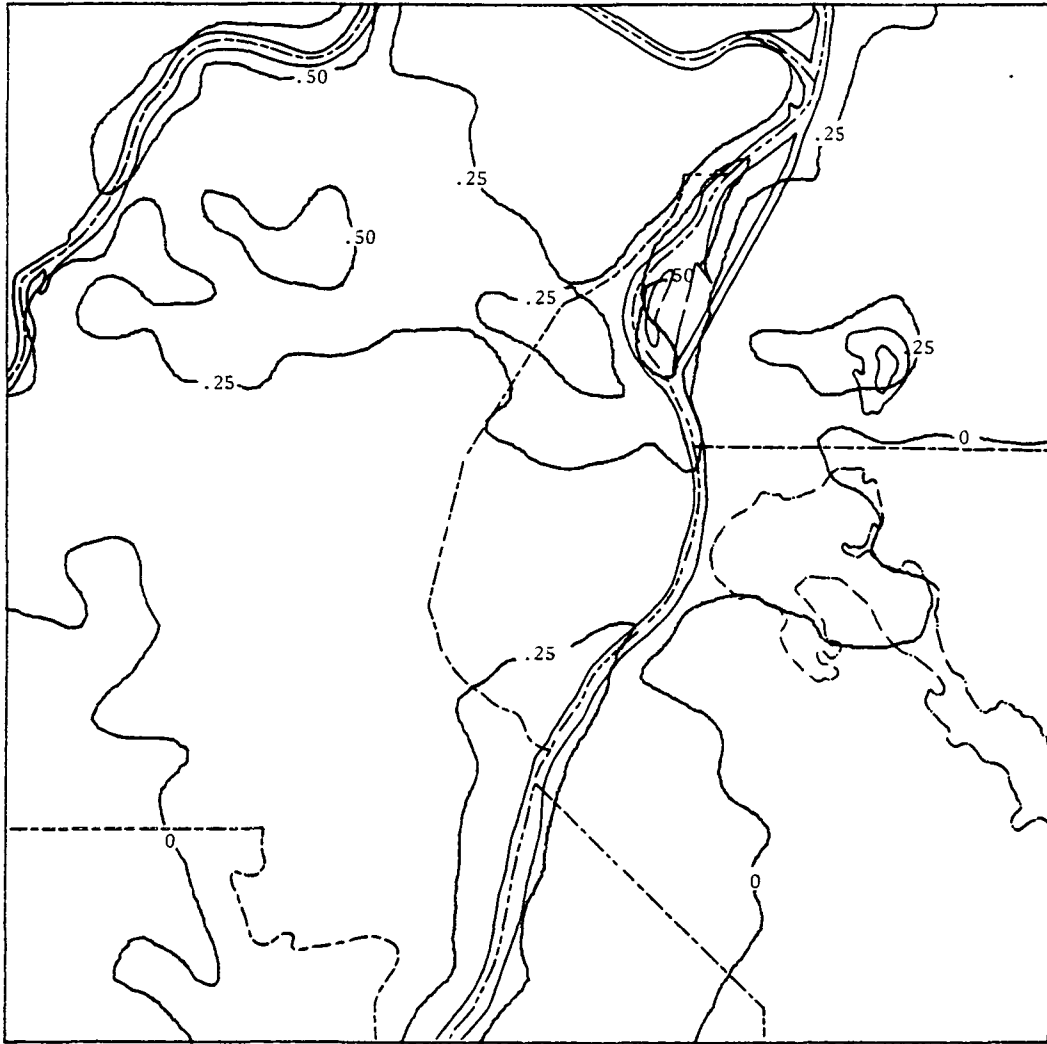


Figure 12. The distribution of the specific humidity depression ($10^{-1} \text{ g kg}^{-1}$) for 14 June 1978.

The flux of water vapor from the air to the ground is greater in the suburban and rural regions than it is over the central portions of St. Louis. These results are similar to the results of Ackerman (1971) and Myers (1974) who indicated that because there is greater cooling in the suburban and rural regions at night, there should be greater dew deposition in those regions also. This should be reflected by a greater flux of water vapor from the air to the ground in the suburban regions than in the urban region. The values of the specific humidity depression range, where positive values exist (these values have the most credibility), from 0 to 0.05 g kg^{-1} . This yields a range for the evaporation from 0 to $-0.15 \text{ kJ m}^{-2} \text{ s}^{-1}$.

Ching et al. (1978) computed average evaporation rates for the St. Louis region for the month of August 1976. They found that in the urban regions, the average evaporation rate was approximately $0.1 \text{ kJ m}^{-2} \text{ s}^{-1}$ and in the rural region, the average rate was $0.2 \text{ kJ m}^{-2} \text{ s}^{-1}$. Their data conveyed the same notion determined in the analysis of the HCMM data; i.e., the evaporation rate is less in the urban region than in the rural and suburban regions (see also Oke, 1974; and Sisterson, 1975). The values calculated using the HCMM data were of the same order of magnitude as those determined by Ching et al.; however, in some cases, the values computed using the HCMM data were as much as six times greater. It must be noted that the values computed by Ching et al. are average values for the month. On the other hand, the values computed using the HCMM data are values determined at the time of maximum and minimum temperatures for specific case studies where the latent heat flux could vary significantly depending on the moisture content of the ground and other factors.

3.6 Eddy Viscosity Distribution

Figures 13 and 14 give the daytime warm (26 June 1978) and cold (26 February 1979) season distribution of the eddy viscosity, K_m , that was computed using Equation (50). The distribution of eddy viscosity was primarily governed by the distribution of the friction velocity, which was governed by the distribution of the wind speeds, and by the stability length, L . Higher values of the eddy viscosity were found where the wind speeds were larger; and lower values were found where there was a positive air-ground temperature difference (a stable environment), which was

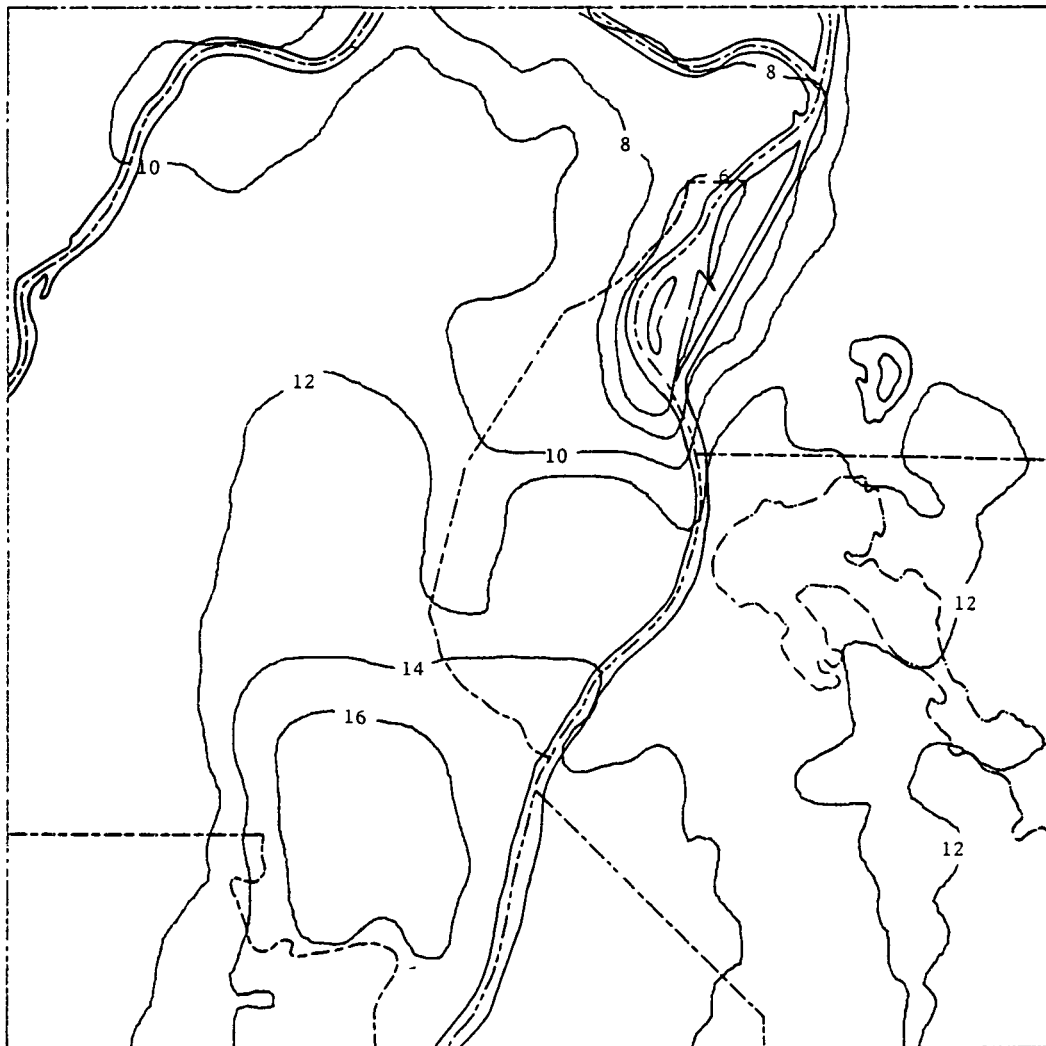


Figure 13. The distribution of the eddy viscosity, K_m , ($\text{m}^2 \text{s}^{-1}$) for 26 June 1978.

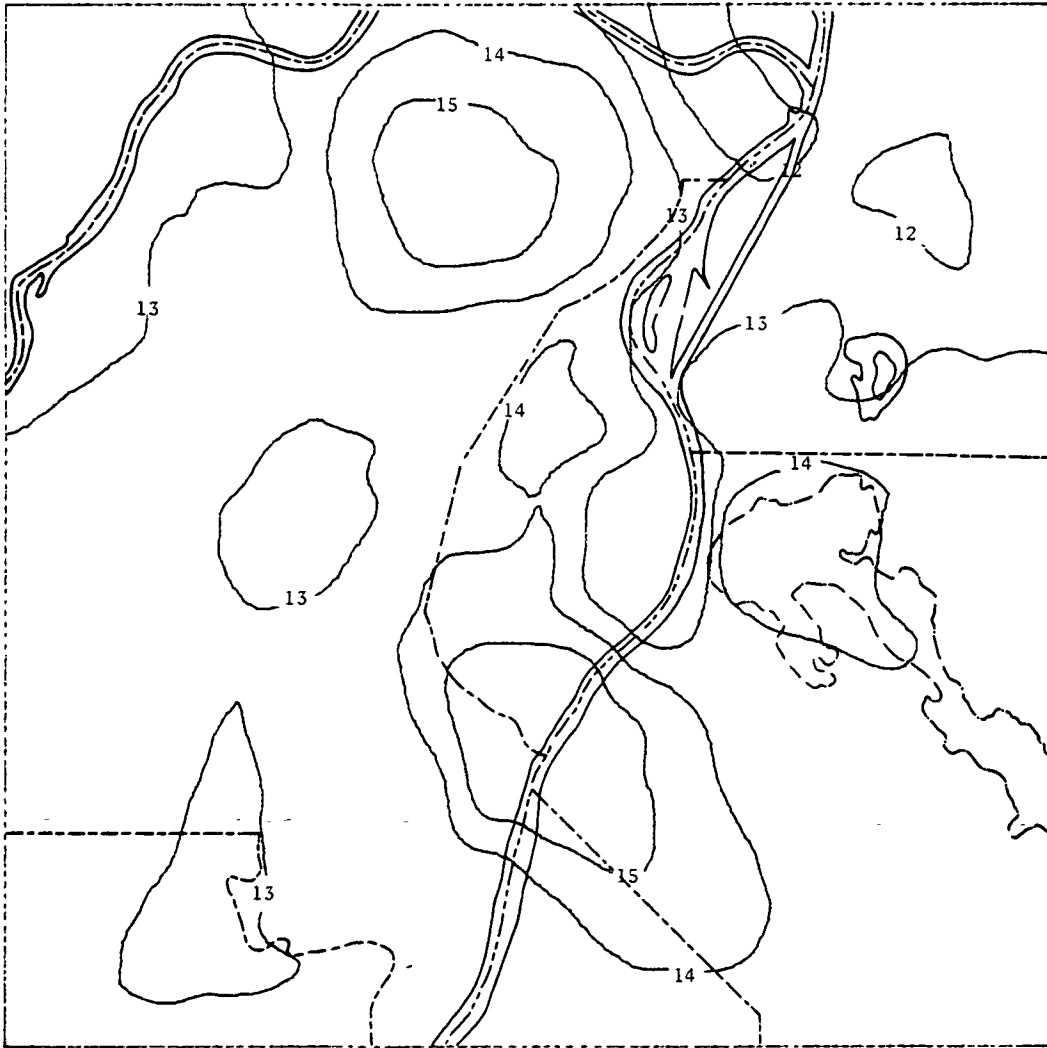


Figure 14. The distribution of the eddy viscosity, K_m , ($\text{m}^2 \text{s}^{-1}$) for 26 February 1979.

primarily where the rivers were located. Because of the increased frictional influence over the cities, the wind speeds over St. Louis and, to a lesser extent, over the cities immediately east of St. Louis had smaller wind speeds than the suburbs and rural regions to the northwest and south. However, instability (the large magnitude negative air-ground temperature differences) maintained large values of the eddy viscosity in the cities. The eddy viscosity was greater in the suburbs and rural regions to the northwest and south than in the city because the wind speeds were greater.

The nighttime warm season distribution of the eddy viscosity which is characterized by the analysis of 14 June 1978 (Figure 15), was governed primarily by the stability length. The largest values of the eddy viscosity were located over the rivers where there was a large negative air-ground temperature difference and in the region surrounding Lambert Field where the wind speed was about 1.5 m s^{-1} greater than the average wind speed using all the remaining stations. The wind pattern for this case was relatively uniform except for the wind speed at the airport. The only explanation for the difference in wind speeds is that the airport anemometer is located in the middle of open runways, whereas most of the other sites are either located in the heart of the city, the heart of the suburbs, or in tree-infested rural regions, and the frictional influence being significantly reduced at the airport site relative to the other sites. The lowest values of the eddy viscosity are located in the suburban and rural regions to the southwest, northeast, and southeast where the air-ground temperature difference is positive (stability).

Clarke et al. (1978) measured the vertical turbulence intensity in St. Louis during the RAPS and determined that for the summer, the turbulence intensity in St. Louis was approximately 33 percent greater than that in the rural region immediately east of East St. Louis. Given the location of the stations used by Clarke et al. to measure the vertical turbulence intensity, the values of the eddy viscosity for the warm season cases were determined at those sites. During the day, the average eddy viscosity for the urban site was approximately 26 percent greater than the average value for the rural site to the east of East St. Louis. At night, the observations of Clarke et al. indicate that the vertical turbulence intensity was approximately 70 percent greater in the city. The eddy viscosity was approximately 43 percent greater in the city.

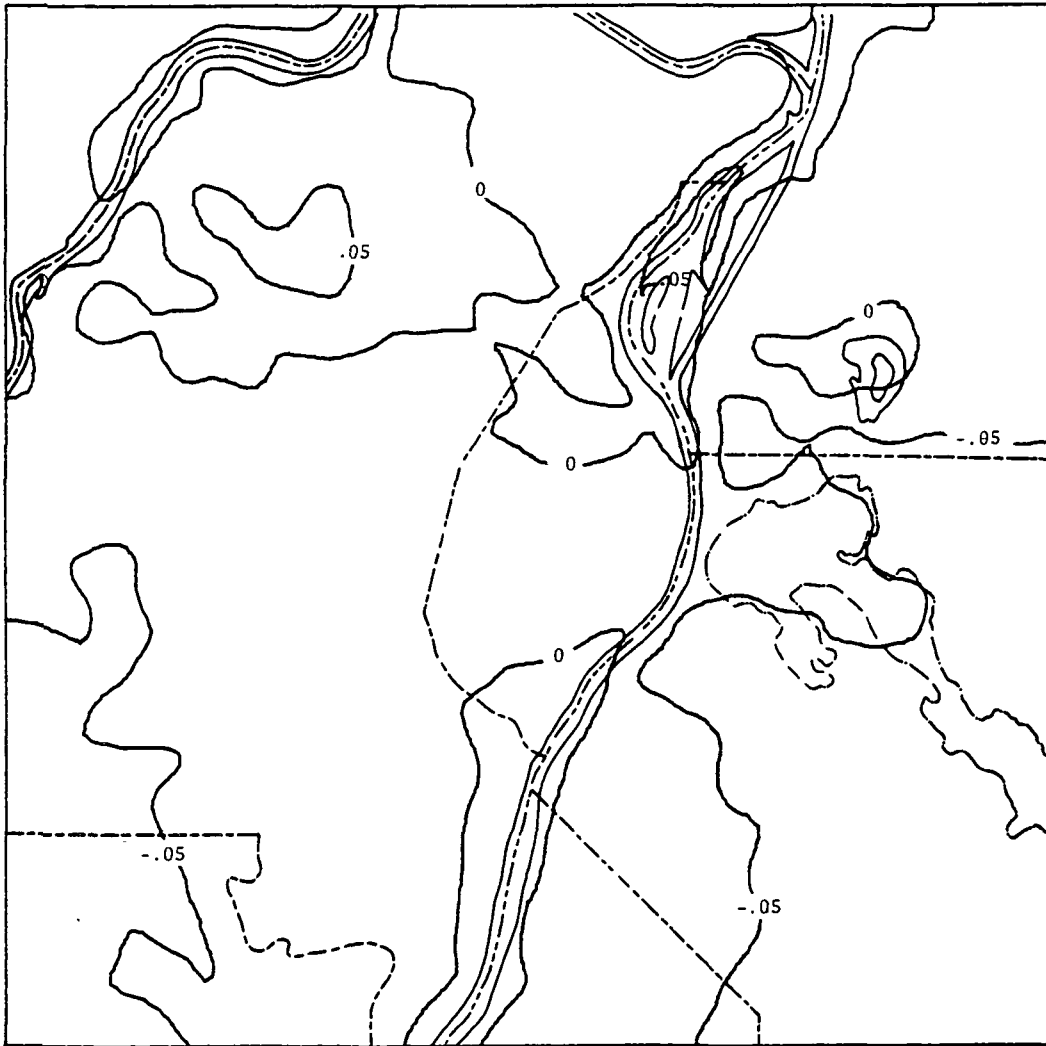


Figure 15. The distribution of the eddy viscosity, K_m , ($\text{m}^2 \text{s}^{-1}$) for 14 June 1978.

4.0 Discussion of Results

The ground temperature pattern in St. Louis indicated a relatively strong temperature contrast between the urban and rural regions during the daytime and in the warm season. Ground temperature contrasts were also noted during the day and in the cold season, but the magnitude of the contrast was smaller than that in the warm season. In both the warm and cold seasons, the daytime distribution of ground temperatures was influenced by small-scale land use features such as parks and other vegetated areas. The magnitude of the horizontal gradient of ground temperature between the urban and rural regions was found to be greater (by as much as 5 times in one case) than the magnitude of the horizontal gradient of air temperature in both the warm and cold seasons. Boundary-layer mixing may be responsible for this factor. The surface heat associated with the ground temperature pattern in the warm season should be able to create a reasonable heat island. The production of the heat island should not necessarily need the added effect of an artificial heat source as suggested by the calculations of Welch et al. (1978). This would suggest that the distribution of surface roughness, soil moisture, and soil diffusivity which affect the ground temperature pattern and, subsequently, the heat flux pattern, might be more important than anthropogenic heating.

At night, the ground temperature contrast between the urban and rural regions was, on the average, smaller than that found during the day. Furthermore, the effect of small-scale land use features such as parks, did not affect the ground temperature pattern as significantly at night as during the day. At night, the magnitude of the horizontal gradient of ground temperature between the urban and rural regions was always less than the magnitude of the horizontal gradient of air temperature, indicating that the differential heat flux pattern was not totally responsible for the air temperature pattern. Other factors, such as radiational effects, must play a significant role.

The diurnal variation of the heat island intensity as defined by the urban-rural air temperature differences has been well documented (Steigerwald, 1981; Mitchell, 1961; Hage, 1972; Landsberg, 1981; and Kellogg, 1977). The heat island intensity as defined by the air temperature is largest at night. Though only two points are available on

the diurnal curve for the heat island intensity as defined by the urban-rural ground temperature difference, the heat island intensity as defined by the ground temperature appears to be opposite of that defined by the air temperature; i.e., the data suggest that the heat island intensity as defined by the ground temperature is largest during the day. The implications of these results are that: 1) during the day, the sensible heat flux at the surface would tend to produce a stronger heat island than at night, but some other process, mixing perhaps, acts against the effect of the sensible heat flux; and 2) at night, the sensible heat flux at the surface is not of sufficient strength to produce the observed magnitude of the air heat island intensity, suggesting that other processes--radiative processes perhaps--might be very influential. However, because there is insufficient data on which to base these results, conclusions and implications are to be considered tentative.

The reflectivity data from the HCMM satellite indicated relatively low values of reflectivity in the central regions of St. Louis. The difference in reflectivity between the urban center and the surrounding suburban and rural regions ranged from 2 to 4 percentage points, consistent with the data of White et al. (1978) and Dabberdt and Davis (1974). The percentage difference was roughly 20 percent, consistent with the modeling results of Craig and Lowry (1972). The magnitude of the reflectivity measured by the HCMM satellite was generally larger than the albedo measurements made by White et al., and Dabberdt and Davis. This may be the result of the following factors: 1) the HCMM measurements are made in a narrow visible band, whereas albedo measurements generally treat the total solar radiation; and 2) previous measurements were made with low-flying aircraft looking through a small atmospheric column, whereas satellite measurements are made at a significantly greater altitude looking through a larger atmospheric column. Atmospheric scattering by water vapor and other constituents will influence the satellite measurement of the albedo.

Though the influence of rivers and lakes was obvious in the reflectivity measurements, the influence of small-scale land use features such as parks was not. This may be a result of the smoothing performed in the analyses. However, smoothing cannot account completely for the lack of discrimination associated with small-scale land use features because such

features were indicated in the ground temperature pattern in which the same kind of smoothing was performed.

The effect of atmospheric pollutants over the center of metropolitan St. Louis has been shown to reduce the incident solar radiation by about 3 percentage points compared to rural regions (Peterson and Stoffel, 1980). The HCMM measurements would suggest that absorption of solar radiation in the urban area is about 2 to 4 percentage points greater than that in the rural region. These results would suggest that the amount of solar energy absorbed at the surface in the urban region was about equivalent to that in the rural region, and that differences in the ground temperature between the urban and rural regions cannot be attributed to incoming radiation differences.

During the day, the pattern of the surface heat flux calculated using the HCMM ground temperature and in situ data indicated relatively large positive values centered about the St. Louis urban complex. The magnitude of the surface heat flux in the urban region ranged from 0.1 to 0.3 $\text{kJ m}^{-2} \text{s}^{-1}$ over the four daytime case studies. The average value was approximately $0.25 \text{ kJ m}^{-2} \text{ s}^{-1}$. In the suburban regions, the magnitude of the heat flux ranged from 0.05 to 0.20 $\text{kJ m}^{-2} \text{ s}^{-1}$ for the four daytime case studies. The average value was $0.1 \text{ kJ m}^{-2} \text{ s}^{-1}$. Godowitch et al. (1981) and Ching et al. (1978) found that the average daytime surface heat flux in urban St. Louis for August 1976 was somewhere between 0.20 to 0.30 $\text{kJ m}^{-2} \text{ s}^{-1}$, and in the suburban region was about $0.15 \text{ kJ m}^{-2} \text{ s}^{-1}$. The comparison between these results suggest that the HCMM data can be used to successfully compute the relative and the absolute magnitudes of the sensible heat flux in spite of some of the simplifications used to make the calculations. The large daytime heat fluxes that were computed using the HCMM data were generally due to the large magnitudes of air-ground temperature differences. For the daytime cases, the air-ground temperature differences ranged from -3.0°C to -11.8°C . The largest air-ground temperature differences generally were found during or immediately after the occurrence of cold air advection under the condition of clear skies. The smallest value of the air-ground temperature difference was found generally during warm air advection and under the condition of clear skies.

At night, the urban region and surrounding suburban regions were characterized by negative heat fluxes. The heat flux in the urban region

was on the order of $-0.02 \text{ kJ m}^{-2} \text{ s}^{-1}$. The magnitude of the heat flux was smallest in the central urban region, and largest in the surrounding suburban and rural regions. The smaller magnitude surface heat flux in the urban region was primarily associated with near-adiabatic conditions. These results, both quantitatively and qualitatively, were consistent with those of Godowitch et al. They further substantiate that the HCMM data may be used to compute the surface heat flux and reasonable estimates of the magnitude in spite of the potential errors.

The daytime distribution of the specific humidity depression in the warm season was characterized, on the average, by small values (small values of evaporation) in the central St. Louis urban region and larger values (larger values of evaporation) in the suburban and rural regions. This leads to the general interpretation that the ground-specific humidity in the urban region is smaller than that in the suburban and rural regions. This interpretation is consistent with the findings of Carlson et al. (1981) and the general interpretations of Dirks (1974), Hage (1975), Kopec (1973), Landsberg and Maisel (1972), and Zanella (1976).

During the day, the specific humidity depression varied from -0.025 to -0.2 g kg^{-1} . This corresponds to a variation in the evaporation from 0.1 to $0.6 \text{ kJ m}^{-2} \text{ s}^{-1}$. Ching et al. (1978) had indicated an average value of evaporation for the month of August 1976 of approximately $0.1 \text{ kJ m}^{-2} \text{ s}^{-1}$ in urban St. Louis. The values computed using the HCMM data were the same order of magnitude determined by Ching et al.; however, in some cases, they were six times greater than the value of Ching et al. The evaporation computed using the HCMM data represent the values around the time of maximum temperature for a specific case study. It is not unexpected that these values are as much as six times different from the value that represents the average over a month. The relative and absolute values of the daytime evaporation rate compare well with observed data in spite of the potential for error associated with the assumption that the local rate of change of the ground temperature is zero. If the evaporation rates are considered reasonable, then the specific humidity depression also must be reasonable.

Nighttime distribution of the specific humidity depression for the warm season was characterized by positive values over most of the region. The largest positive values were found over rivers and lakes. The positive

values found over the suburban and rural regions were larger than those over the central portions of St. Louis, which is also consistent with the results of Ackerman (1971) and Myers (1974).

The daytime distribution of the eddy viscosity was governed by the distribution of the wind speeds and stability. Higher values for the eddy viscosity were found where the wind speeds were higher, and lower values where there was a stable environment. Because of the increased frictional influence over the cities, wind speeds over St. Louis were smaller than in the suburbs and rural regions to the northwest and south. However, the instability in the city maintained large values for the eddy viscosity. The nighttime distribution of the eddy viscosity in the two cases analyzed was primarily governed by the stability. The largest values of the eddy viscosity were located over rivers where there was an unstable environment. The lowest values were located in the suburban and rural regions to the southwest and southeast where the environment was stable. There were no observations available with which to compare the calculated distribution of the eddy viscosity. The variation of the eddy viscosity between the urban and rural regions compared reasonably well with the observations of turbulent intensity made in St. Louis in the summer by Clarke et al. (1978) in both daytime and nighttime cases.

The results indicate that a reasonable estimate of the surface heat flux, urban albedo, and specific humidity depression can be obtained utilizing HCMM satellite data. (Values of the ground-specific humidity can be obtained if the distributions of the air-specific humidity are available.) These three parameters--the ground temperature distribution, the albedo distribution, and the ground-specific humidity distribution--are needed by mesoscale modelers as part of the specification of initial and boundary conditions. Another important term is the surface roughness. Attempts were made to utilize a wind profile model to acquire the surface roughness. However, because of limitations of the model, results were limited. A brief description of the results are given in Appendix J.

The eddy viscosity is not a parameter necessary for input into hydrodynamic models. However, there is a potential utilization for the eddy viscosity distribution in diffusion models. As in the case of the specific humidity depression and the surface roughness, more research is required with fundamental comparisons between the calculated and observed values.

Furthermore, these results must be qualified until there is an actual case of the application of the HCMM data in a numerical model, even though this preliminary effort indicates that the potential results are good.

5.0 Recommended Research

Due to the preliminary nature of this research and limited resources, very little effort could be made to determine the effect on the calculations of the parameters used in the various models used to derive the surface heat flux, the friction velocity, the specific humidity depression, and other boundary layer parameters. Future research should examine the effect of these parameters. Future research should also examine the possibility of determining other boundary layer terms required for meso-scale models including the surface roughness. Initial attempts to compute the surface roughness examined one model and were not as successful. Other models should be investigated which might yield better results.

The long-term goal of this research project is to develop initial data and parameters which can be used in mesoscale prediction models. The use of the remote-sensing data is encouraged because it is only through these data that the required resolution for mesoscale models can be ascertained. Research should concentrate on the utilization of the parameters derived from the various models to develop initial fields of the boundary layer temperature, the ground-specific humidity, the boundary-layer-specific humidity, the boundary layer pressure, and, potentially, the boundary layer winds. The procedures which should be tested for the development of such initial fields are the utilization of objective variational analysis. The data determined from energy balance models and other boundary layer models can be used as input data for an objective variational analysis model. For example, objective variational models can use the distribution of the specific humidity depression and limited in situ data to derive the 10-m distribution of the specific humidity. This, together with the distribution of the specific humidity depression can be utilized to derive the distribution of the ground-specific humidity. Similar techniques can be used to develop the temperature distribution at various levels in the boundary layer. If the boundary layer temperature distribution can be determined, hydrostatic and geostrophic assumptions can be utilized to obtain an initial estimate of the pressure and wind distribution. The objective analysis procedures can be used to adjust the wind field estimates given a model for the vertical distribution of the exchange coefficient.

6.0 References

1. B. Ackerman. Moisture content of city and country air. Proceedings of Conf. Air Pollution Meteorology, Raleigh, NC, 1971. pp. 154-158. Amer. Meteorol. Soc., Boston.
2. T. P. Ackerman. A model of the effect of aerosols on urban climates with particular applications to the Los Angeles Basin. J. Atmos. Sci., 1977. 34, pp. 531-547.
3. M. Aida and M. Yaji. Observations of atmospheric downward radiation in the Tokyo area. Bound. Layer Meteorol., 1979. 16, pp. 453-465.
4. A. Arakawa. Design of the UCLA general circulation model. Tech. Rep. 7, Dept. of Meteorol., Univ. of California, Los Angeles, 1972. 103 pp.
5. R. D. Bornstein. The two-dimensional URBMET boundary layer model. J. Appl. Meteorol., 1975. 14, pp. 1459-1477.
6. J. R. Bray, J. E. Sanger, and A. L. Archer. The visible albedo of surfaces in central Minnesota. Ecology, 1966. 47, pp. 524-531.
7. T. N. Carlson, J. N. Augustine, and F. E. Boland. Potential application of satellite temperature measurements in the analysis of land use over urban areas. Bull. Amer. Meteorol. Soc., 1977. 58, pp. 1301-1303.
8. T. N. Carlson, J. K. Dodd, S. G. Benjamin, and J. N. Cooper. Satellite estimation of the surface energy balance, moisture availability, and thermal inertia. J. Appl. Meteorol., 1981. 20:1, pp. 67-87.
9. T. J. Chandler. The Climate of London. Hutchinson, London, 1965. p. 150.
10. T. J. Chandler. Urban climatology--inventory and prospect. Urban climates. Tech. Note No. 108, WMO No. 254, TP. 141, 1970. pp. 1-14.
11. J. K. S. Ching, J. F. Clarke, and J. M. Godowitch. The variability of the heat flux and mixed layer depth over St. Louis, MO. Presented at the WMO Symposium on Boundary Layer Physics Applied to Special Problems of Air Pollution, Norrkoping, Sweden, June 14-23, 1978.
12. C. F. Chow, E. C. Kinde, and F. M. Vukovich. Study of atmospheric behavior using a quasi-geostrophic, diabatic, two-layer model. Mon. Weather Rev., 1972. 100:6, pp. 477-486.
13. J. F. Clarke, J. K. S. Ching, F. S. Binkowski, and J. M. Godowitch. Turbulent structure of the urban surface boundary layer. Presented at the NATO/CCMS Ninth International Technical Meeting on Air Pollution Modeling and Its Application, Toronto, Canada, August 28-31, 1978.

14. C. D. Craig and W. P. Lowry. Reflections on the urban albedo. Conference on the Urban Environment and Sec. Conference on Biomet., Philadelphia, PA, Oct. 31-Nov. 2, 1972. pp. 159-164.
15. W. F. Dabberdt and P. A. Davis. Determination of energetic characteristics of urban-rural surfaces in the greater St. Louis area. Preprint, Symp. Atmos. Diffusion and Air Pollut., Santa Barbara, 1974. pp. 133-141. Amer. Meteorol. Soc., Boston, MA.
16. J. A. Davies, W. Schertzer, and M. Nunez. Estimating global solar radiation. Bound. Layer Meteorol., 1975. 9, pp. 33-52.
17. J. W. Deardorff. Efficient prediction of ground surface temperature and moisture, with inclusion of a layer of vegetation. J. Geophys. Res., 1978. 83, pp. 1889-1903.
18. R. A. Dirks. Urban atmosphere: Warm dry envelope over St. Louis. J. Environ. Res., 1974. 79:24, pp. 3473-3475.
19. M. A. Estoque and C. M. Bhumralkar. Flow over a localized heat source. Mon. Weather Rev., 1969. 97:12, pp. 850-859.
20. R. Geiger. The climate near the ground. Harvard University Press, 1965. 610 pp.
21. J. M. Godowitch, J. K. S. Ching, and J. F. Clarke. Urban/rural and temporal variations in PBL turbulence parameters and length scales over St. Louis, MO. Fifth Symp. on Turb., Diff. and Air Pollut., Atlanta, GA, March 9-13, 1981. Preprints, Amer. Meteorol. Soc., Boston, MA.
22. K. D. Hage. Nocturnal temperatures in Edmonton, Alberta. J. Appl. Meteorol., 1972. 11, pp. 123-129.
23. K. D. Hage. Urban-rural humidity differences. J. Appl. Meteorol., 1975. 14, pp. 1277-1283.
24. G. J. Haltiner and F. L. Martin. Dynamical and Physical Meteorology. McGraw-Hill, New York, 1957.
25. Heat Capacity Mapping Mission User's Guide. Goddard Space Flight Center, Greenbelt, MD, 1980. 120 pp.
26. H. G. Houghton. On the heat balance of the northern hemisphere. J. Meteorol., 1954. 11, pp. 1-9.
27. F. A. Huff and S. A. Changnon, Jr. Precipitation modification by major urban areas. Bull. Amer. Meteorol. Soc., 1973. 54, pp. 1220-1232.
28. F. A. Huff and E. E. Schlessman. 1971-1972 studies of monthly, seasonal, and storm rainfall. Summary Report of METROMEX studies, F. A. Huff, ed., Illinois State Water Survey, Urbana, 1973. pp. 5-27.

29. R. J. Hutcheon, R. H. Johnson, W. P. Lowry, C. H. Black, and D. Hadley. Observations of the urban heat island of a small city. Bull. Amer. Meteorol. Soc., 1967. 48, pp. 7-9.
30. W. W. Kellogg. Effects of human activities on global climate--Part 1. WMO Bull., 1977. 26, pp. 229-240.
31. R. J. Kopec. Daily spatial and secular variations of atmospheric humidity in a small city. J. Appl. Meteorol., 1973. 12, pp. 639-648.
32. H. E. Landsberg. Man-made climatic changes. Science, 1970. 170, pp. 1265-1274.
33. H. E. Landsberg. The Urban Climate. International Geophysics Series, Vol. 28, Academic Press, New York, 1981.
34. H. E. Landsberg and T. N. Maisel. Micrometeorological observations in an area of urban growth. Bound. Layer Meteorol., 1972. 1, pp. 61-63.
35. E. N. Lawrence. Urban climate and day of the week. Atmos. Environ., 1971. 5, pp. 935-948.
36. C. L. Mateer. Note on the effect of the weekly cycle of air pollution on solar radiation at Toronto. Int. J. Air and Water Poll., 1961. 4, pp. 52-54.
37. M. Matson, E. P. McClain, D. F. McGinnis, Jr., and J. A. Pritchard. Satellite detection of urban heat islands. Mon. Weather Rev., 1978. 106, pp. 1725-1734.
38. R. A. McCormick and J. H. Ludwig. Climate modification by atmospheric aerosols. Science, 1967. 156, pp. 1358-1359.
39. J. E. McDonald. Direct absorption of solar radiation by atmospheric water vapor. J. Meteorol., 1960. 17, pp. 319-328.
40. J. L. McElroy. A numerical study of the nocturnal heat island over a medium-sized mid-latitude city (Columbus, OH). Bound. Layer Meteorol., 1973. 3:4, pp. 442-453.
41. J. M. Mitchell, Jr. The thermal climate of cities. Symposium on Air Over Cities, Cincinnati, OH, November 6-7, 1961. pp. 131-145.
42. A. S. Monin and A. M. Obukhov. Fundamentale Gesetzmässigkeiten der turbulenten Vermischung in der bodennahen Schicht der Atmosphäre. In "Sammelband zur statistischen Theorie der Turbulenz," (H. Goering, ed.), 1954. pp. 199-226. Akademie Verlag, Berlin (1958). Trans. Inst. Geophys. Akad. Nauk. SSSR No. 24, p. 151.
43. T. M. Myers. Dew as a visual indicator of the urban heat island in Washington, DC. Master's Thesis, Univ. of Maryland., College Park, 1974. 54 pp.

44. L. O. Myrup. A numerical model of the urban heat island. J. Appl. Meteorol., 1969. 8, pp. 908-918. Corrigendum, ibid. 1970. 9, p. 54.
45. C. J. Nappo. A numerical study of the urban heat island. Proc. of Conf. on Urban Environ. and Sec. Conf. on Biomet., Philadelphia, PA, 1972.
46. T. R. Oke. Review of urban climatology 1968-1973. WMO Technical Note No. 134, 1974. 132 pp.
47. T. R. Oke and C. East. The urban boundary layer in Montreal. Bound. Layer Meteorol., 1971. 1, pp. 411-437.
48. J. P. Pandolpho, M. A. Atwater, and E. E. Anderson. Prediction by numerical models of transport and diffusion in an urban boundary layer. CEM report, EPA Contract No. CPA-70-62, 1971. 139 pp.
49. J. T. Peterson and T. L. Stoffel. Analysis of urban-rural solar radiation data from St. Louis, MO. J. Appl. Meteorol., 1980. 19, pp. 275-283.
50. J. C. Price. Assessment of the urban heat island effect through the use of satellite data. Mon. Weather Rev., 1979. 107, pp. 1554-1557.
51. P. K. Rao. Remote sensing of urban heat islands from an environmental satellite. Bull. Amer. Meteorol. Soc., 1972. 53, pp. 647-648.
52. P. T. Schickendanz. Inadvertent rain modification as indicated by surface raincells. J. Appl. Meteorol., 1974. 13:8, pp. 891-900.
53. R. G. Semonin and S. A. Changnon, Jr. METROMEX: Summary of 1971-1972 results. Bull. Amer. Meteorol. Soc., 1974. 55, pp. 95-100.
54. D. L. Sisterson. Studies on the urban moisture budget. Rept. No. AS114, Dept. Atmos. Sci., Univ. of Wyoming, Laramie, 1975. 52 pp.
55. J. E. Steigerwald. Climatological aspects of the St. Louis heat island. Master's Thesis. North Carolina State University, Raleigh, NC, 1981. 74 pp.
56. F. M. Vukovich. A comparison of Explorer VII infrared radiation values with various atmospheric parameters. Master's Thesis. St. Louis University, St. Louis, MO, 1972. 73 pp.
57. F. M. Vukovich. Theoretical analysis of mean wind and stability on heat island circulation of an urban complex. Mon. Weather Rev., 1971. 99, pp. 919-926.
58. F. M. Vukovich. A study of the atmospheric response due to a diurnal function characteristic of an urban complex. Mon. Weather Rev., 1973. 101, pp. 467-474.
59. F. M. Vukovich. Urban Meteorology and Related Air Pollution Distribution. Air Pollution Control Part IV, G. M. Bragg and W. Strauss, ed., John Wiley and Sons, Inc., New York, 1981.

60. F. M. Vukovich and J. W. Dunn. A theoretical study of the St. Louis heat island: Some parameter variations. J. Appl. Meteorol., 1978. 17, pp. 1585-1599.
61. F. M. Vukovich, J. W. Dunn, and B. Crissman. A theoretical study of the St. Louis heat island: The wind and temperature distribution. J. Appl. Meteorol., 1976. 15, pp. 417-440.
62. F. M. Vukovich, W. J. King, J. W. Dunn, and J. J. B. Worth. Observations and simulations of the diurnal variation of the urban heat island circulation and associated variations of the ozone distribution: A case study. J. Appl. Meteorol., 1979. 18:7, pp. 836-854.
63. R. W. Welch, J. Pugle, and W. G. Zdunkowski. Two-dimensional numerical simulation of the effects of air pollution upon the urban-rural complex. Tellus, 1978. 30, pp. 136-150.
64. J. M. White, F. D. Eaton, and A. H. Auer, Jr. The net radiation budget of the St. Louis metropolitan area. J. Appl. Meteorol., 1978. 17, pp. 539-599.
65. P. J. Wyatt, G. N. Plass, and V. R. Stull. The infrared transmittance of carbon dioxide. J. Appl. Optics, 1964a. 3:2, pp. 243-254.
66. P. J. Wyatt, G. N. Plass, and V. R. Stull. The infrared transmittance of water vapor. J. Appl. Optics, 1964b. 3:2, pp. 229-241.
67. G. Zanella. Il clima urbano di Parma. Riv. Meteorol. Aeronaut., 1976. 36, pp. 125-146.

APPENDIX A
HCMM DAYTIME GROUND TEMPERATURE ANALYSES
FOR ST. LOUIS, MO

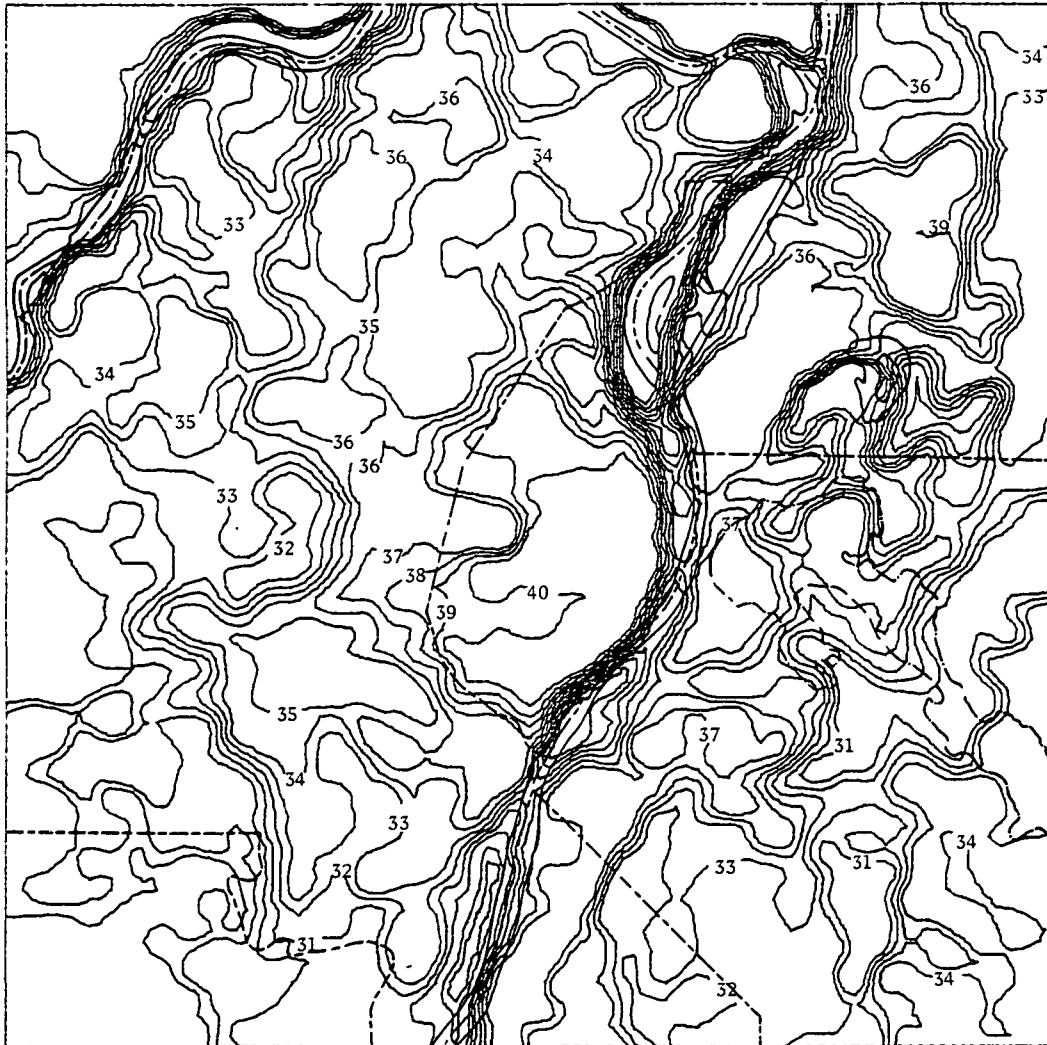


Figure 1A. HCMM daytime ground temperature ($^{\circ}\text{C}$) analysis for 10 June 1978.

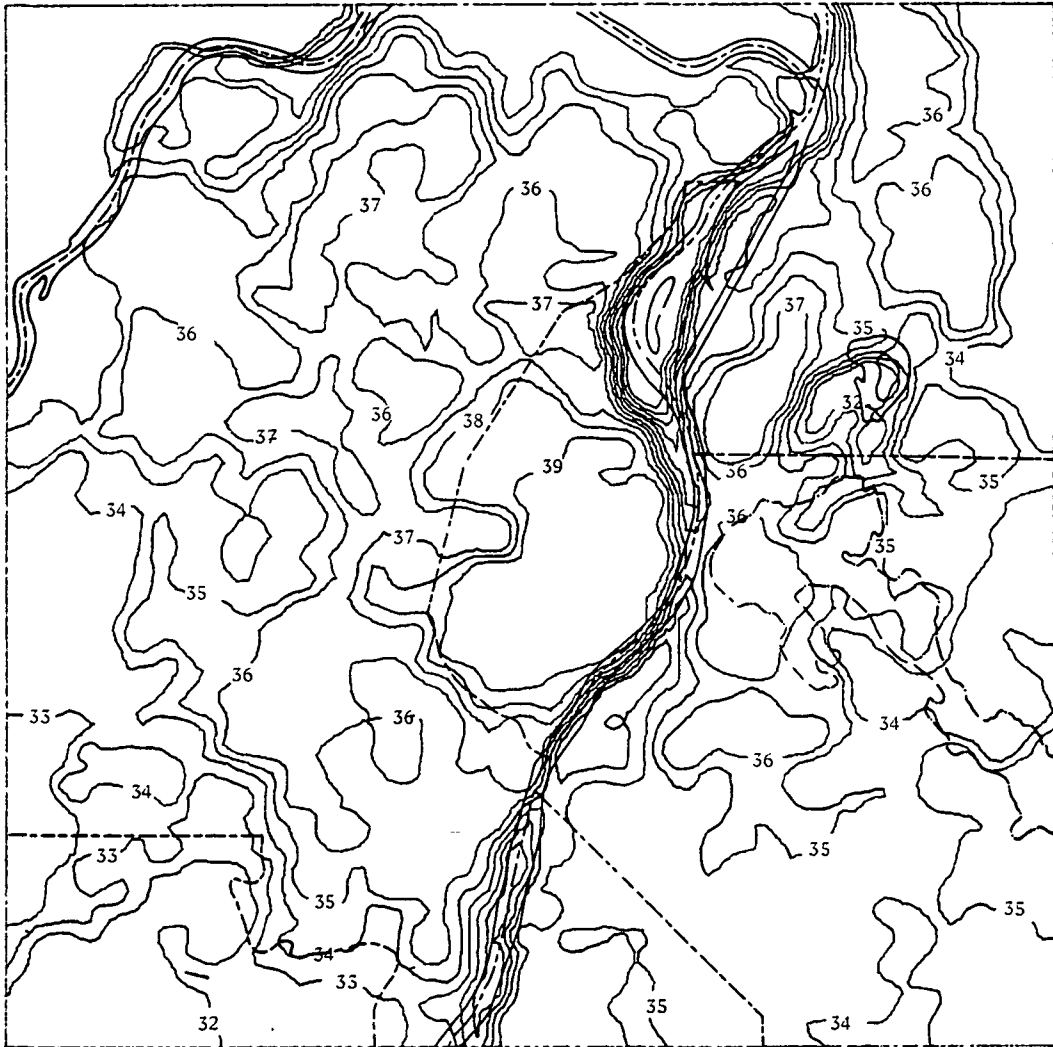


Figure 2A. HCMM daytime ground temperature ($^{\circ}\text{C}$) analysis for 26 June 1978.

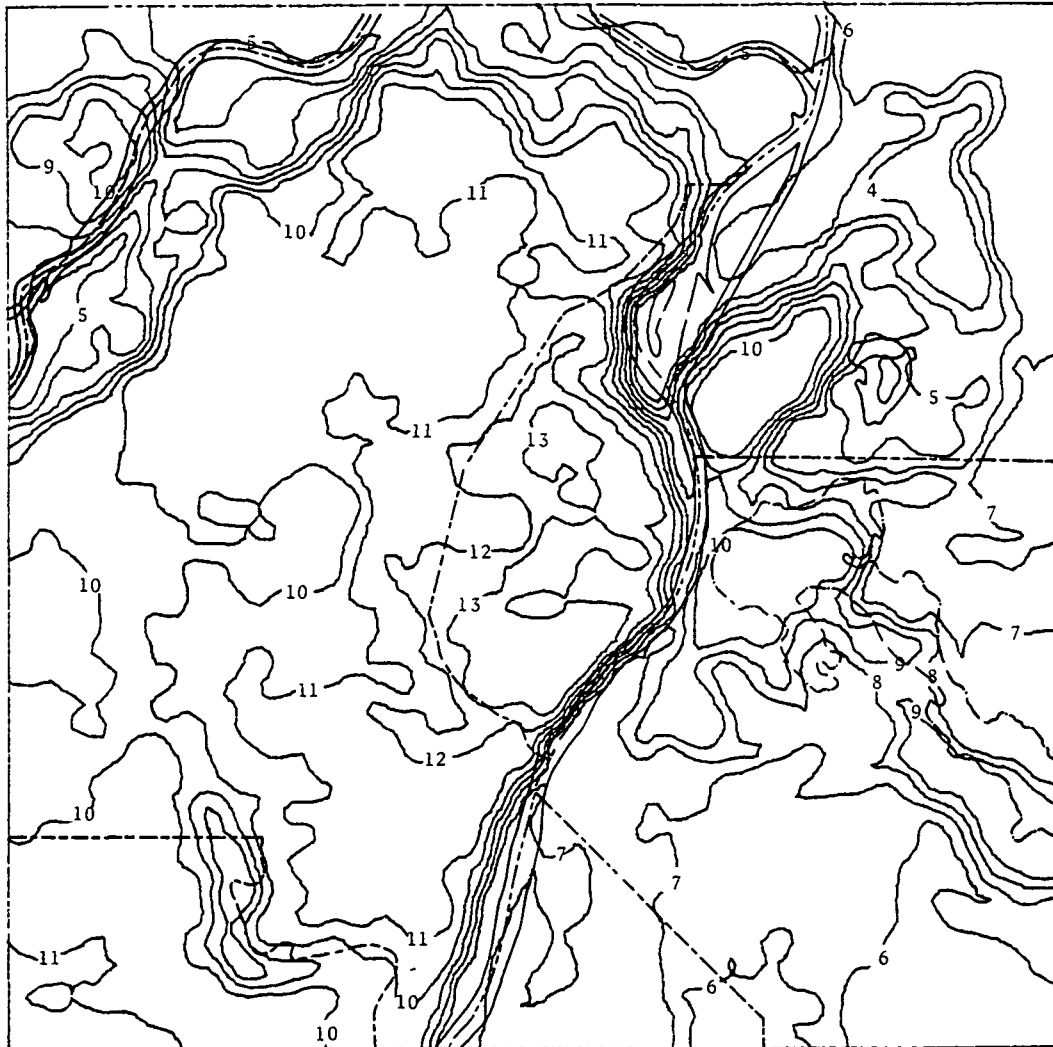


Figure 3A. HCMM daytime ground temperature ($^{\circ}\text{C}$) analysis for 26 February 1979.

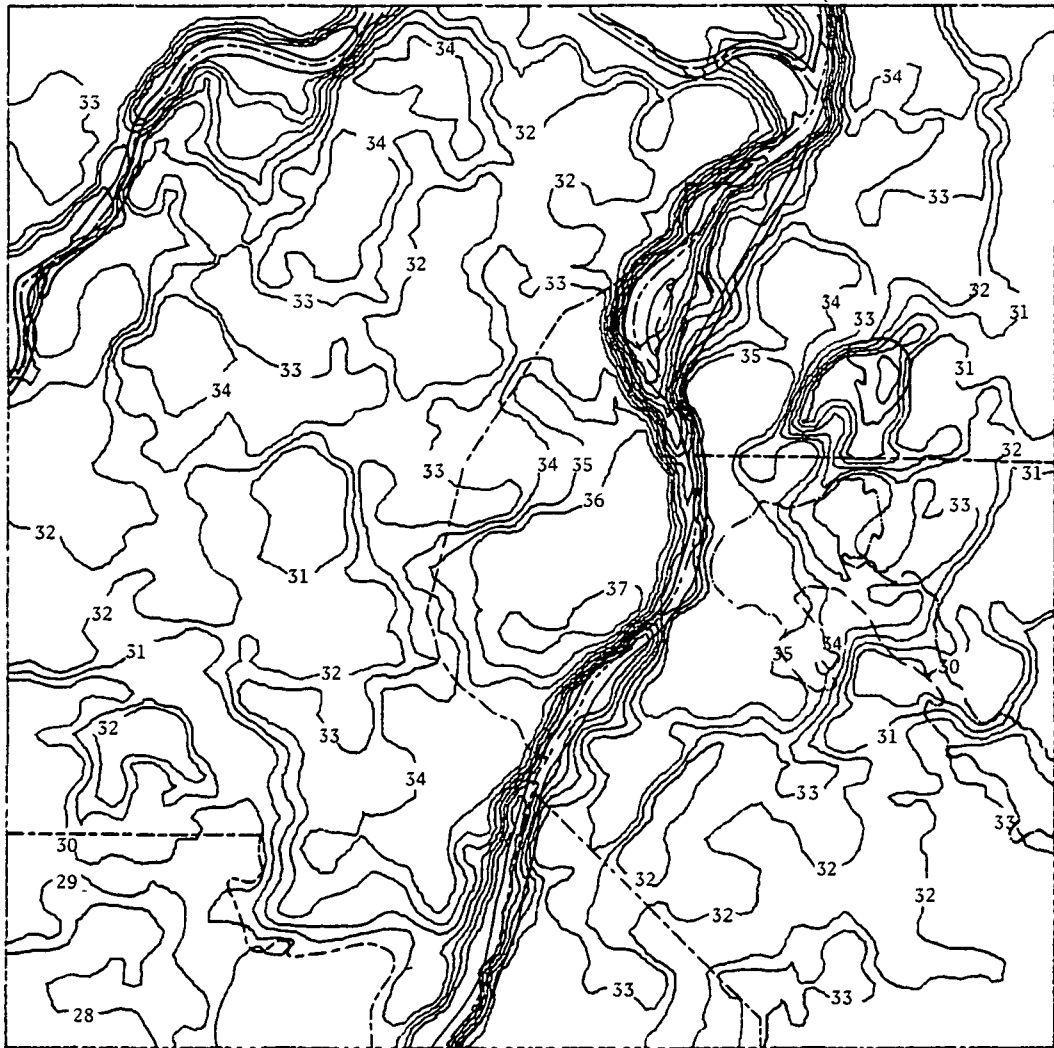


Figure 4A. HCMM daytime ground temperature (°C) analysis for 27 September 1979.

APPENDIX B
HCMM NIGHTTIME GROUND TEMPERATURE ANALYSES
FOR ST. LOUIS, MO



Figure 1B. HCMM nighttime ground temperature ($^{\circ}\text{C}$) analysis for 9 June 1978.

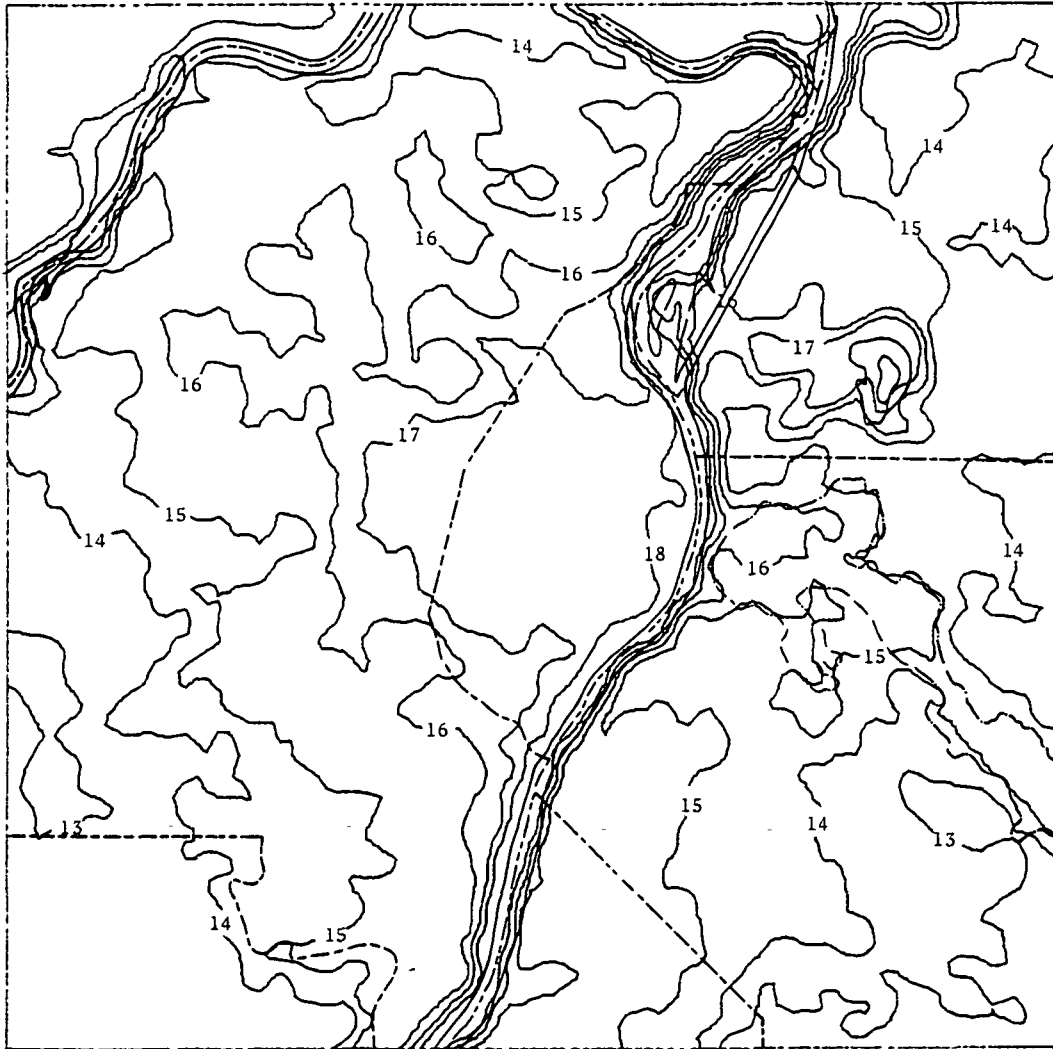


Figure 2B. HCMM nighttime ground temperature (°C) analysis for 14 June 1978.

APPENDIX C
HCMM REFLECTIVITY ANALYSES
FOR ST. LOUIS, MO

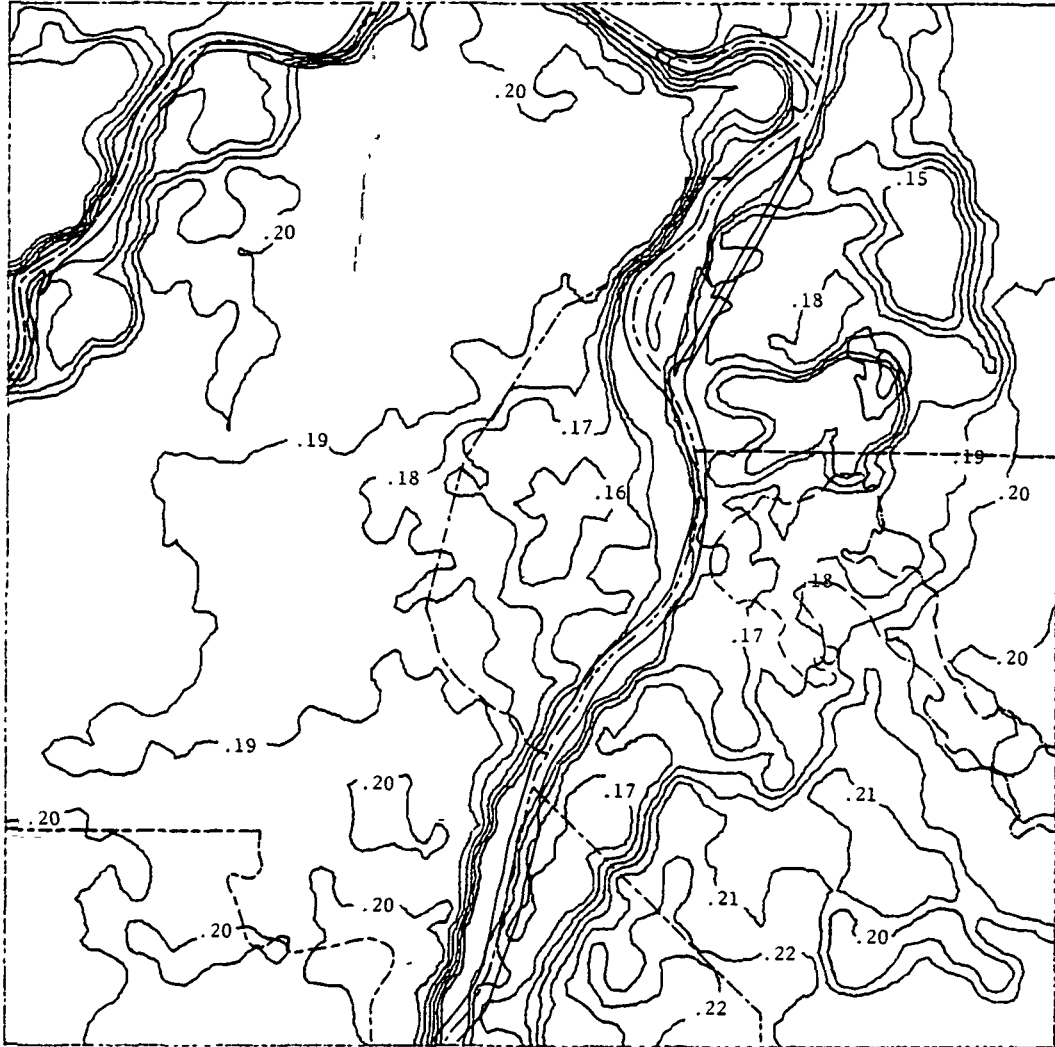


Figure 1C. Reflectivity distribution for 10 June 1978.

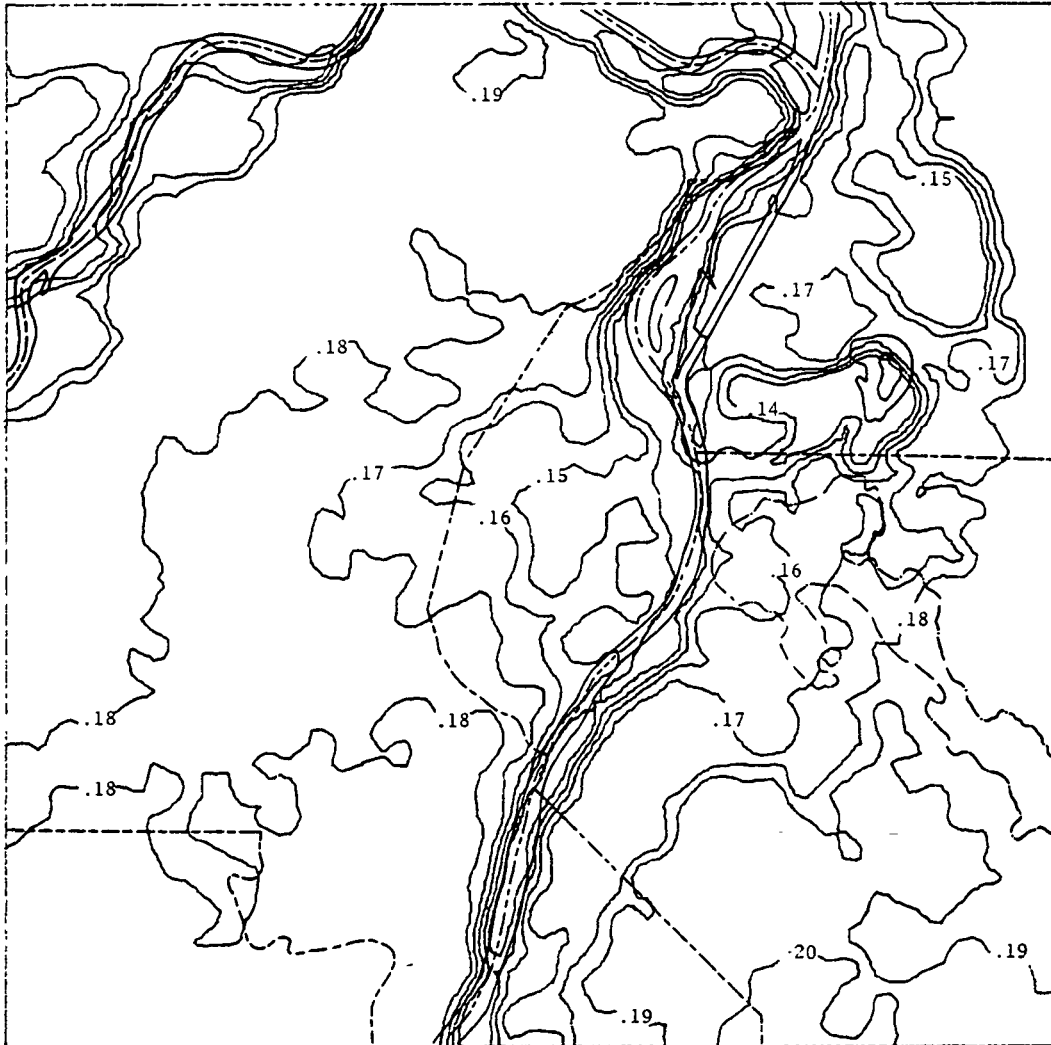


Figure 2C. Reflectivity distribution for 26 June 1978.

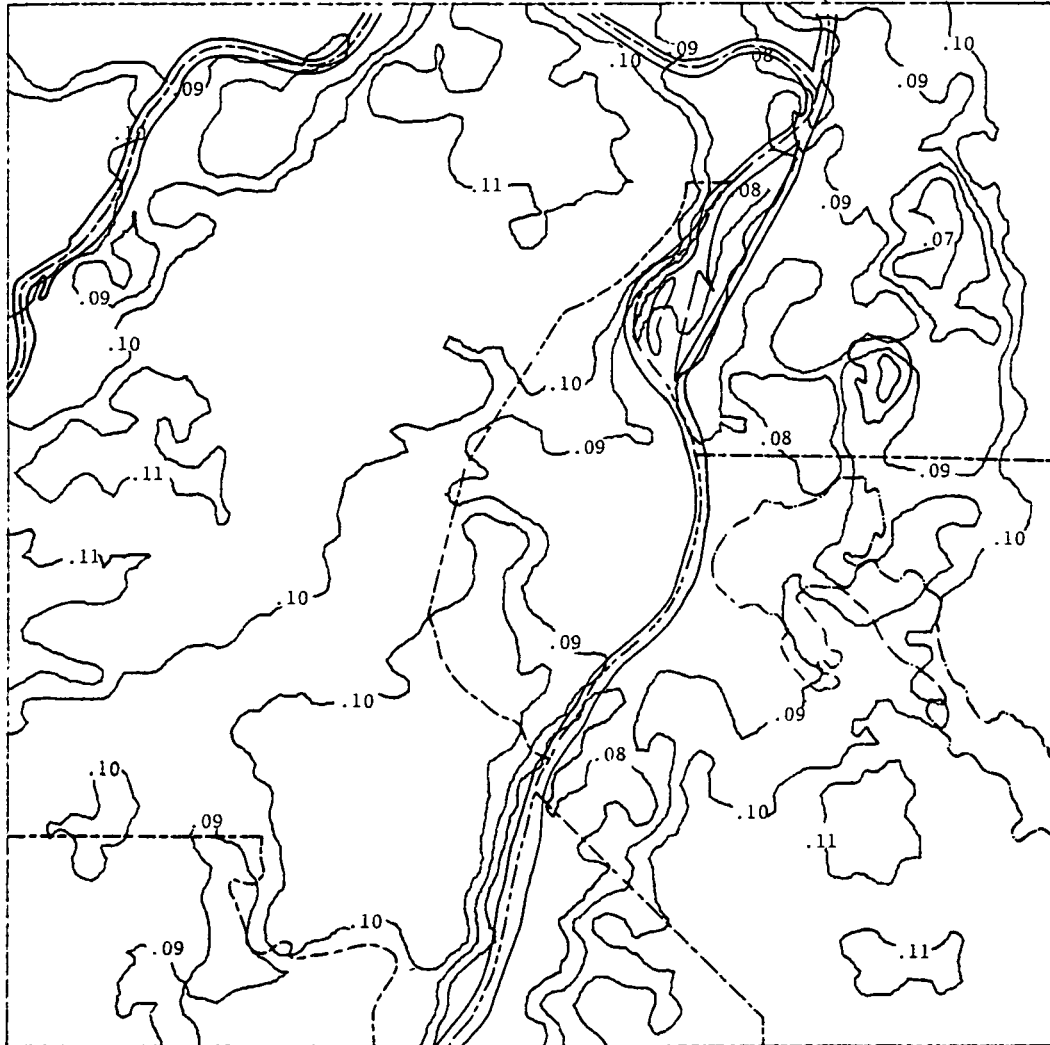


Figure 3C. Reflectivity distribution for 26 February 1979.

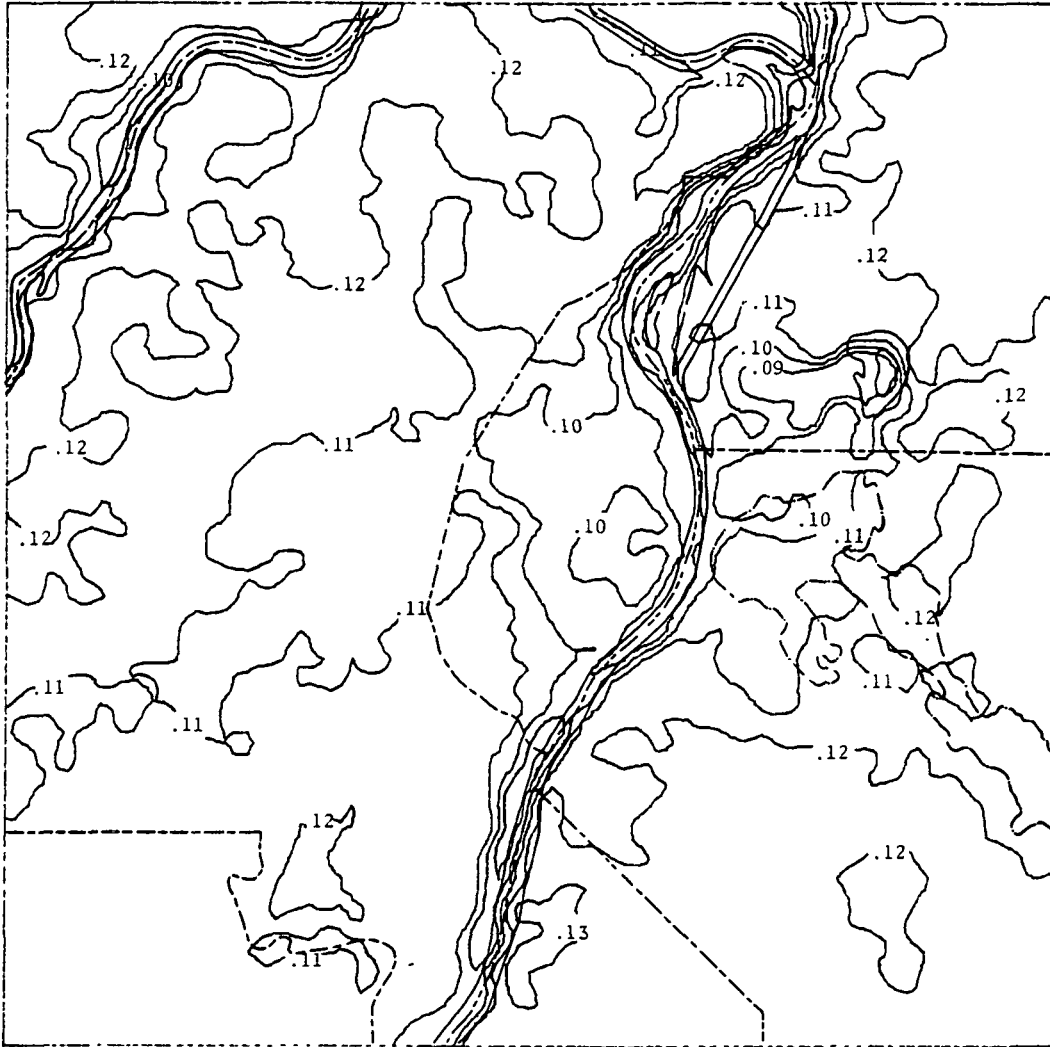


Figure 4C. Reflectivity distribution for 27 September 1979.

APPENDIX D
DAYTIME SURFACE HEAT FLUX ANALYSES

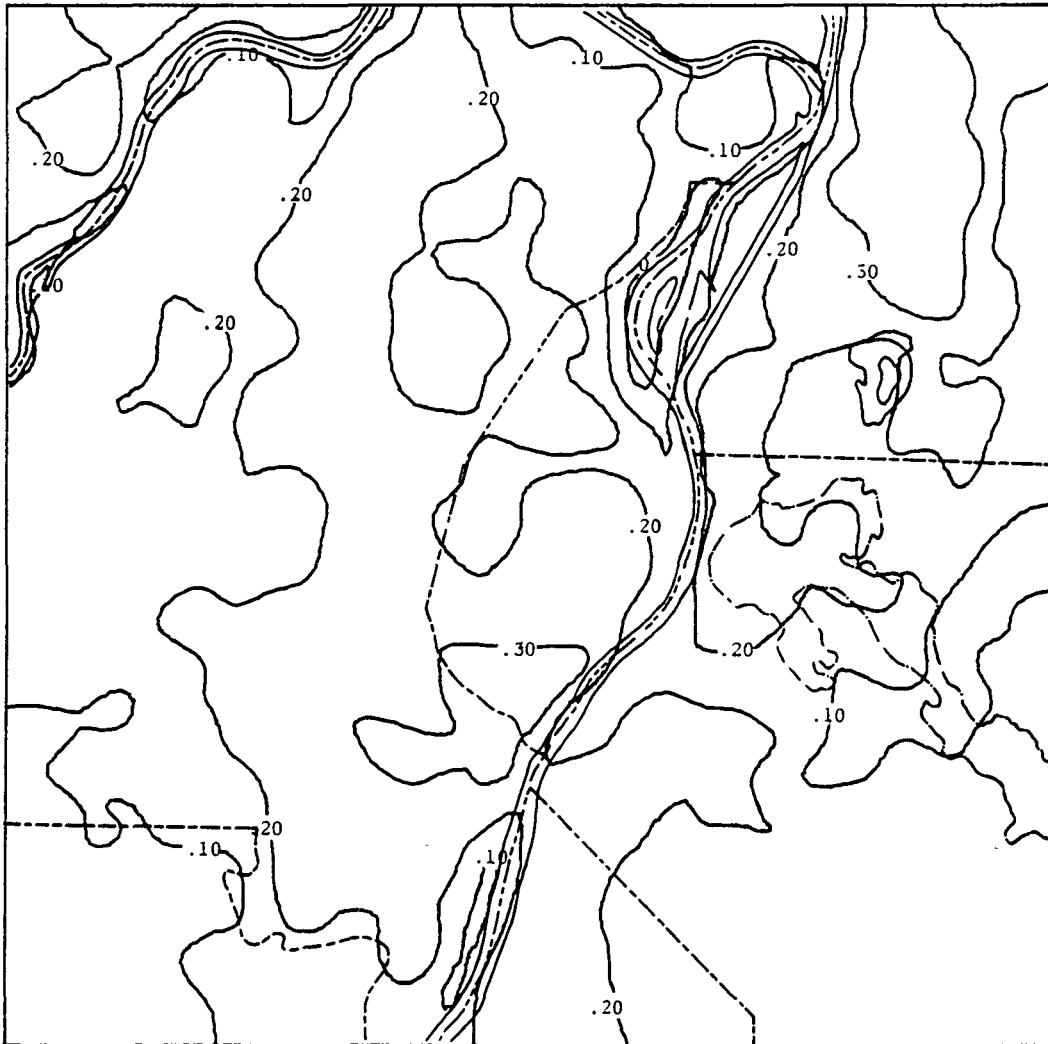


Figure 1D. Surface heat flux ($\text{kJ m}^{-2} \text{s}^{-1}$) distribution for 10 June 1978.

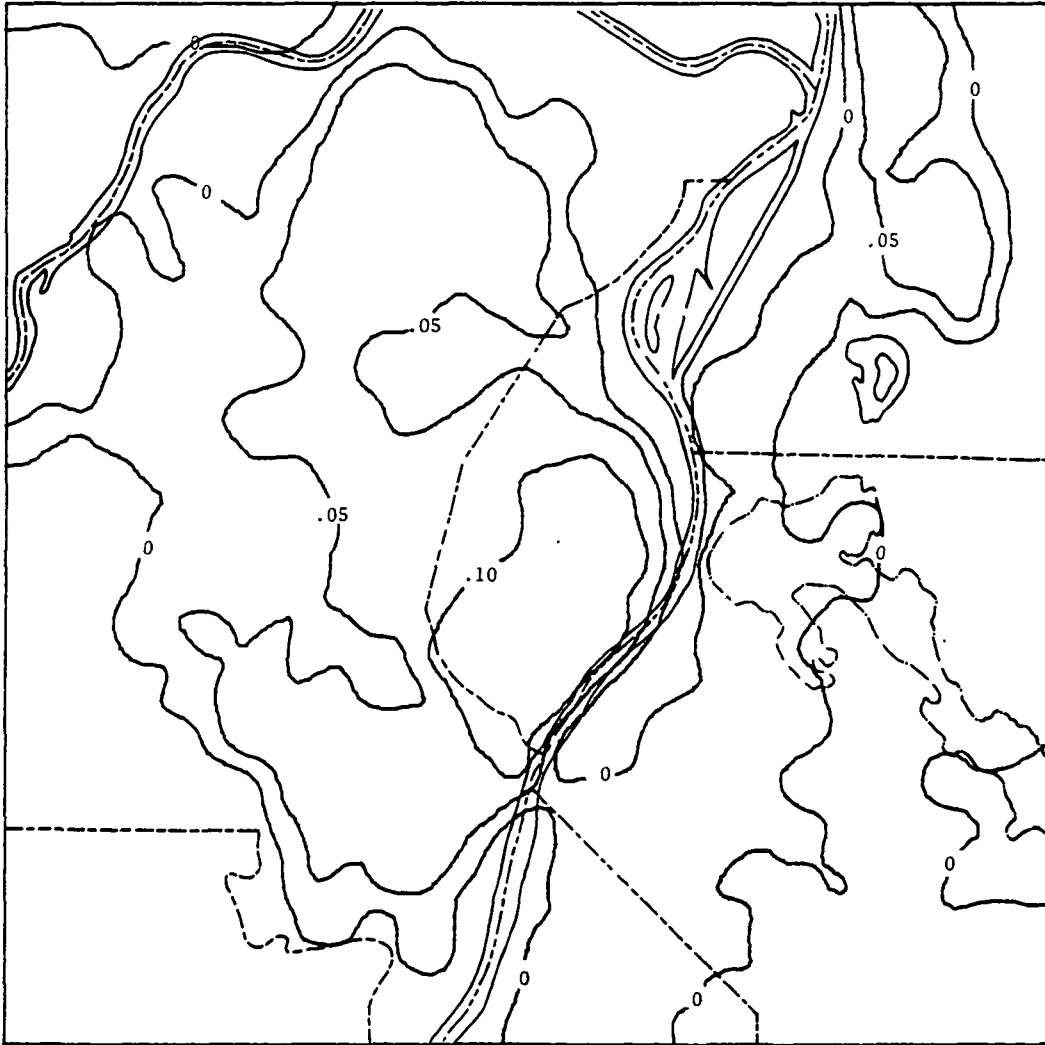


Figure 2D. Surface heat flux ($\text{kJ m}^{-2} \text{s}^{-1}$) distribution for 26 June 1978.

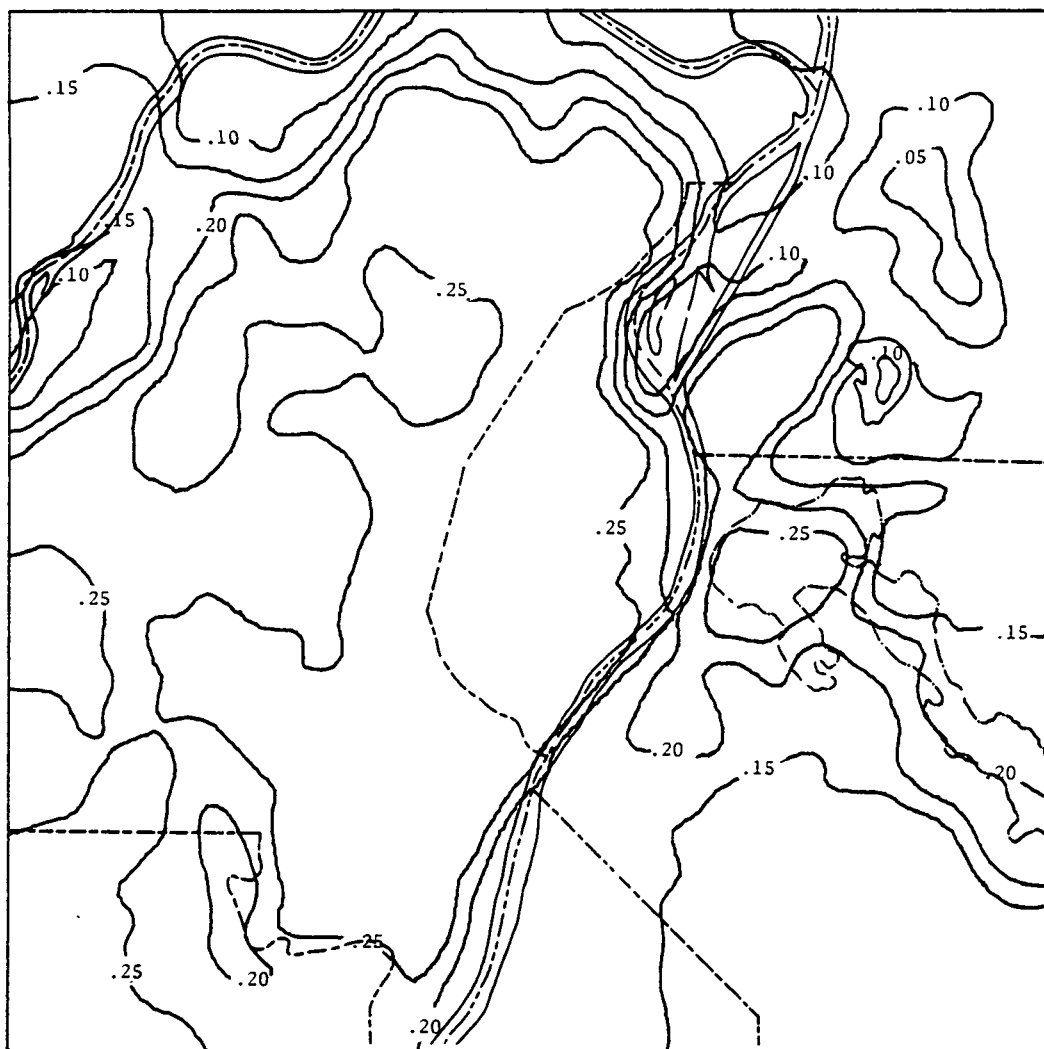


Figure 3D. Surface heat flux ($\text{kJ m}^{-2} \text{s}^{-1}$) distribution for 26 February 1979.

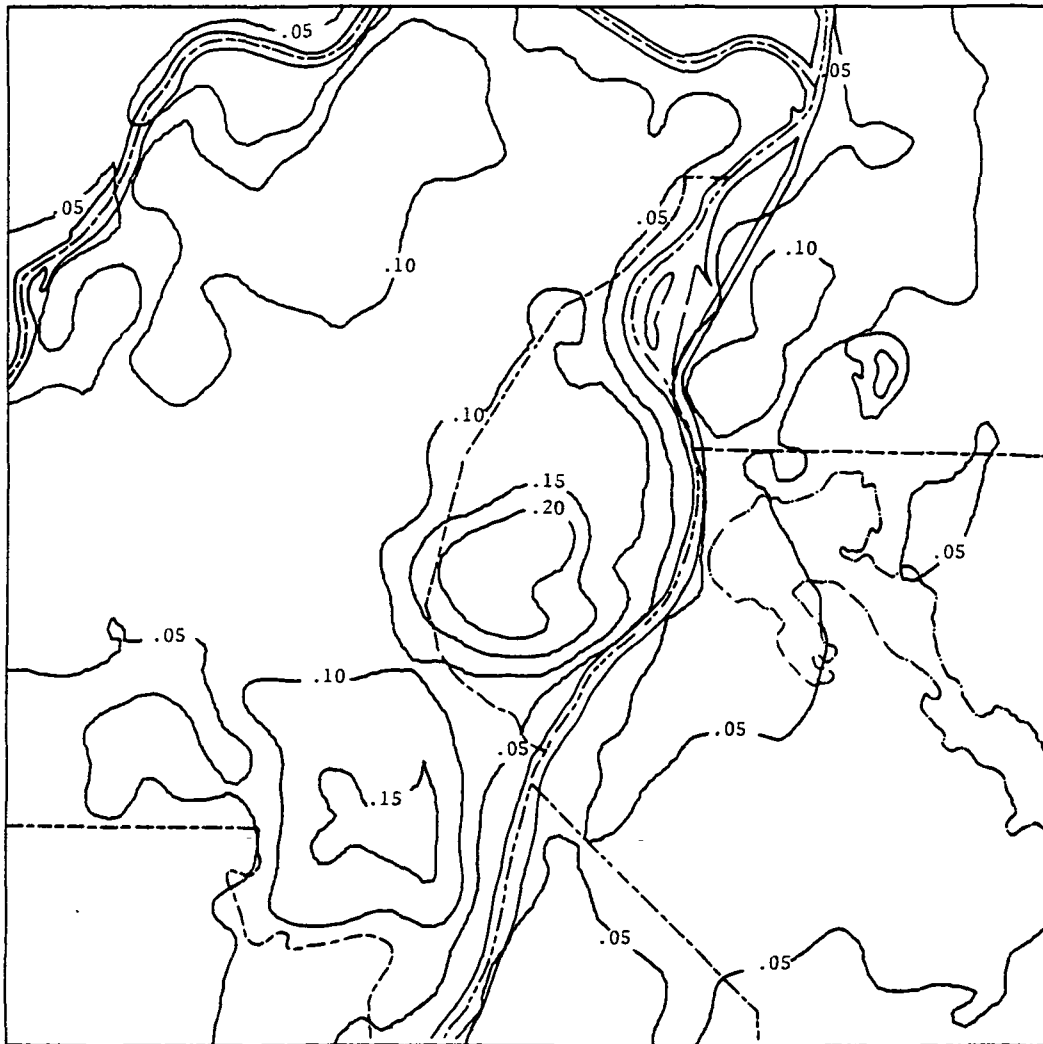


Figure 4D. Surface heat flux ($\text{kJ m}^{-2} \text{s}^{-1}$) distribution for 27 September 1979.

APPENDIX E
NIGHTTIME SURFACE HEAT FLUX ANALYSES

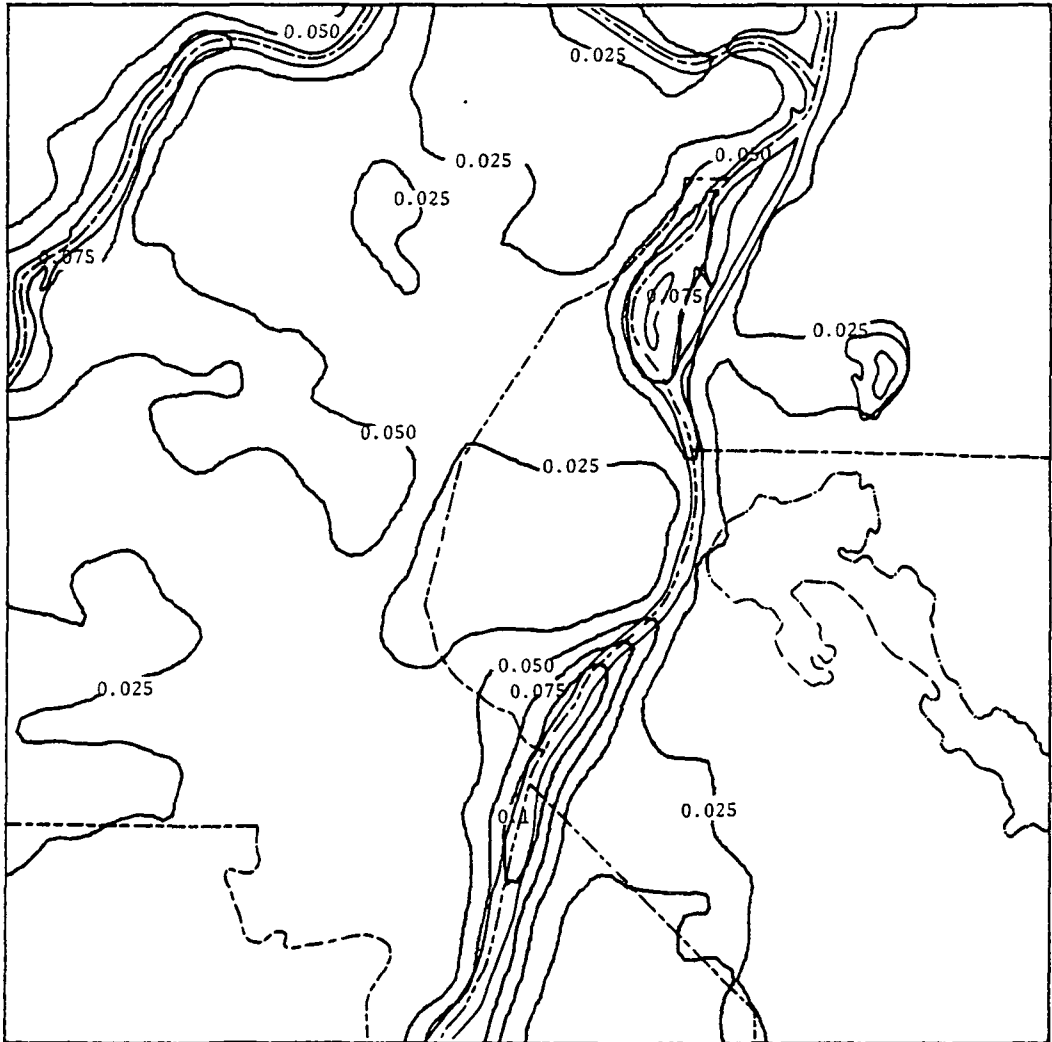


Figure 1E. Surface heat flux ($\text{kJ m}^{-2} \text{s}^{-1}$) distribution for 9 June 1978.

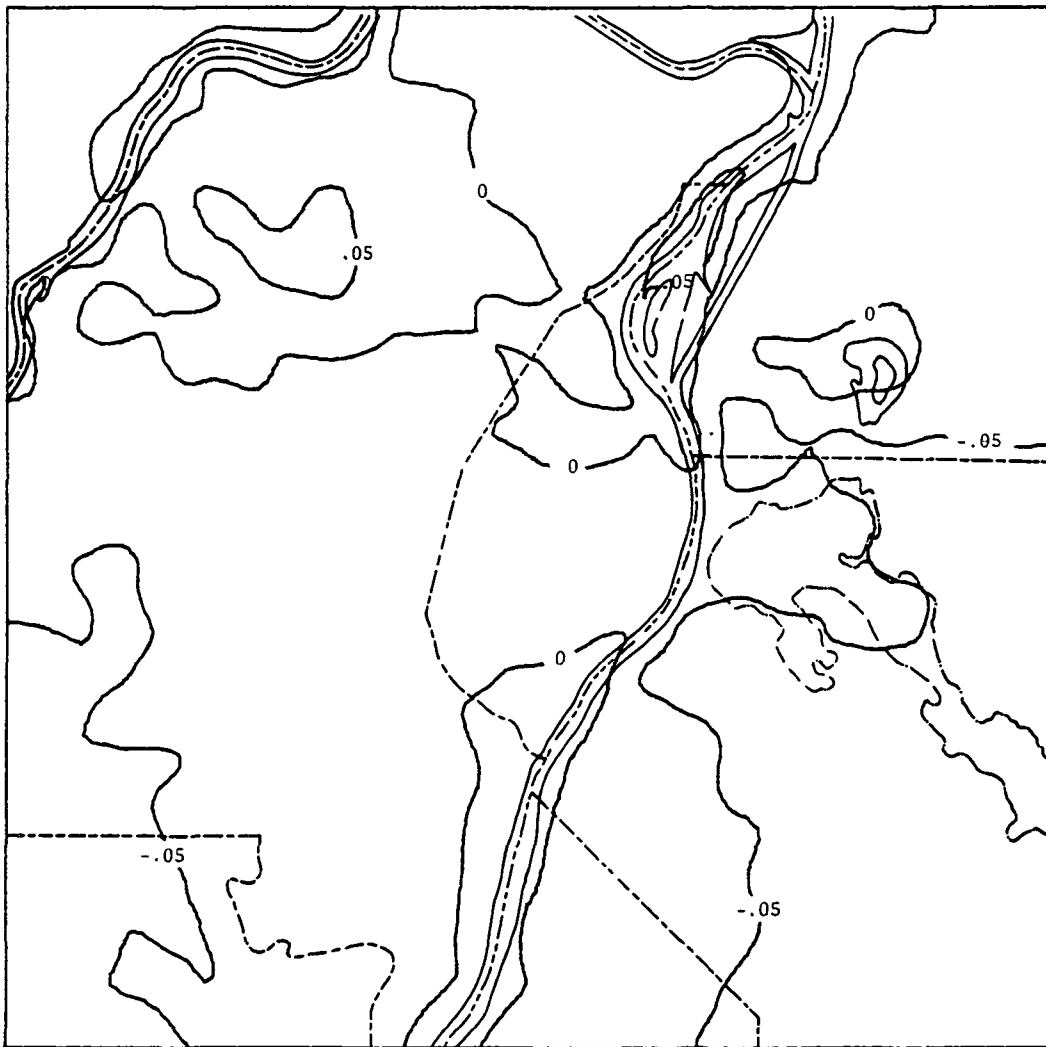


Figure 2E. Surface heat flux ($\text{kJ m}^{-2} \text{s}^{-1}$) distribution for 14 June 1978.

APPENDIX F
THE DAYTIME SPECIFIC HUMIDITY
DEPRESSION DISTRIBUTION

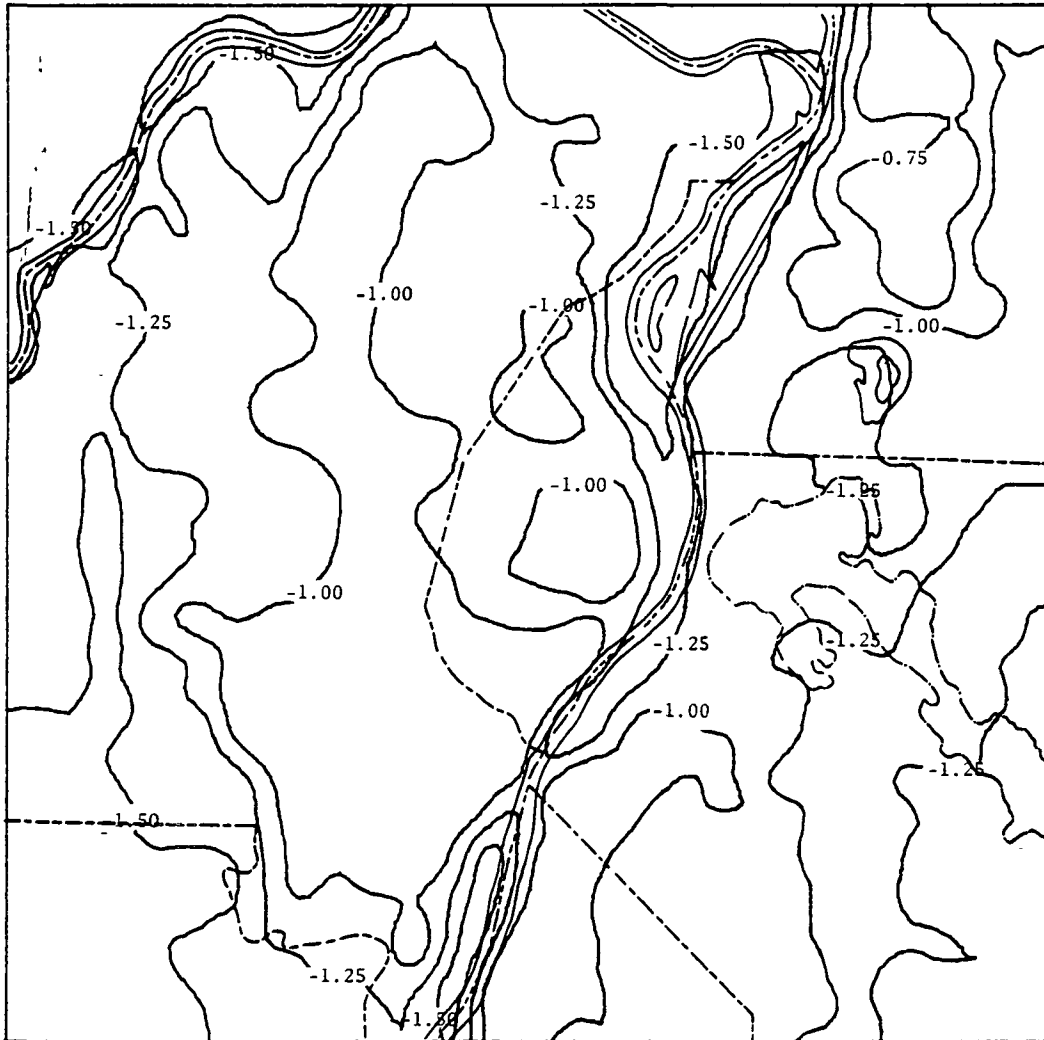


Figure 1F. The distribution of the specific humidity ($10^{-1} \text{ g kg}^{-1}$) depression for 10 June 1978.



Figure 2F. The distribution of the specific humidity ($10^{-1} \text{ g kg}^{-1}$) depression for 26 June 1978.

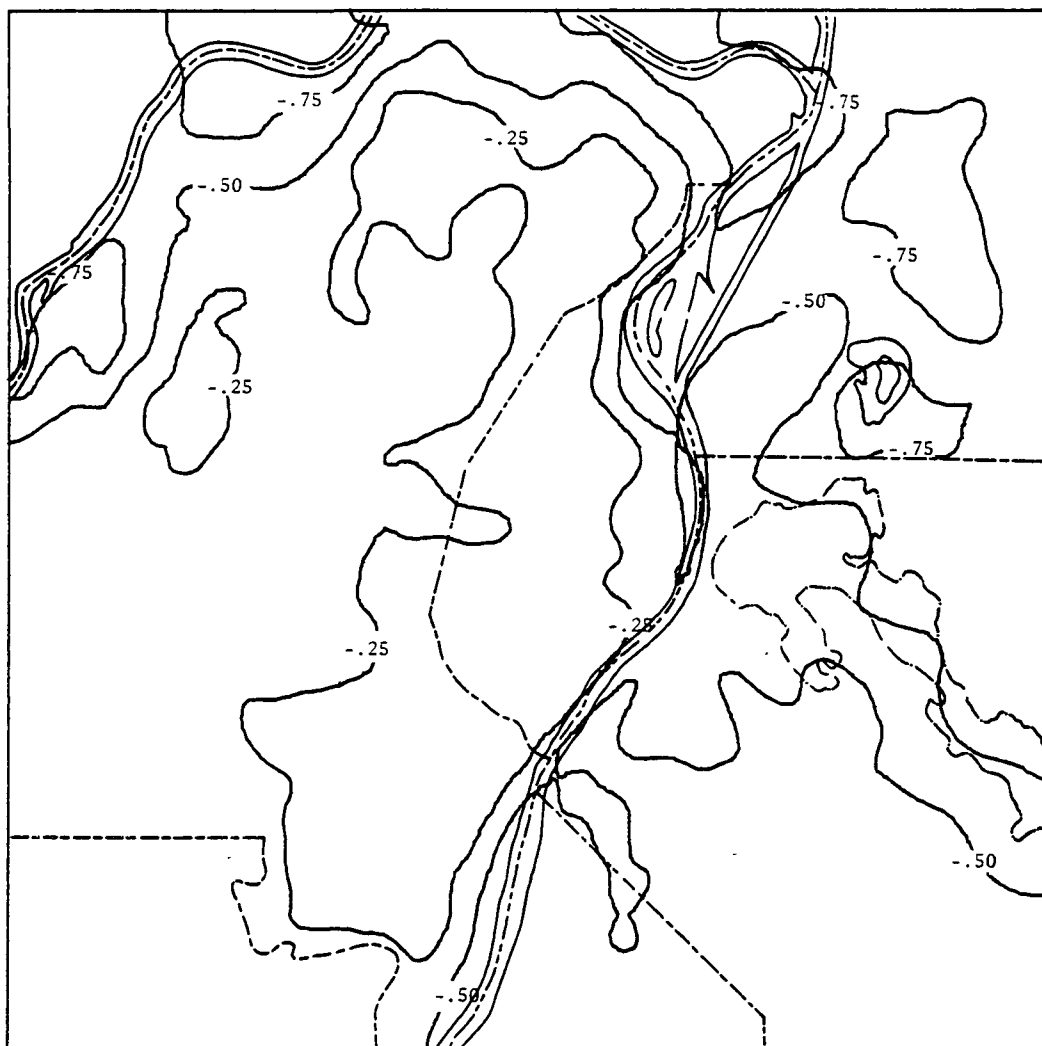


Figure 3F. The distribution of the specific humidity ($10^{-1} \text{ g kg}^{-1}$) depression for 26 February 1979.

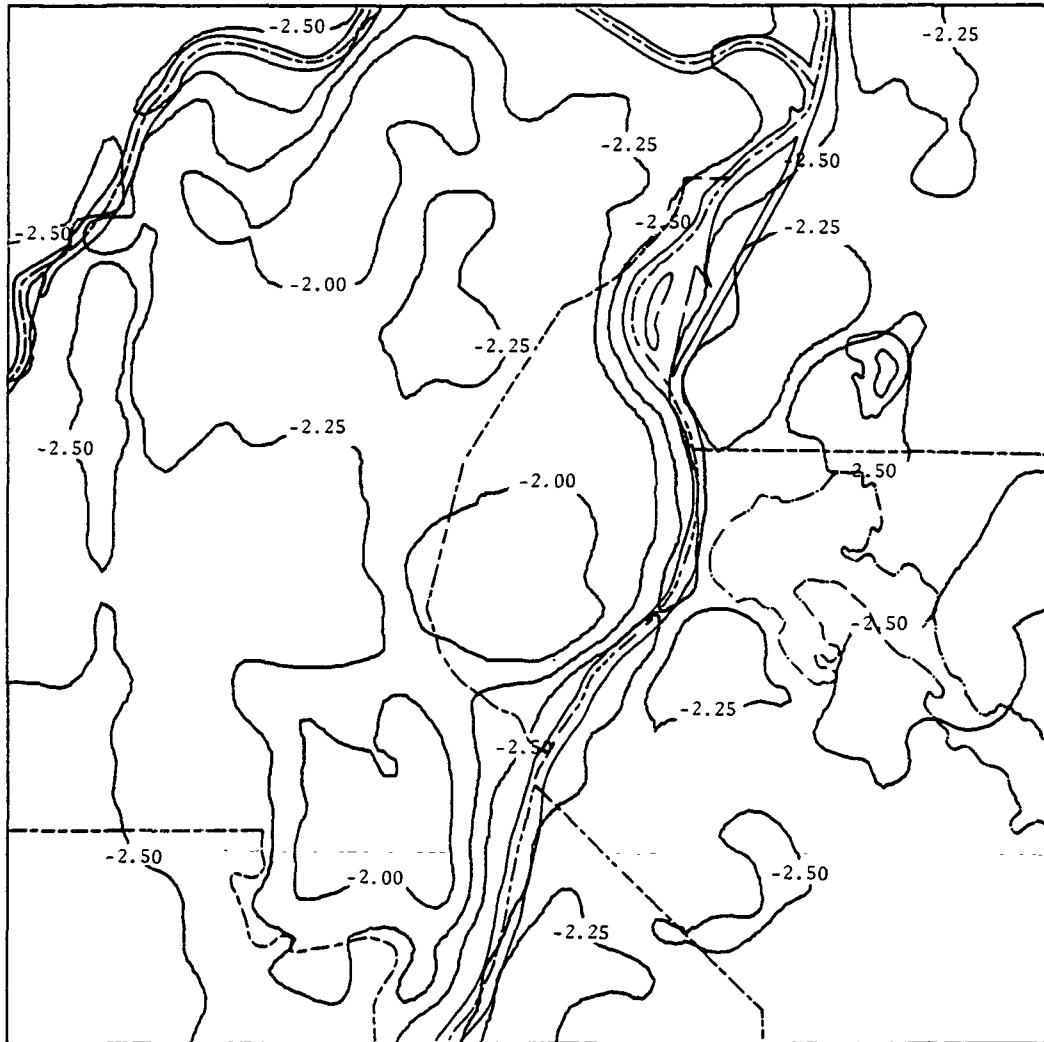


Figure 4F. The distribution of the specific humidity ($10^{-1} \text{ g kg}^{-1}$) depression for 27 September 1979.

APPENDIX G
THE NIGHTTIME SPECIFIC HUMIDITY
DEPRESSION DISTRIBUTION

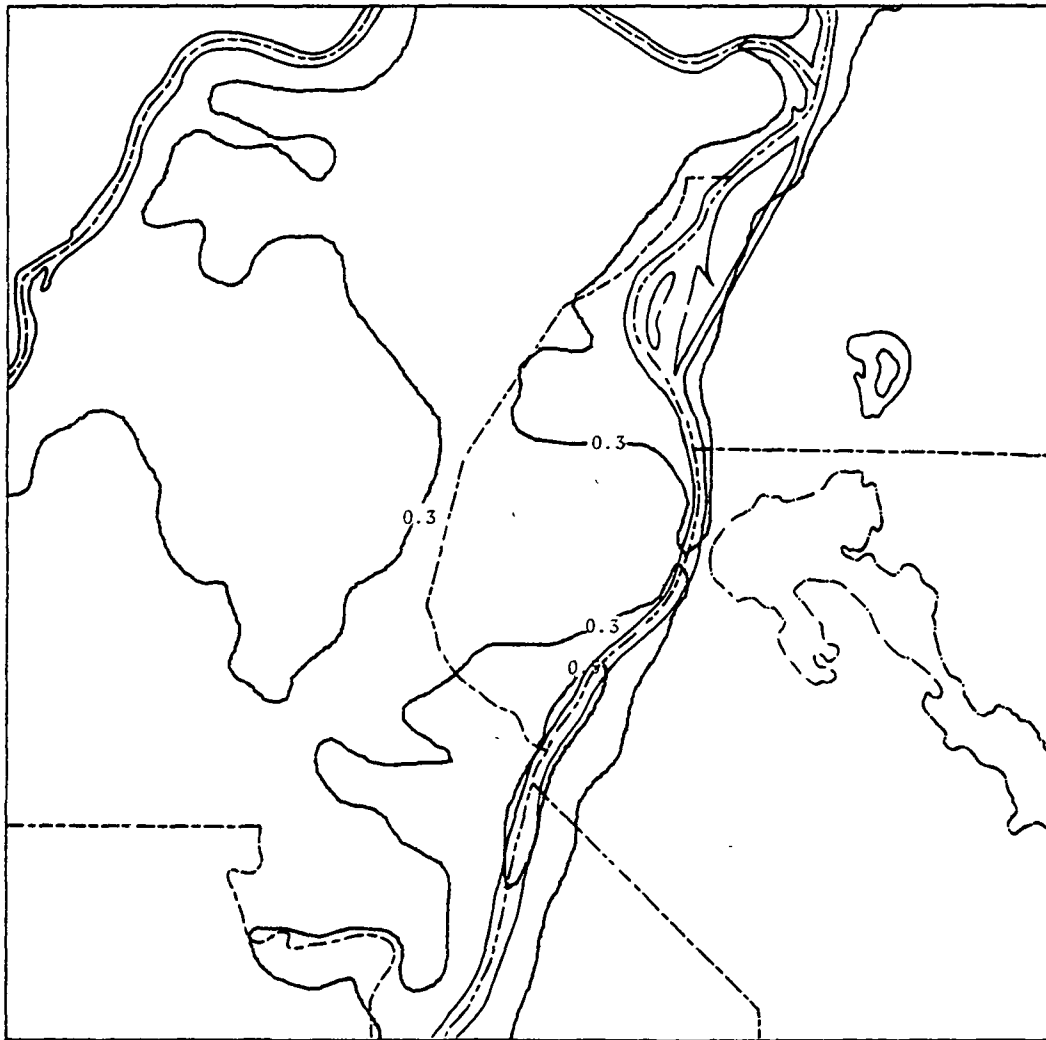


Figure 1G. The distribution of the specific humidity ($10^{-1} \text{ g kg}^{-1}$) depression for 9 June 1978.

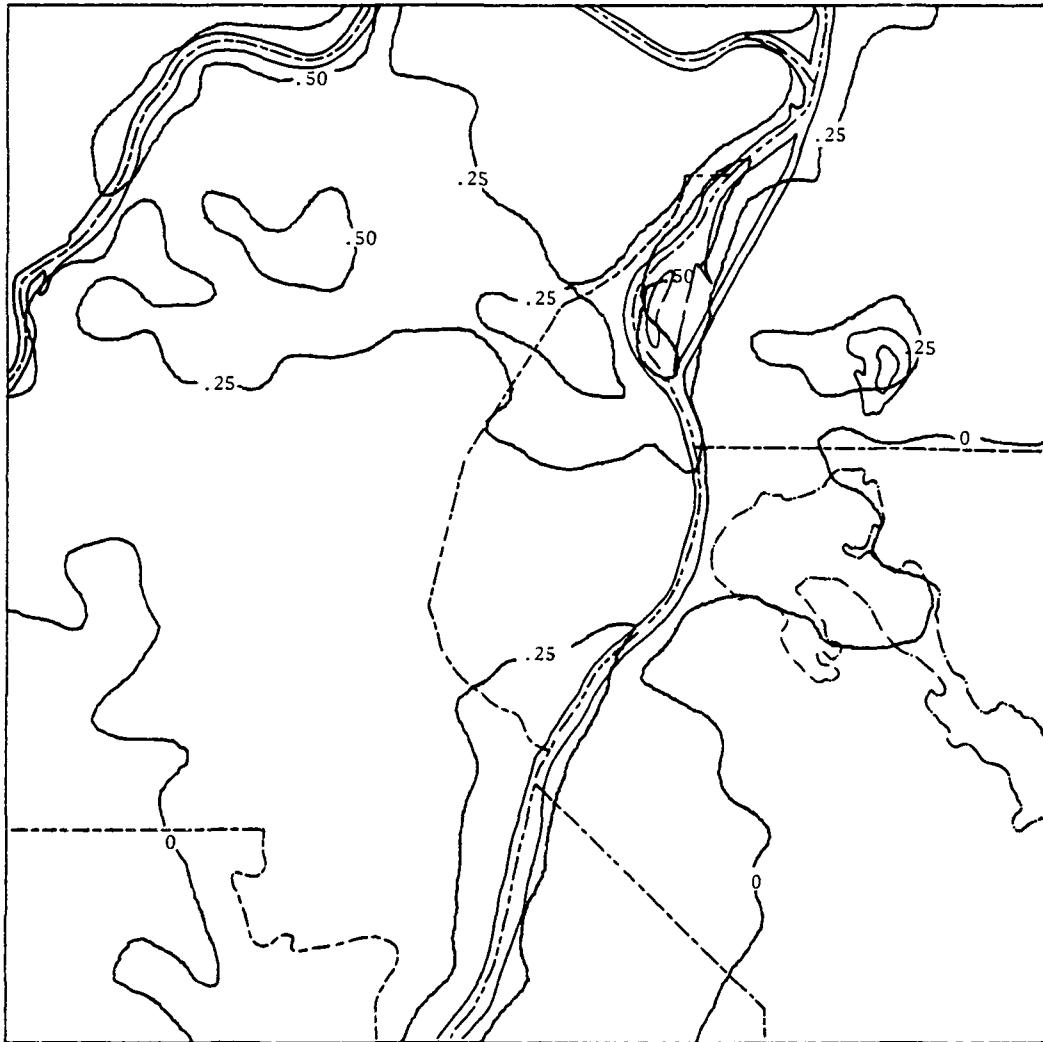


Figure 2G. The distribution of the specific humidity ($10^{-1} \text{ g kg}^{-1}$) depression for 14 June 1978.

APPENDIX H
THE DISTRIBUTION OF THE EDDY VISCOSITY
FOR THE DAYTIME CASES

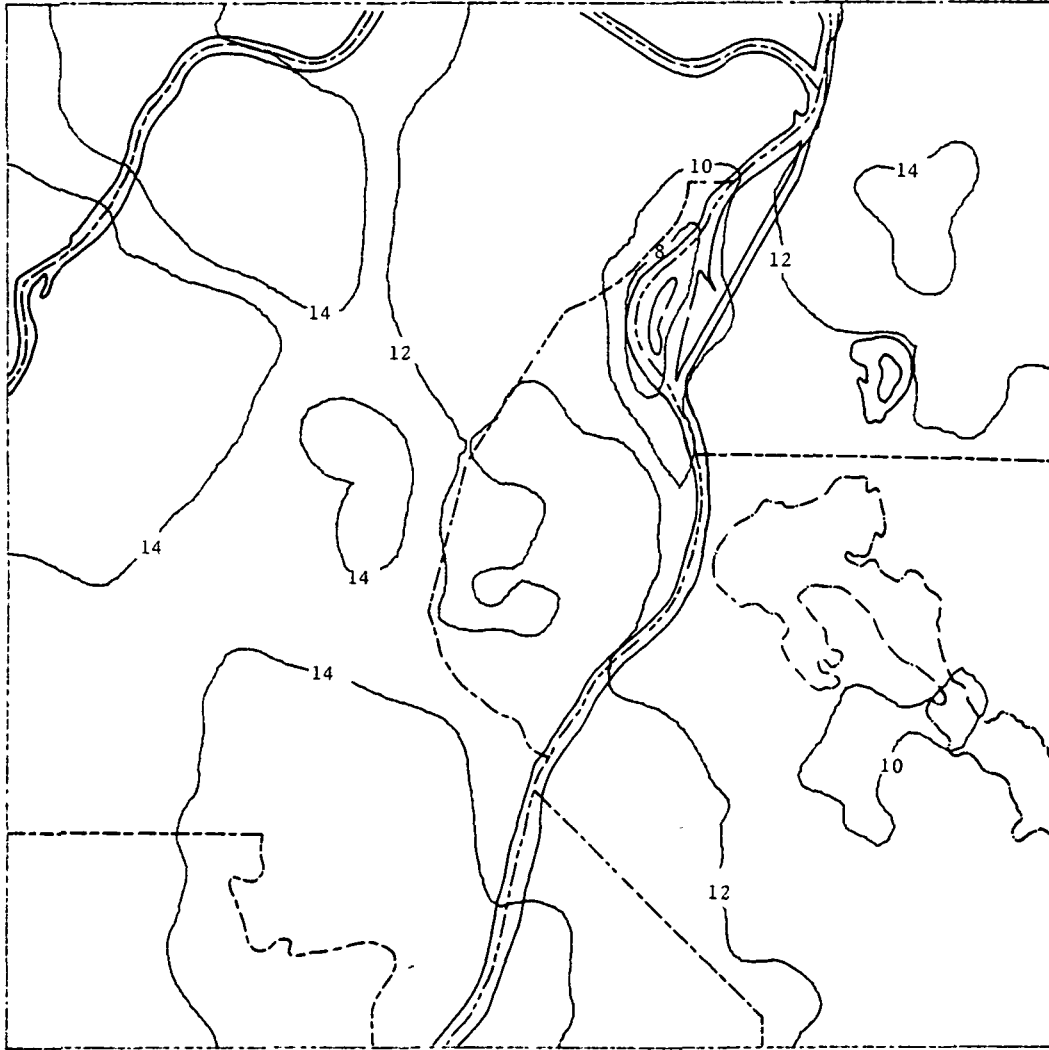


Figure 1H. The distribution of the eddy viscosity ($\text{m}^2 \text{s}^{-1}$) for 10 June 1978.

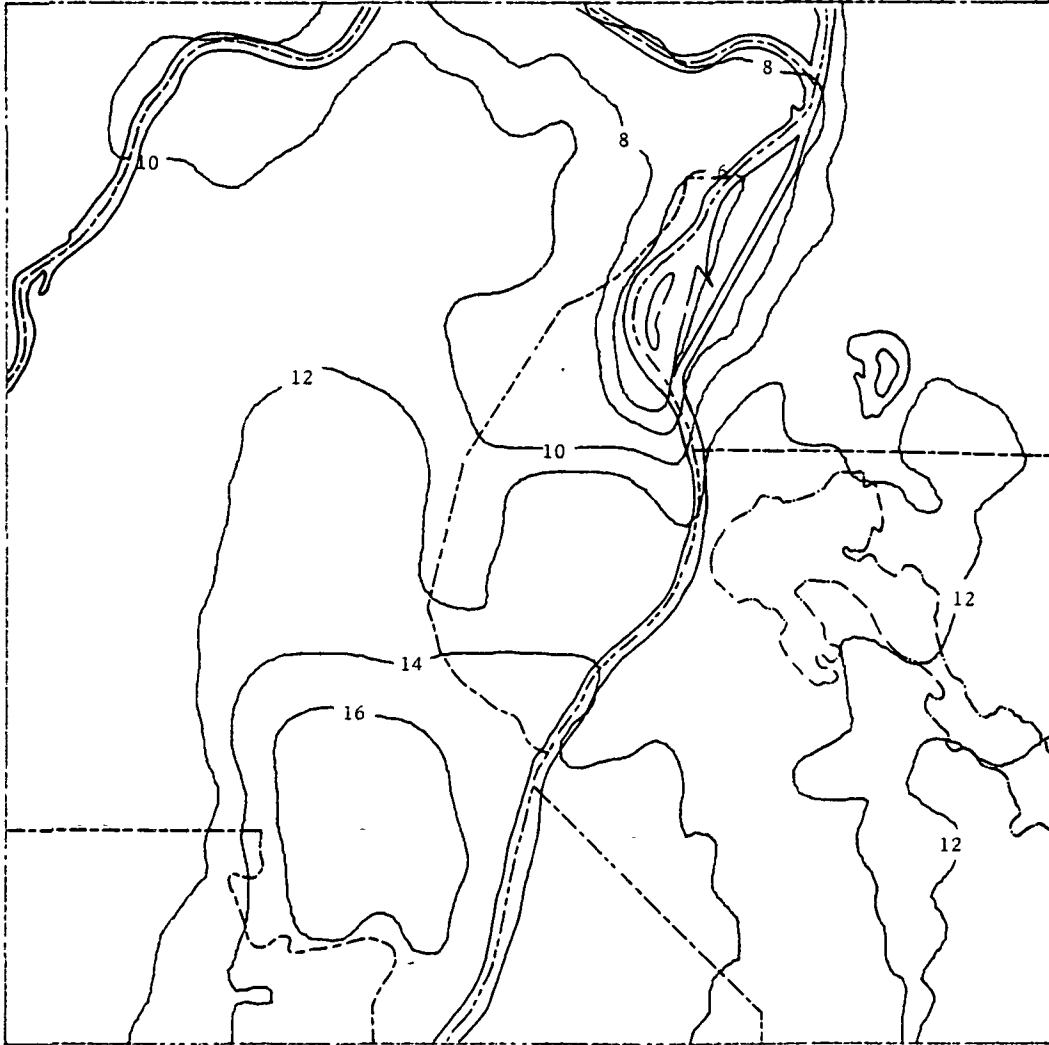


Figure 2H. The distribution of the eddy viscosity ($\text{m}^2 \text{s}^{-1}$) for 26 June 1978.

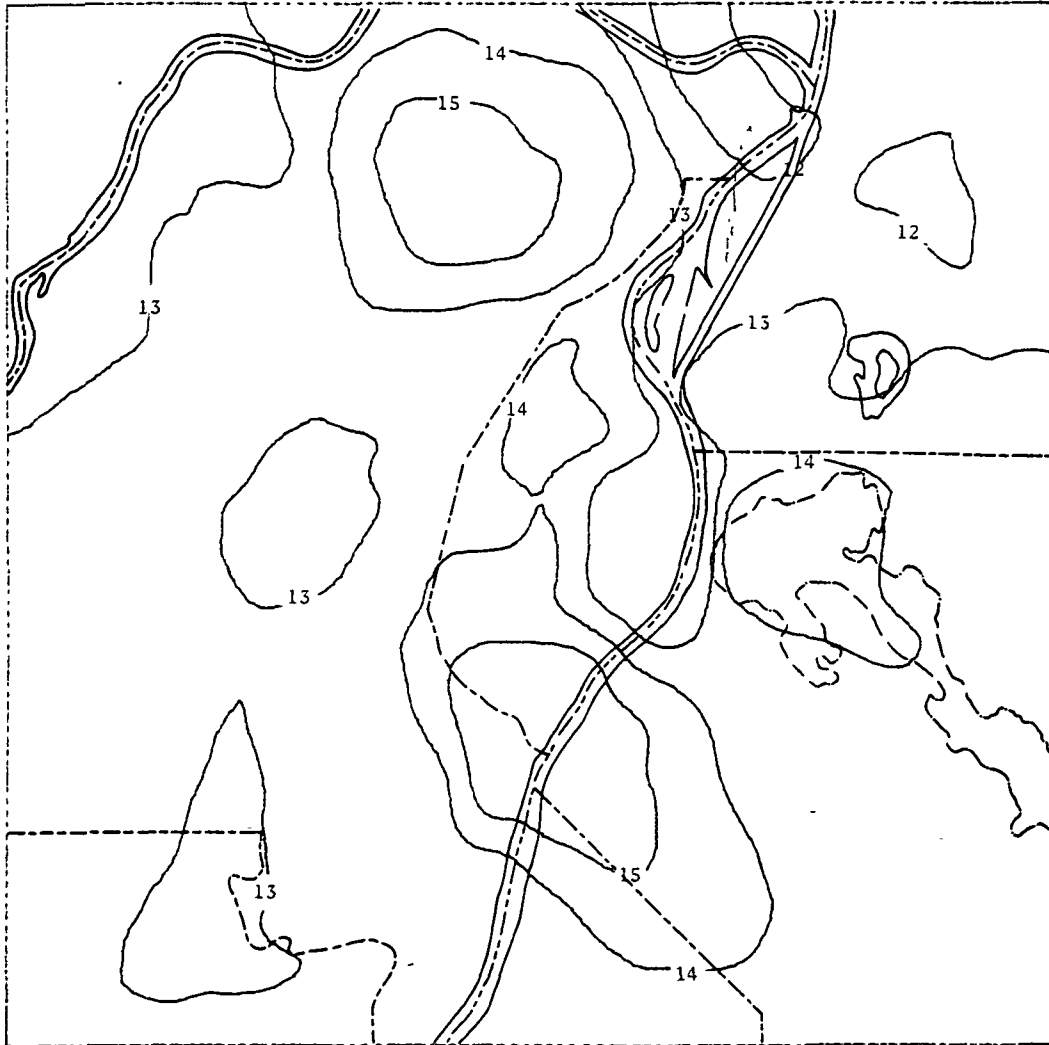


Figure 3H. The distribution of the eddy viscosity ($\text{m}^2 \text{s}^{-1}$) for 26 February 1979.



Figure 4H. The distribution of the eddy viscosity ($\text{m}^2 \text{s}^{-1}$) for 27 September 1979.

APPENDIX I
THE DISTRIBUTION OF THE EDDY VISCOSITY
FOR THE NIGHTTIME CASES

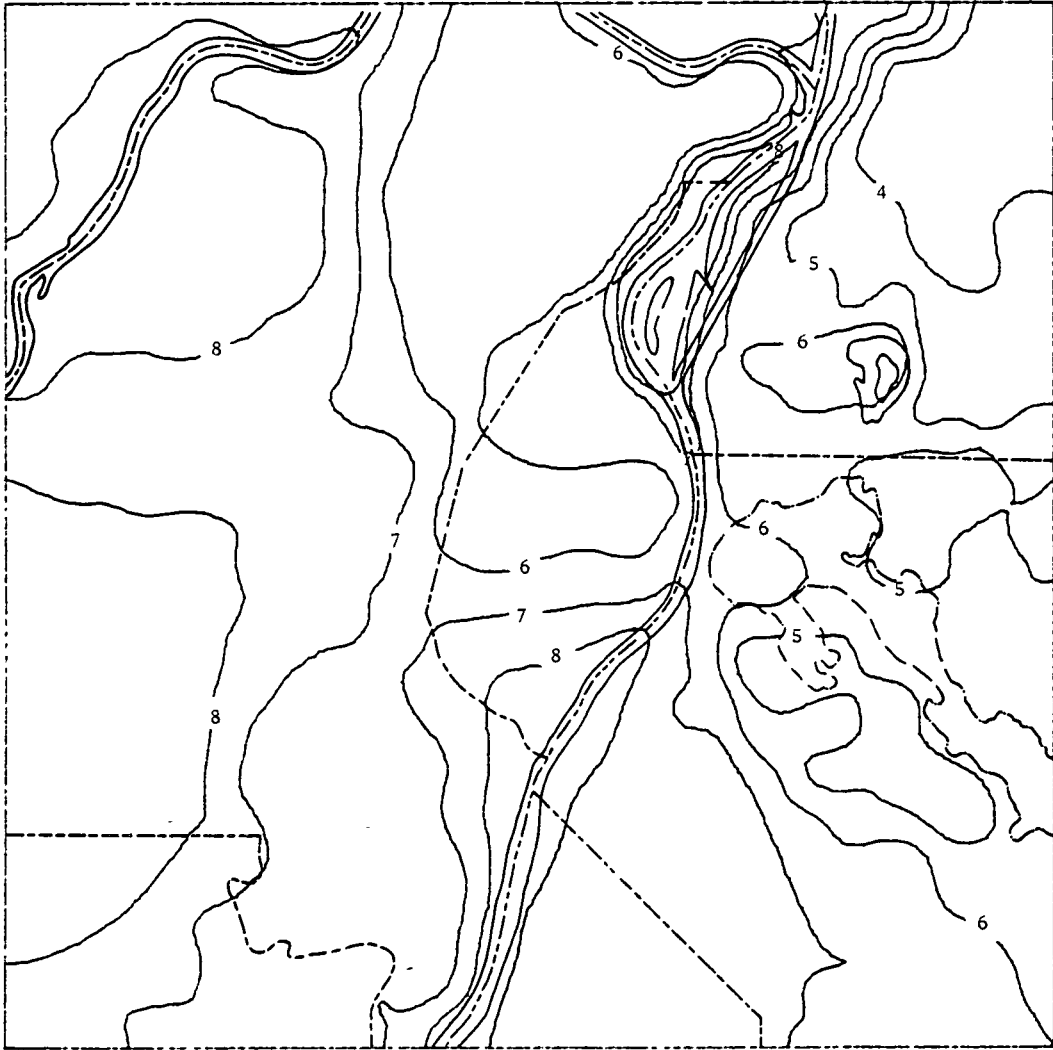


Figure 11. The distribution of the eddy viscosity ($\text{m}^2 \text{s}^{-1}$) for 9 June 1978.

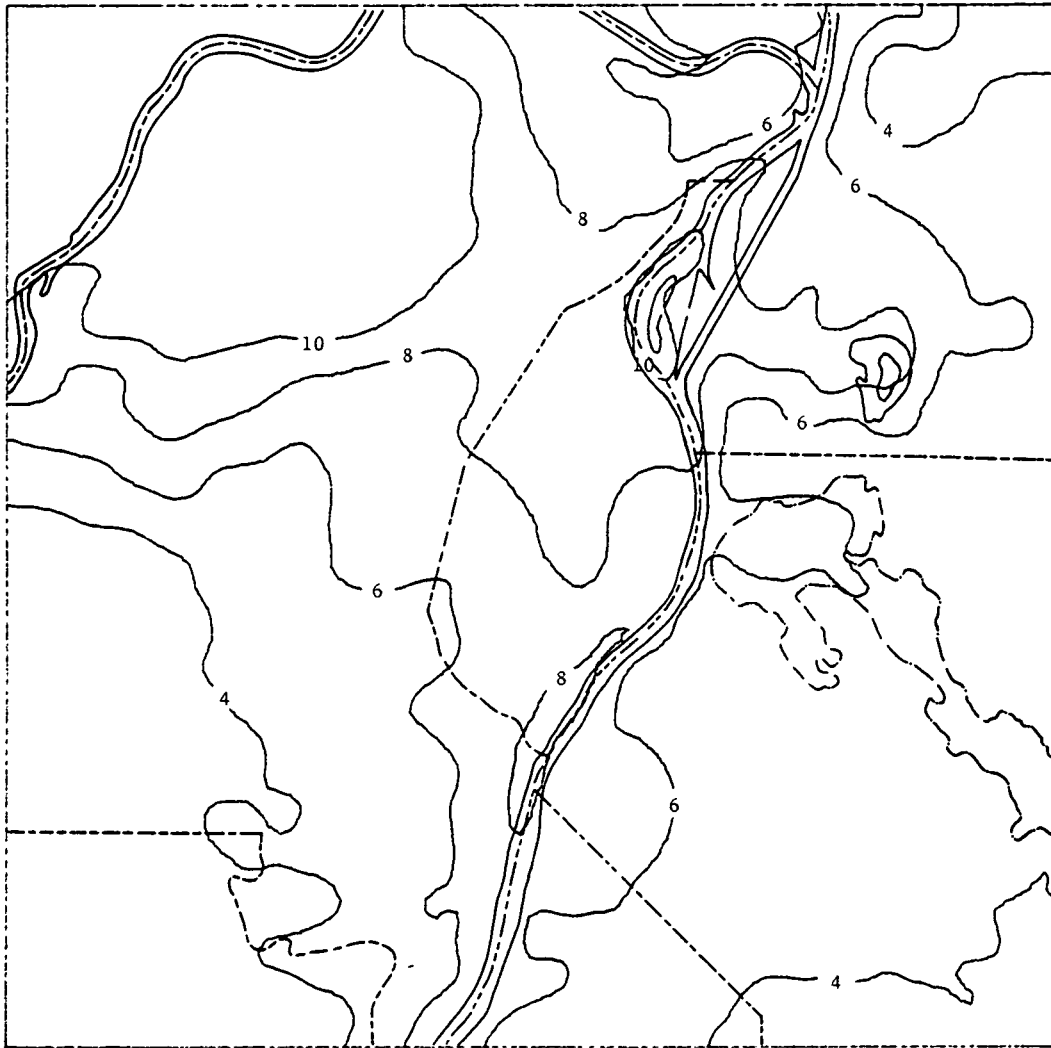


Figure 2I. The distribution of the eddy viscosity ($\text{m}^2 \text{s}^{-1}$) for 14 June 1978.

APPENDIX J
ESTIMATION OF THE SURFACE ROUGHNESS DISTRIBUTION
USING HCMM SATELLITE DATA

APPENDIX J

ESTIMATION OF THE SURFACE ROUGHNESS DISTRIBUTION USING HCMM SATELLITE DATA

An attempt was made to estimate the distribution of the surface roughness, z_0 , using the profile equation derived by Monin and Obukhov (1954): i.e.,

$$U(z) = \frac{U_*}{k} \left[\ln \left(\frac{z + z_0}{z_0} \right) + \frac{\alpha}{L} z \right], \quad (1-J)$$

where $U(z)$ is the wind speed, U_* is the friction velocity, k is the Von Kármán constant, z is the altitude, α is the constant, and L is the Monin-Obukhov stability length. Rearranging terms, Equation (1-J) takes the form

$$\ln \left(\frac{z + z_0}{z_0} \right) = x, \quad (2-J)$$

where

$$x = \frac{kU(z)}{U_*} - \frac{\alpha z}{L}. \quad (3-J)$$

Exponentiating and rearranging terms, the following solution for the surface roughness is obtained:

$$z_0 = z(\exp[x] - 1.0)^{-1}. \quad (4-J)$$

The expression in the exponential, x , is generally a small difference between larger terms, and is very sensitive to the accuracy of those terms. Furthermore, the profile equation, Equation (1-J), is only applicable when the stability does not differ greatly from the adiabatic. Therefore, application of Equation (4-J) has significant limitation in determining the distribution of the surface roughness. Only one case study, 9 June 1978,

had conditions that approached the requirement that the stability be very near the adiabatic. The results of the calculations for that case study is shown in Figure 1J.

The distribution of the surface roughness for 9 June 1978 shows larger values for the surface roughness (on the order of 0.6 m) around the central region of St. Louis relative to the immediate suburban regions. However, there are larger values for the surface roughness (values on the order of 0.7 m) immediately to the north and south of the East St. Louis-Belleville urban complex. Comparable values of the surface roughness found in the central urban complex of St. Louis are noted in the northwestern and southwestern portions of the region of interest. Since the wind speed was generally uniform over the region of interest, the variations in surface roughness are generally a result of variations in stability.

The values of the surface roughness calculated using the HCMM satellite data are smaller than the values generally found in the central portions of the city. Clarke et al. (1978) considered the surface roughness for an adiabatic boundary layer at various sites around the St. Louis urban complex using RAPS data. They found that in the central portions of the city, the surface roughness varied from 0.7 to 1.7 m, and values in the rural region to the east of East St. Louis were around 0.3 m. The values in the surface roughness calculated using the HCMM data appeared to be small by a factor of 2 or 3 in the central portions of the St. Louis urban complex, and appeared to be too large by a factor of 2 in the rural region east of East St. Louis.

The results of this study suggests that considerably more research must be performed before it can be conclusively determined whether the distribution of the surface roughness can be derived using satellite data. A study should be initiated which would examine the applicability of other profile equations and the first-order differential equation [Equation (45) in Section 2.4.3] used to derive the profile equations to estimate the surface roughness. The resources were not available for this study to perform the in-depth research necessary to determine which technique might yield the good results.

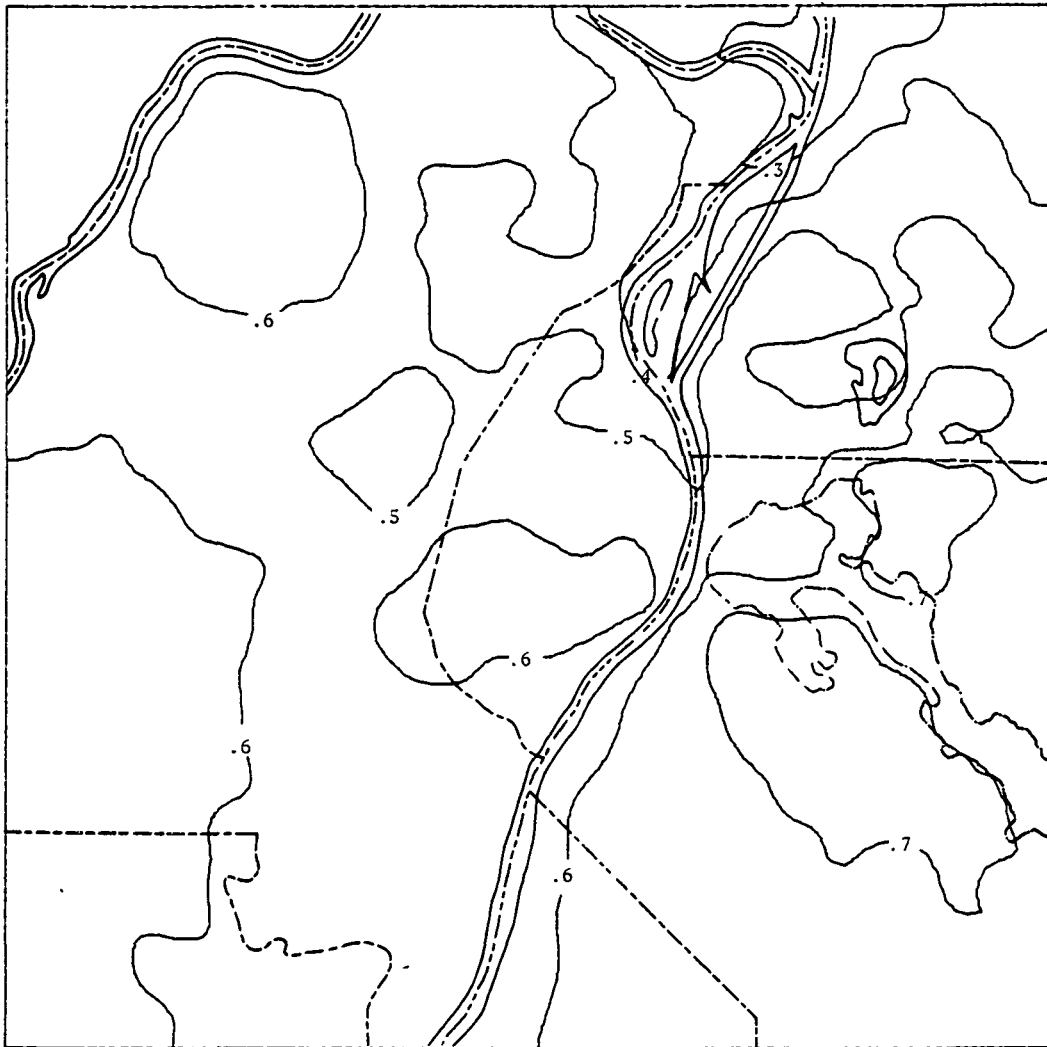


Figure 1J. Distribution of the surface roughness (m) for 9 June 1978.